Cutting Soft Materials

Svetlana Glukhova

▶ **To cite this version:**

Svetlana Glukhova. Cutting Soft Materials. Theoretical and/or physical chemistry. Sorbonne Université, 2024. English. NNT : 2024SORUS448 . tel-04923598

HAL Id: tel-04923598
https://theses.hal.science/tel-04923598v1

Submitted on 31 Jan 2025

HAL is a multi-disciplinary open access archive for the deposit and dissemination of scientific research documents, whether they are published or not. The documents may come from teaching and research institutions in France or abroad, or from public or private research centers.

L'archive ouverte pluridisciplinaire **HAL**, est destinée au dépôt et à la diffusion de documents scientifiques de niveau recherche, publiés ou non, émanant des établissements d'enseignement et de recherche français ou étrangers, des laboratoires publics ou privés.

Doctoral Thesis

CUTTING SOFT MATERIALS

Physics and Chemistry of Materials Doctoral School 397

Prepared at the École Supérieure de Physique et de Chimie Industrielles de la Ville de Paris (ESPCI Paris) and Laboratoire de Physique de l'Ecole Normale Supérieure(ENS Paris)

Svetlana Glukhova

Dissertation Defence Committee:

Veronique LAZARUS Professor, ENSTA Paris	Reviewer
Prof. Shelby HUTCHENS Assistant Professor, IL (UIUC)	Reviewer
Prof. Benoit ROMAN Research Director, ESPCI, CNRS	Examiner
Prof. Mokhtar ADDA-BEDIA Research Director, ENS de Lyon	Examiner
Prof. Matteo CICCOTTI Professor, ESPCI	Director
Prof. Frederic LECHENAULT Researcher, ENS Paris	Co-Director

Substantial summary in French

La découpe des matériaux mous représente un défi fascinant, qui reflète les complexités des actions quotidiennes telles que trancher de la mozzarella ou des tissus chirurgicaux. Derrière ces actions apparemment simples se cache un monde de mécaniques complexes, où déformation, fracture et propriétés des matériaux interagissent pour façonner les résultats de la découpe. Cette thèse entreprend un voyage pour dévoiler les mécanismes de découpe des matériaux mous, explorant trois projets expérimentaux distincts qui progressent en complexité et en portée. Des feuilles minces d'élastomères à la découpe par fil dans des hydrogels, et enfin à la découpe en bordure avec des lames flexibles, chaque chapitre s'appuie sur les résultats des précédents, tissant un récit complet sur la science de la découpe et ses implications.

Découpe de Feuilles Minces d'Élastomères Le voyage commence avec la découpe de feuilles minces de polydiméthylsiloxane (PDMS), un élastomère largement utilisé. La question centrale était simple mais profonde : comment la netteté de la lame, la vitesse de coupe et les propriétés du matériau influencent-elles le processus de découpe ? Dans ce cadre contrôlé, la lame était déplacée perpendiculairement le long d'un chemin prédéfini, permettant aux chercheurs d'isoler et d'examiner les interactions mécaniques en jeu.

Les expériences ont révélé que l'interaction entre la lame et le matériau était loin d'être simple. Notamment, deux types d'instabilités sont apparus : des ondulations hors plan et des oscillations dans le plan, comme illustré dans la Fig.1. Ces instabilités étaient profondément liées aux propriétés mécaniques du PDMS, telles que son énergie de fracture (Γ) et son module d'élasticité (E). Une découverte clé a été l'identification d'un paramètre adimensionnel seuil, Γ/E, qui déterminait l'apparition de ces phénomènes. Ce ratio, appelé la *longueur tomoélastique* (ℓ_{TE}), est devenu un thème récurrent dans la thèse, agissant comme une échelle critique pour comprendre la dynamique de découpe.

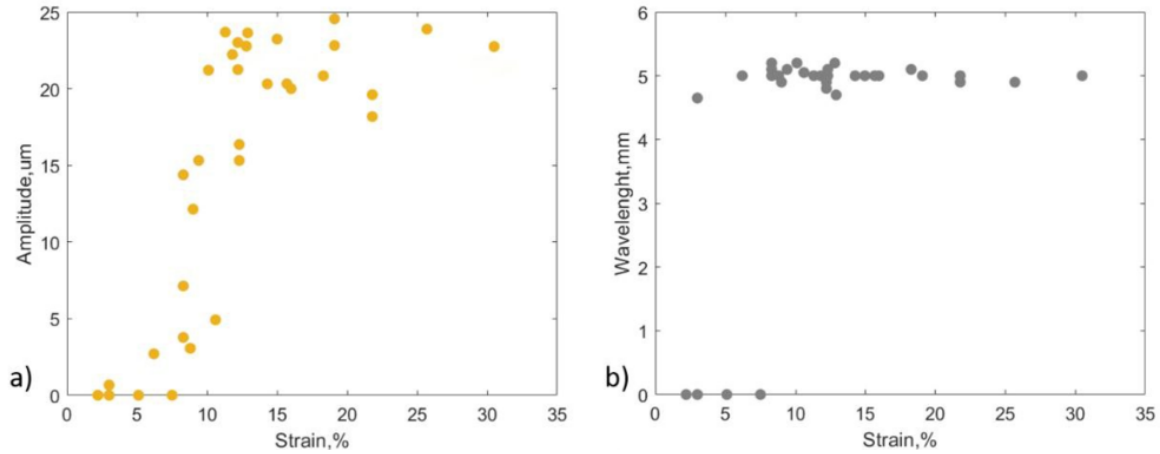

Figure 1: Données du profilomètre mécanique : a) amplitude des oscillations sur les surfaces après découpe d'E32 en fonction de la contrainte appliquée. Un seuil indique l'apparition des oscillations après 5% de contrainte appliquée, b) longueur d'onde des oscillations en fonction de la contrainte appliquée.

En établissant une analogie avec les fissures thermiques dans des plaques de verre, l'étude a proposé un cadre pour prédire le comportement oscillatoire lors de la découpe. Ce chapitre a posé les bases pour comprendre comment les propriétés des matériaux et des lames interagissent, offrant un point de départ pour explorer des scénarios de découpe plus complexes.

Découpe par Fil dans des Gels de Gélatine En s'appuyant sur les expériences contrôlées du premier chapitre, la recherche est passée à un nouveau paradigme : permettre à l'outil de découpe – un fil – de choisir son propre chemin. Le matériau choisi était un hydrogel de gélatine, un matériau mou et homogène avec des propriétés élastiques bien caractérisées. Ici, le montage expérimental a introduit des conditions de charge combinées, où l'échantillon était étiré pendant que le fil coupait sous son propre poids.

L'introduction de la liberté directionnelle a ajouté une couche de complexité à l'étude. Contrairement à la lame rigidement guidée dans le chapitre précédent, la trajectoire du fil était influencée par l'interaction entre les forces d'étirement et le poids du fil. Cela a conduit à des découvertes fascinantes sur la propagation des fissures et la directionnalité (Fig.2).

Les expériences ont révélé que le chemin de la fissure n'était pas uniquement déterminé par l'alignement initial du fil mais était également façonné par des instabilités résultant du couplage entre les forces d'étirement et de découpe.

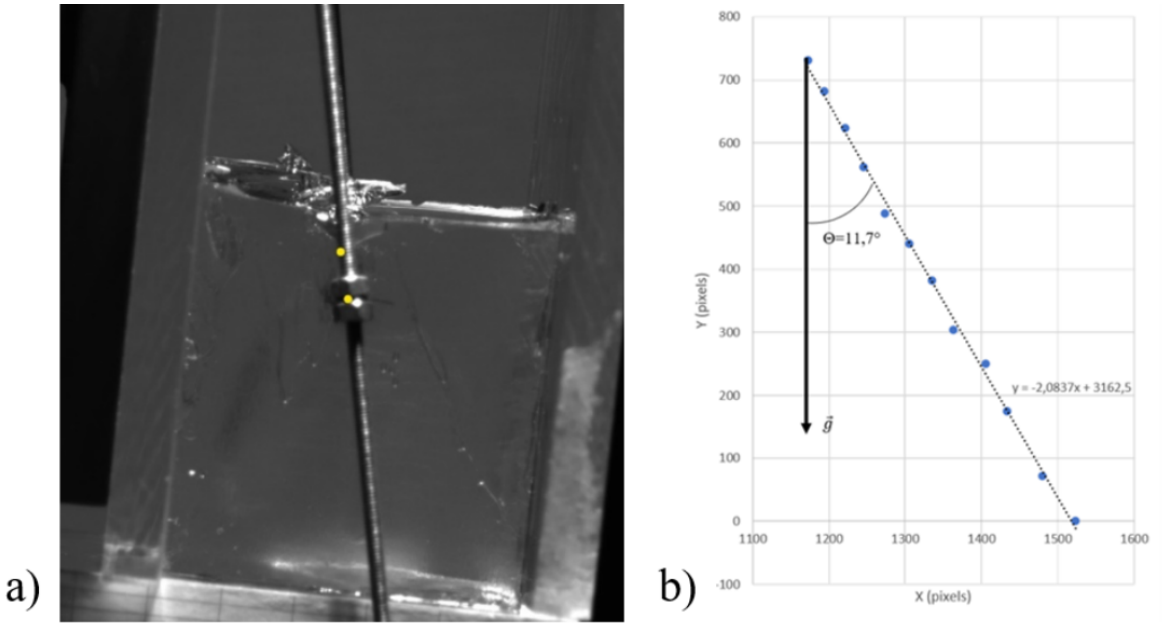

Figure 2: Cube de gélatine sous une compression de 20% avec une masse de fil de 29,6 g : a) angle mesuré entre la fissure et la verticale b).

Une découverte inattendue a été l'émergence d'un comportement de fracture en mode mixte, où la trajectoire de la fissure déviait d'un chemin rectiligne. Ce phénomène a souligné l'importance de considérer les effets de charge combinés dans les processus de découpe. Ce chapitre a mis en lumière les défis liés à la prédiction des chemins de fissures dans les matériaux mous, ouvrant la voie à des modèles et des conceptions expérimentales plus sophistiqués.

Découpe de Barres d'Élastomères sur le Bord Le dernier chapitre a abordé le concept de découpe sous sa forme la plus complexe : découper des élastomères mous près d'un bord à l'aide d'une lame rigide montée sur des supports flexibles. La motivation pour cette étude provenait des limites des expériences précédentes. Bien que la découpe par fil ait permis une liberté directionnelle, elle manquait de rigidité nécessaire pour des coupes

précises dans les applications industrielles. Pour combler cette lacune, les chercheurs ont conçu un système où la flexibilité de la lame, plutôt que son chemin, dictait le comportement de la découpe (Fig.3).

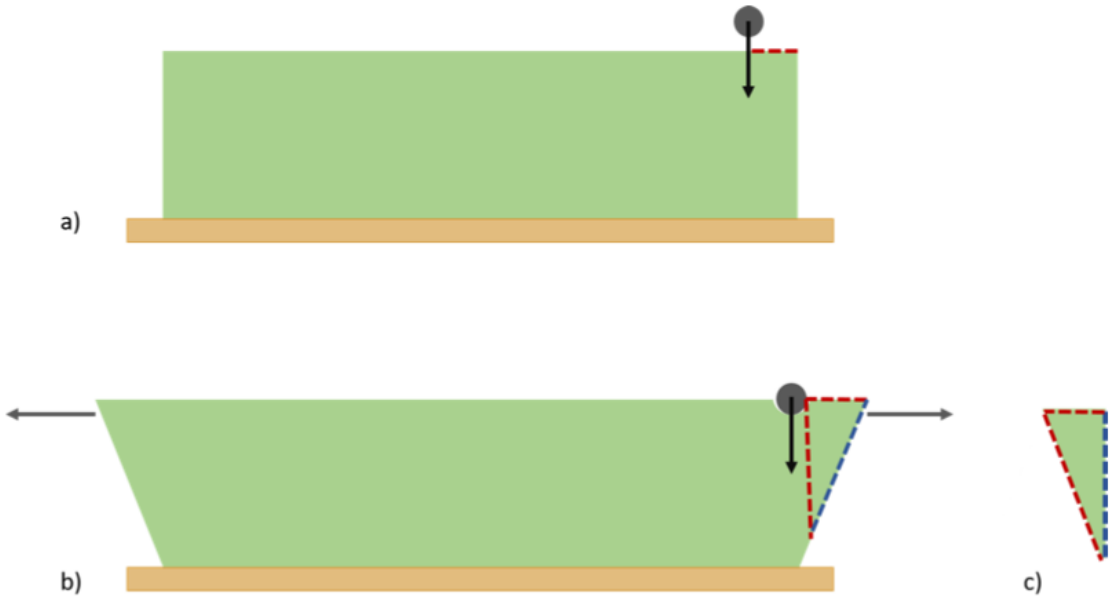

Figure 3: a) Échantillon original avant que la lame ne touche le bord, b) la lame pénètre dans l'échantillon, provoquant un étirement sous pression après contact, jusqu'à l'initiation de la coupe, et c) fragment de l'échantillon après découpe.

Ce montage a introduit une nouvelle dimension à l'étude : l'interaction entre la rigidité en flexion de la lame (B) et la longueur tomoélastique (ℓ_{TE}) du matériau. Lorsque la distance de coupe (d) par rapport au bord était petite par rapport à ℓ_{TE}, de grandes déformations dans le matériau dominaient le comportement de la découpe, entraînant une morphogenèse significative – la formation de formes complexes et non planes. À l'inverse, à des distances plus grandes, la mécanique de la fracture gouvernait le processus, conduisant à des résultats plus prévisibles.

Les expériences ont également révélé le double rôle de la flexibilité de la lame. Bien que la flexibilité ait permis à la lame de s'adapter à la déformation du matériau, elle a également introduit des non-linéarités, compliquant la prédiction des chemins de découpe. En normalisant les données avec d/ℓ_{TE}, les chercheurs ont proposé un cadre unifié pour comprendre

la transition entre les régimes dominés par la déformation élastique et ceux dominés par la fracture.

Conclusion et Perspectives Chaque chapitre de cette thèse représente une avancée dans la compréhension des complexités de la découpe des matériaux mous. La progression, des lames guidées rigidement aux fils libres de leurs trajectoires, puis aux lames flexibles, reflète une compréhension évolutive de l'influence des propriétés des matériaux, des conditions de charge et de la conception des outils sur les résultats de la découpe.

Le concept de la longueur tomoélastique (ℓ_{TE}) émerge comme un thème unificateur, fournissant une échelle critique pour prédire le comportement de découpe dans différents matériaux et configurations.

Perspectives Futures Des questions restent ouvertes. Les recherches futures pourraient explorer :

- **Diversité des Matériaux :** Étendre l'étude à des matériaux avec une gamme plus large de ratios Γ/E, permettant une compréhension plus complète du rôle de la longueur tomoélastique.
- **Nouvelles Conceptions de Lames :** Étudier des géométries et matériaux de lames innovants qui combinent rigidité et flexibilité pour optimiser les performances de découpe.
- **Applications Réelles :** Traduire ces découvertes dans des contextes industriels tels que la transformation alimentaire, la fabrication de dispositifs médicaux et la robotique souple.

En relevant ces défis, les chercheurs pourront continuer à développer les bases établies par cette thèse, faisant progresser la science de la découpe et ses applications dans divers domaines.

Acknowledgements

I extend my deepest gratitude to my supervisors, Matteo Ciccotty and Frederic Lechenault, whose guidance, support, and encouragement were invaluable throughout this journey. Your expertise and insightful feedback have shaped this dissertation and my academic growth profoundly.

I would like to express my sincere thanks to my committee members, Veronique Lazarus, Shelby Hutchens, Benoit Roman, and Mokhtar Adda-Bedia, for their willingness to share their knowledge and for the time and effort they will dedicate to reviewing my work. Their expertise is highly respected, and I look forward to their feedback during my defense.

I am indebted to ESPCI PSL for providing the resources and facilities necessary for conducting this research. The financial support from Sorbonne University is gratefully acknowledged.

Special thanks go to my colleagues and friends for their unwavering support and encouragement during challenging times. Your camaraderie and understanding have made this academic journey fulfilling and enjoyable.

I am deeply grateful to my family for their unconditional love, patience, and unwavering belief in my abilities. Their support has been the cornerstone of my perseverance and success.

Lastly, I would like to express my appreciation to all individuals who participated in this study, whose contributions were essential to its completion.

Their support and encouragement have been instrumental in the completion of this dissertation.

Context

Abstract

This research explores the mechanics of cutting and fracture in soft materials, with a particular focus on understanding crack propagation under combined cutting and stretching loads. Soft materials, such as elastomers and gelatin gels, exhibit complex mechanical behaviors that pose challenges in predicting and controlling crack initiation and propagation during cutting processes. Through a series of meticulously designed experiments, this study investigates how different factors—such as applied strain, cutting speed, and blade sharpness—affect the stability and efficiency of cutting in soft materials.

The research identifies distinct cutting regimes that emerge based on varying levels of applied strain, highlighting the transition between stable and unstable crack propagation. Additionally, novel instabilities, such as out-of-plane wrinkling and in-plane sinusoidal oscillations, are observed during the cutting process, with these patterns being strongly influenced by material properties and the degree of applied strain. These findings are crucial for applications where precision in cutting is essential, such as in biomedical engineering and food processing.

The study contributes to the development of predictive models that integrate fracture mechanics with cutting processes, providing a deeper understanding of the conditions that lead to unexpected morphology after cutting. While a comprehensive model has yet to be fully realized, the insights gained lay the foundation for future work aimed at optimizing cutting techniques and improving material performance in industrial applications.

Chapter 1

Introduction and chapters organisation

1.1 Industrial Context and Scientific Question of the Study

Cutting processes have long been a cornerstone of industrial applications, with extensive research and technological advancements dedicated to materials like metals, ceramics, and composites. Techniques such as laser cutting, waterjet cutting, and abrasive machining have revolutionized manufacturing processes, ensuring precision and efficiency. However, these well-established methods often falter when applied to soft materials such as elastomers, gels, and biological tissues. This limitation arises from the fundamentally different mechanical behaviors exhibited by soft materials, which challenge conventional cutting principles.

Figure 1.1: Different examples of soft materials industrial cutting.

In industries such as food processing, medical device manufacturing, and packaging, the need for precise and efficient cutting of soft materials is ever-growing. The texture and appearance of sliced food products, the safety and accuracy of surgical instruments, and the performance of elastomeric seals are all directly influenced by the cutting process. Yet, achieving consistent results remains elusive due to the inherent properties of soft materials, including their viscoelasticity, high deformability, and nonlinear elastic behavior. Traditional models developed for brittle materials fail to account for these complexities, often leading to unpredictable outcomes like tearing, excessive energy consumption, and uneven cuts [1, 2].

Cutting soft materials poses several unique challenges. For example, the elastic recovery of these materials can cause deviations in the cutting path, while their tendency to deform under load complicates the application of precise cutting forces. Additionally, the interaction between cutting tools and soft materials often leads to instabilities, such as jagged fracture surfaces or localized tearing, which compromise product quality and process efficiency.

Addressing these challenges requires a paradigm shift in the understanding of cutting mechanics. The present study seeks to fill this gap by investigating the fundamental mecha-

nisms governing the cutting of soft materials. A key aspect of this research is the deliberate design and execution of experiments to observe unusual cutting phenomena. By creating controlled conditions to provoke instabilities and deviations, the study aims to uncover the underlying factors that influence cutting behavior.

This research not only focuses on the material properties but also emphasizes the interplay between cutting tool geometry, process parameters (such as speed and force), and the specific characteristics of the soft material being cut. The ultimate goal is to develop predictive models and practical guidelines that can be applied across a range of industries, ensuring greater reliability and precision in cutting processes.

Moreover, the implications of this work extend beyond traditional industrial applications. Insights gained from understanding and controlling cutting mechanics could drive innovations in fields such as robotics, where soft actuators and components are increasingly used, and in medicine, where precision cutting is critical for minimally invasive procedures. By bridging the gap between material science and industrial engineering, this study has the potential to significantly advance both scientific knowledge and practical applications.

1.2 Organization of the Study

The study is systematically organized to address the complexities associated with cutting soft materials through a series of experimental investigations and theoretical analyses. It begins with a broad review of the state of the art in fracture mechanics, particularly focusing on the challenges posed by soft and elastic materials.

Following the literature review, the study transitions into an extensive experimental phase, structured into several key sections. The first set of experiments focuses on mixed loading between the cutting of thin elastomer sheets and stretching. This phase of the research investigates how various factors, such as blade sharpness, cutting speed, and the intrinsic properties of the elastomers, influence the fracture behavior of the material. The primary focus is placed on understanding the onset and progression of instabilities during the cutting process, which can lead to unpredictable outcomes, such as uneven cuts or the formation

of complex fracture patterns.

The subsequent experimental section examines the wire-cutting of gelatin gels, serving as a model system for exploring crack propagation in soft, homogeneous materials. These experiments are designed to investigate the effects of strain and the weight of the cutting wire, which directly impact the cutting speed and the directionality of each cut. Additionally, this part of the study delves into the instabilities that arise during crack initiation and propagation, providing valuable data to refine existing models and develop new theoretical frameworks.

In addition to the above, the study includes a critical examination of cutting soft elastomers on an edge, detailed in the fourth chapter. This aspect of the research addresses a specific cutting scenario that was investigated to gain a deeper understanding of the nonlinear effects that could arise due to the elastic nature of the materials during the cutting process.

The study concludes with a synthesis of the experimental findings and proposes how these insights might be utilized to create a framework for predicting and controlling fracture and cutting in soft materials. These contributions are expected to enhance the reliability, efficiency, and precision of cutting processes in industries that handle soft materials, ultimately driving innovation in both existing technologies and future developments.

Chapter 2

State of the Art

2.1 Relation between Cutting and Fracture of Soft Materials

Cutting is a fundamental process with significant implications across both cultural and technological domains. The application of orthogonal compression to the cutting plane plays a crucial role in guiding the cutting process. However, the forces exerted during cutting and the necessity of holding the material can induce substantial strain, thereby distorting the final shape of the fabricated parts. Beyond these common applications, the cutting of soft materials holds particular significance in industrial sectors such as food processing and tissue analysis in histology [3, 4, 5, 6].

An example of the influence of different cutting speeds on the final shape of salami is shown in Fig.2.1. Salami, a soft material with a heterogeneous structure, contains a significant amount of macroscopic filler that resists transection. It has been observed that at low cutting velocities, these fillers are squeezed rather than dissected, causing the cutting forces to superimpose. At higher velocities, the filler particles are separated due to internal stiffening [5]. The rough cutting surfaces of the salami and the residues remaining on the cutting edge of the blade when cutting at velocities up to 1 m/s demonstrate this effect. At 10^{-1} m/s, the cutting path is rough, while at 10 m/s, the surface and the cutting path are smooth. These observations highlight the effect of velocity changes on the overall fracture behavior.

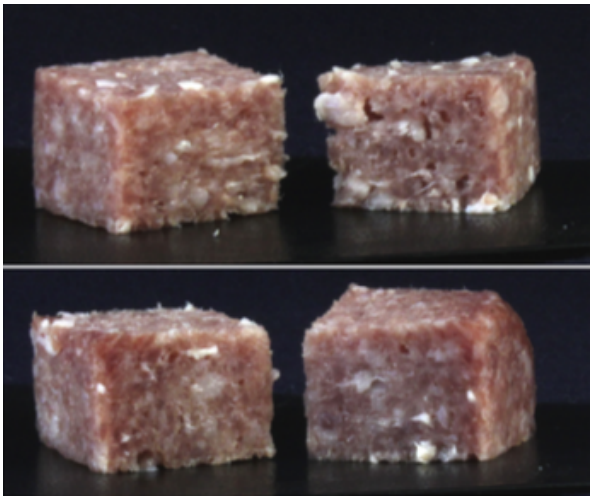

Figure 2.1: Surface of salami after cutting at 10^{-1} m/s (rough, upper image) and at 10 m/s (smooth, lower image).

The behavior of soft materials differs significantly from that of strong ductile solids, such as metals, soils, or hard polymers. A key distinction lies in the fracture mechanics of soft matter. The challenge of working with soft materials arises from their nonlinear deformation characteristics across various scales, complicating the attainment of desired part shapes and surface finishes. This necessitates the use of specialized tools and methodologies tailored to address these complexities [7].

Due to the nonlinear effects inherent in soft materials, cutting does not always lead to predictable fracture propagation. This complexity underscores a significant challenge in contemporary materials science: accurately describing and predicting crack propagation in soft materials. Currently, there is a notable gap in the development of comprehensive models that effectively integrate cutting and fracture processes into a unified framework applicable across a wide range of soft materials. While fracture mechanics provides a solid foundation for understanding crack propagation under stress—primarily through energy-based and stress-based approaches within Linear Elastic Fracture Mechanics—it remains unclear how these principles can be applied to the cutting processes of soft materials. In our study, we aim to explore whether the tools and concepts from fracture mechanics can be effectively used to analyze and predict cutting behavior in soft materials.

Developing such models is crucial for advancing our understanding and improving the precision of cutting soft materials. Effective models would not only enhance the predictability of cutting outcomes but also optimize industrial applications. For instance, in the food processing industry, more accurate models could result in higher-quality products with reduced waste [5]. In medical fields, such models could improve surgical techniques and outcomes by offering better predictions of how soft tissues will behave under cutting stresses [6]. Similarly, in the manufacturing of elastomeric components, improved models could lead to more efficient production processes and higher-quality final products [8, 9]. However, developing these comprehensive models necessitates advanced tools for accurately describing the elastic behavior of materials.

2.1.1 Introduction to Linear Elastic Fracture Mechanics (LEFM)

In the context of cutting, where soft materials with complex, nonlinear behavior are involved, a crucial question arises: can the propagation criteria derived from fracture mechanics be effectively applied to understand and predict cutting processes? Linear Elastic Fracture Mechanics (LEFM) is a critical framework within the broader field of fracture mechanics, specifically addressing the behavior of cracks in elastic solids. The inception of LEFM can be traced back to the pioneering work of A.A. Griffith in the early 20th century [10]. Griffith's seminal experiments with glass fibers laid the foundation for understanding crack propagation in brittle materials. His tensile tests of glass fibers revealed that the actual fracture strengths were significantly lower than theoretical predictions based on atomic bond strengths. This discrepancy led Griffith to propose that the presence of microscopic cracks or flaws in the material could account for the reduced strength. He hypothesized that these flaws act as stress concentrators, significantly amplifying local stress and ultimately leading to crack propagation.

Griffith's energy criterion for crack propagation posits that a crack will grow when the release of elastic strain energy exceeds the energy required to create new crack surfaces. This relationship is mathematically represented as:

$$G \geq G_c = 2\gamma$$

where G is the strain energy release rate, G_c is the critical energy release rate for crack propagation, and γ is the surface energy per unit area. This criterion established a quantitative basis for understanding why materials often fail at stresses much lower than their theoretical strength.

Prior to Griffith's work, C.E. Inglis [11] made significant contributions by addressing the problem of stress concentration around elliptical holes and cracks in materials. Inglis derived expressions to quantify the stress concentration factor, showing that the stress at the tip of an elliptical crack increases significantly as the radius of curvature at the crack tip decreases. This insight was instrumental in understanding the amplification of stress around crack tips, further reinforcing Griffith's energy-based approach to fracture.

Inglis' work on stress concentration can be summarized by the following relation:

$$\sigma_{\text{max}} = \sigma \left(1 + 2\frac{a}{\rho}\right)$$

where σ_{max} is the maximum stress at the crack tip, σ is the nominal stress, a is the half-length of the crack, and ρ is the radius of curvature at the crack tip. This relationship highlights the dramatic increase in stress near the crack tip, a fundamental aspect of crack propagation in brittle materials.

2.1.2 Surface Energy and Energy Release Rate

Central to Griffith's theory was the concept of surface energy [10]. In a brittle material, the creation of new surfaces during crack propagation requires energy, which is supplied by the elastic strain energy stored in the material. The critical condition for crack growth can be expressed in terms of the energy release rate G, which represents the rate at which energy is released from the elastic field as the crack propagates. For a crack to propagate, the energy release rate must reach a critical value G_c, related to the material's fracture toughness.

The energy release rate G is defined as:

$$G = \frac{dU_w}{dA} - \frac{dU_{el}}{dA} \geq \Gamma$$

where G is the energy release rate, U_w is the work done, U_{el} is the elastic energy, and Γ represents the material's surface energy. When G reaches Γ, the crack will propagate, linking the energy approach directly with the material's intrinsic properties.

2.1.3 Stress-Intensity Factors

Building on the work of Griffith and Inglis, G.R. Irwin [12, 13] introduced the concept of the stress-intensity factor K, which characterizes the stress field near the crack tip. Irwin calculated the singular stress field produced around a loaded crack and found a square root dependence of the stress on the distance from the crack tip, expressed as:

$$\sigma \sim \frac{K}{\sqrt{r}}$$

Using this approach, an equivalent condition for crack propagation in terms of stress can be expressed as $K \geq K_c$, where K_c is the critical stress-intensity factor, also known as the fracture toughness of the material.

For linear elastic materials, it can be demonstrated that the energy-based approach and the stress-based approach are equivalent. This equivalence is expressed through the relationship:

$$K \sim \sqrt{EG}$$

where E is the elastic modulus of the material. Thus, in LEFM, both the energy criterion and the stress criterion are equivalent. The maximum stress achieved at the crack tip is essentially defined by the external work or input energy provided to the entire sample. The stress-intensity factor depends on the applied load, crack size, and geometry of the specimen.

Irwin also identified three fundamental modes of crack propagation based on the loading

conditions at the crack tip (Fig.2.2):

- **Mode I (Opening Mode)**: The crack faces are pulled apart perpendicular to the crack plane. This mode is characterized by the stress-intensity factor K_I.
- **Mode II (Sliding Mode)**: The crack faces slide relative to each other in the plane of the crack, driven by in-plane shear stresses. This mode is characterized by the stress-intensity factor K_{II}.
- **Mode III (Tearing Mode)**: The crack faces slide relative to each other out of the plane of the crack, driven by out-of-plane shear stresses. This mode is characterized by the stress-intensity factor K_{III}.

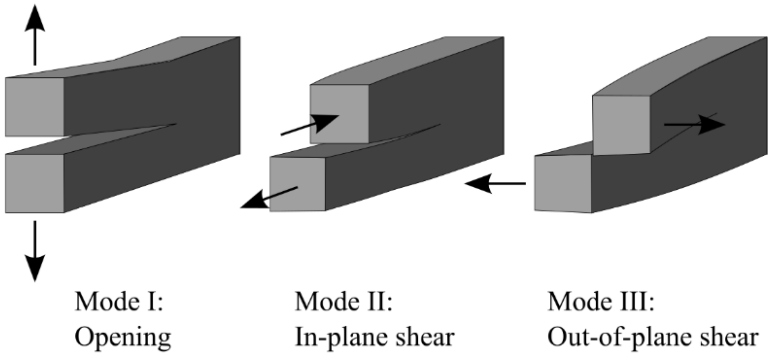

Figure 2.2: Illustration of the three fundamental fracture modes: Mode I (opening mode), Mode II (sliding mode), and Mode III (tearing mode).

Each mode of crack propagation can be analyzed using the corresponding stress-intensity factors, providing a comprehensive framework for predicting the onset of fracture under various loading conditions.

The stress-intensity factor K for each mode can be expressed as:

$$K_I = \sigma\sqrt{\pi a}$$

$$K_{II} = \tau\sqrt{\pi a}$$

$$K_{III} = \tau\sqrt{\pi a}$$

where σ is the applied stress, τ is the applied shear stress, and a is the crack length. These equations illustrate how the stress intensity at the crack tip is influenced by the applied loads and the size of the crack.

2.2 Predicting Crack Paths in Soft Materials

Predicting the path of a crack is a significant challenge in fracture mechanics, as it hinges on accurately modeling the motion of the crack tip and understanding the fundamental mechanisms of material separation. This task becomes even more complex in soft polymers, where crack behavior is both intricate and critical to materials science and engineering. The process involves comprehending how cracks initiate, propagate, and ultimately lead to failure.

Soft polymers often exhibit diverse crack growth behaviors, including both stable and unstable propagation modes. Stable crack growth occurs under controlled loading conditions, where the crack advances gradually with increasing stress, demonstrating a degree of resilience against sudden failure [14]. This gradual progression allows for some predictability and control over the crack path. In contrast, unstable crack growth involves rapid propagation under critical stress conditions, leading to catastrophic failure. In such cases, cracks can propagate at speeds approaching the speed of sound in the material, making them difficult to predict and control.

The transition from stable to unstable crack growth is often marked by a critical stress intensity factor, beyond which the crack propagates uncontrollably. To address this challenge, one must ask: if a crack propagates, can the criteria from fracture mechanics be used to describe the stability of this propagation? Initially, this involves understanding linear propagation and whether phenomena such as stick-slip behavior occur. Additionally, can the tools of fracture mechanics be applied to predict the direction in which the crack will propagate? Furthermore, can fracture mechanics criteria predict whether the crack direction will remain stable or become unstable—specifically, whether perturbations will cause a change in the crack's path?

Understanding these aspects is crucial for developing more accurate predictive models for crack behavior in soft polymers, with implications for both material design and failure prevention.

2.2.1 Historical Approaches to Crack Path Prediction

LEFM forms the foundation of our understanding of simple cracks [15]. Building on Griffith's pioneering work [10], LEFM incorporates the concept of energy balance as a criterion for crack propagation. According to Griffith's theory, a crack will extend if the decrease in elastic strain energy equals or exceeds the increase in surface energy due to the creation of new crack surfaces. This fundamental principle can be expressed mathematically as:

$$\frac{dU}{da} = \Gamma$$

where $\frac{dU}{da}$ is the rate of decrease in elastic energy per unit increase in crack length, and Γ is the surface energy per unit area of the crack, considered a characteristic material property. Once crack propagation initiates, the dynamics of simple cracks are comprehensively governed by this energy balance principle [16]. LEFM provides a robust quantitative framework for describing the behavior of a crack tip, applicable to scenarios such as a semi-infinite crack propagating within an infinite medium or an infinitely long strip.

Understanding the stability behavior of crack propagation is crucial for predicting the integrity and durability of materials and structures under stress. The stability of a crack influences the material's ability to withstand loading conditions without catastrophic failure.

T-stresses characterize the stress state around the crack tip, affecting the direction and stability of crack growth, and play a crucial role in the stability of crack propagation. While the stress intensity factors (SIFs) K_I, K_{II}, and K_{III} are primary parameters in LEFM used to describe the intensity of singular stress fields near the crack tip, T-stresses represent the non-singular term in the Williams expansion of the stress field. Understanding T-stresses is essential for assessing the stability and direction of crack growth, particularly under complex loading conditions.

$\sigma_{ij} = \frac{K}{\sqrt{2\pi r}} f_{ij}(\theta) + T g_{ij}(\theta) +$ higher order terms

where σ_{ij} is the stress tensor, r and θ are polar coordinates centered at the crack tip, and $f_{ij}(\theta)$ and $g_{ij}(\theta)$ are angular functions. The T-stress is independent of the distance from the crack tip, making it a constant stress component parallel to the crack plane.

2.2.2 Influence on Crack Propagation

The T-stress influences the stress state around the crack tip, thereby affecting the stability and direction of crack propagation. Positive T-stress tends to open the crack faces, promoting mode I (opening mode) propagation, while negative T-stress can close the crack faces, potentially leading to crack path deflection or kinking. The effect of T-stress on crack propagation can be summarized as follows:

Positive T-Stress: Enhances crack-tip opening, increasing the likelihood of straight-ahead propagation in mode I.

Negative T-Stress: May cause crack closure or kinking, leading to deviations from the initial crack path and mixed-mode propagation.

The criteria for the propagation of a crack determine when a crack will start to grow or continue to propagate under applied stress. These criteria focus on the conditions necessary for crack growth initiation and sustainment. The primary criteria are as follows:

Griffith Criterion:

A crack propagates when the energy release rate G exceeds the critical energy release rate G_c.

G is the amount of energy available for crack growth per unit area of crack extension.

G_c is a material property representing the energy required to create new surfaces.

Stress-Intensity Factor Criterion:

A crack propagates if the stress intensity factor K exceeds the fracture toughness K_c.

K represents the intensity of the stress field near the crack tip.

K_c is a material property indicating the critical stress intensity factor for crack propagation.

Rate of Change of Energy Release Rate:

Stability can also be evaluated using the rate of change of the energy release rate with respect to crack length, $\frac{dG}{da}$.

A crack is stable if $\frac{dG}{da} < 0$, indicating that the energy available for crack growth decreases as the crack propagates.

T-stress modifies the stress field at the crack tip, influencing both the energy release rate and the stress-intensity factor. This modification can either stabilize or destabilize crack propagation, depending on the sign and magnitude of the T-stress:

Stabilization: Positive T-stress can stabilize crack propagation by promoting mode I fracture and reducing the likelihood of crack path deviation.

Destabilization: Negative T-stress can destabilize crack propagation by inducing crack kinking or deflection, leading to mixed-mode fracture and potentially increasing the energy release rate.

2.3 Direction of Crack Propagation in Fracture Mechanics

The direction of crack propagation is a fundamental concern in fracture mechanics, as it determines the failure paths and integrity of materials under stress. In soft materials, including polymers, gels, and biological tissues, understanding crack propagation direction is crucial due to their unique mechanical properties. This section explores various theories and methodologies used to predict crack propagation direction in soft materials, supported by examples from recent research.

Fracture mechanics offers several theoretical approaches to predict the direction of crack propagation, including the Principle of Local Symmetry (PLS), the maximization of energy release rate, and the maximal stress direction.

The Principle of Local Symmetry (PLS) posits that a crack will propagate in a direction that minimizes the stress intensity factors for shear modes (Mode II and Mode III), resulting in a pure Mode I (opening mode) propagation. This principle is based on the assumption that the crack advances in a way that maintains local symmetry of the stress field around the crack tip.

Maximization of Energy Release Rate suggests that a crack will propagate in the direction where the energy release rate is maximized. The energy release rate (G) is defined as the amount of energy available for crack growth per unit area of crack extension. This criterion ensures that the crack advances in the most energetically favorable direction.

The Maximal Stress Direction proposes that cracks propagate in the direction where the stress at the crack tip is highest. This method is particularly relevant for materials with high toughness and complex stress fields, as it considers the local stress environment's influence on crack growth.

Predicting crack propagation direction in soft materials involves various experimental techniques, including digital image correlation (DIC), finite element analysis (FEA), and photoelasticity. These methods provide insights into the stress fields and deformation patterns around crack tips.

In materials science, understanding crack propagation in soft polymers and composites is essential for developing materials with enhanced toughness and reliability. This knowledge helps in tailoring the microstructure and composition of materials to achieve desired mechanical properties.

2.4 Experimental Investigations of Cutting

2.4.1 Fracture Tests in Soft Viscoelastic Materials

Fracture tests provide insights into how materials respond to stress and how cracks initiate and propagate. This information is crucial for predicting material behavior during cutting, especially crack formation and propagation, which directly affect cutting quality and efficiency. Understanding the conditions under which a material may fail, as revealed by fracture tests, is vital for ensuring the safety and reliability of cutting operations.

Typically, fracture tests are conducted on unconfined samples such as films, sheets, or thick specimens. These materials generally exhibit lower viscoelasticity than soft adhesives, making fracture behavior more complex. The results of these tests are significantly influenced by the material properties and the dimensions of the sample. For instance, fracture

can occur under plane stress conditions in thin samples or plane strain conditions in thick samples, each leading to different outcomes for the energy release rate, denoted as $\Gamma(v)$, where v represents the crack velocity. The challenge in defining the energy release rate lies in determining the direction of energy release. For example, peeling scotch tape from a surface involves an interface that is mechanically weaker than the bulk material, creating a preferential crack path. However, in fracture tests, such preferential crack paths do not exist in bulk material, leading to potential crack deviations even under pure mode I loading conditions.

Various test geometries are employed to study fracture propagation in soft viscoelastic materials, such as rubber. The choice of geometry often depends on practical considerations. Common geometries include the trousers test, pure shear test, and single or double edge notch tests (Fig. 2.3).

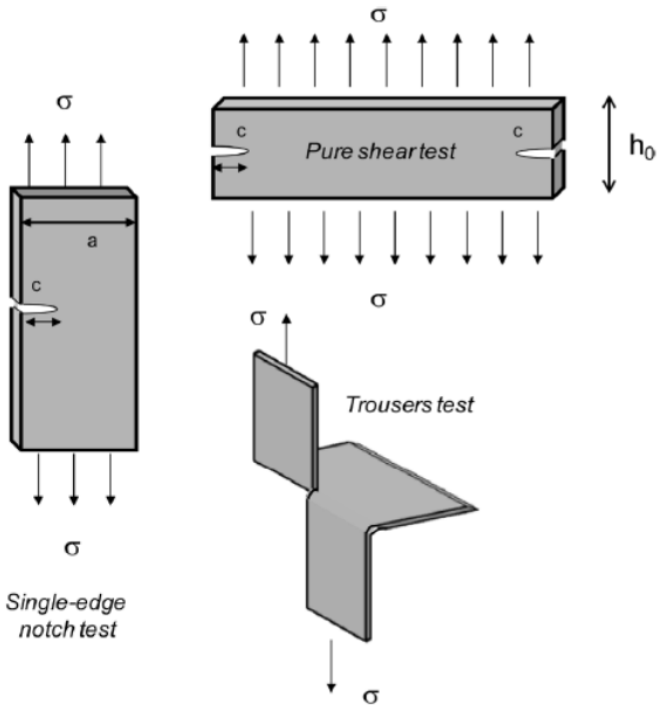

Figure 2.3: Schematic of the most common geometries used for fracture of rubbers: single-edge notch test, trousers test (also called tear test), and pure shear test [17].

Trousers Test:

This test weakens the material at a side groove, reducing the sample thickness to create a weak plane for crack propagation. It is suitable for very tough materials but involves significant dissipative processes. As a result, it measures the apparent work of fracture, $\Gamma_{\text{app}}(v)$, instead of the intrinsic fracture energy, $\Gamma(v)$.

Pure Shear Test:

This test geometry has the advantage of applying an energy release rate, G, that remains constant regardless of crack length if the material is elastic in the bulk and the crack length, c, is greater than half the undeformed sample height, h_0. For purely elastic materials, the energy release rate is expressed as:

$$G = W(\lambda)h_0$$

where $W(\lambda)$ represents the strain energy per unit volume ahead of the crack tip under a fixed stretch, λ. This geometry is suitable for both steady-state and fatigue crack propagation but requires specific sample preparation and careful gripping, which is feasible in industrial settings but challenging in laboratory environments with small samples. Consequently, it has been rarely used for hydrogels [18].

Single or Double Edge Notch Test:

This test involves stretching a pre-notched strip of material in tension. For elastomers, which typically exhibit Neo-Hookean elasticity under moderate stretch, Greensmith (1963) proposed an empirical expression for the energy release rate:

$$G = \frac{6W(\lambda)c}{\sqrt{\lambda}}$$

where $W(\lambda)$ is the strain energy per unit volume, obtained from the stress-strain curve of an unnotched sample of identical dimensions. In this geometry, the energy release rate increases with crack length, implying that dG/dc is positive. As a result, once the crack starts moving, it will accelerate, leading to spontaneous and uncontrolled propagation.

The study of fracture propagation in soft viscoelastic materials necessitates careful se-

lection of test geometries to ensure accurate measurements of fracture energy. While the trousers test is suitable for tough materials, the pure shear test provides a consistent energy release rate for elastic materials. The single or double edge notch test, commonly used in academic studies, allows for empirical estimation of the energy release rate but poses challenges in controlling crack propagation. Each test geometry has its advantages and limitations, necessitating careful consideration in experimental design and interpretation of results.

2.4.2 Cutting Tests

Two pivotal testing methods specifically tailored for analyzing the mechanical behavior of soft, rubber-like materials during cutting processes, are the Y-shaped test and the pure shear test, as initially introduced by Lake and Yeoh [19]. These tests are designed to characterize the mechanical properties of soft materials under cutting conditions, which is crucial for developing predictive models and optimizing cutting techniques.

In these tests, the cutting process can be executed in two primary ways: one where a constant force is applied, and the cutting rate is measured, and another where the blade moves at a constant rate relative to the test piece, with the cutting force being measured [19].

This section delves deeply into the methodologies and applications of these tests, highlighting their critical role in advancing the study and development of soft materials.

Y-Shaped Test The Y-shaped test is specifically designed to investigate the initiation and propagation of cracks in soft materials. This test involves a specimen with a pre-cut notch in the shape of a ”Y”, where the arms of the ”Y” act as guides for crack propagation (fig. 2.4). The geometry of the Y-shaped specimen is critical as it creates a controlled environment for observing crack initiation and growth under applied stresses.

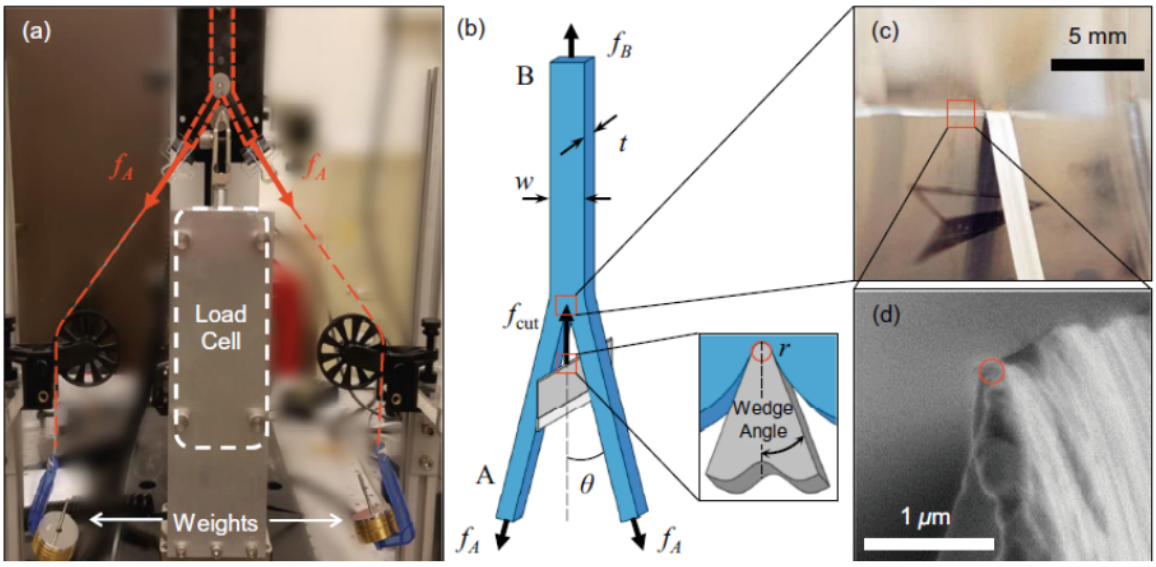

Figure 2.4: Cutting with a Y-shaped geometry. (a) A photograph of the cutting instrument shows the position of the sample (orange dashed lines), relative to the load cell (white dashed lines) upon which the cutting blade is mounted. Hanging weights apply load f_A to two sample legs. (b) Schematics of the Y-shaped sample and blade geometries illustrate variable parameters and the free-body diagram during steady-state cutting. The cutting force applied by the blade (c) is measured by the load cell. Blade radius, r, (b)-inset is determined from a scanning electron microscopy (SEM) image (d) [20].

The sample, typically made from a soft material, is prepared with a Y-shaped notch. The arms of the ”Y” are aligned with the principal directions of the expected stress field. The specimen is subjected to tensile loading in a controlled environment to ensure uniform stress distribution. High-speed cameras or other imaging techniques are used to observe the crack initiation and propagation, capturing the dynamic behavior of the crack as it interacts with the material’s internal structure.

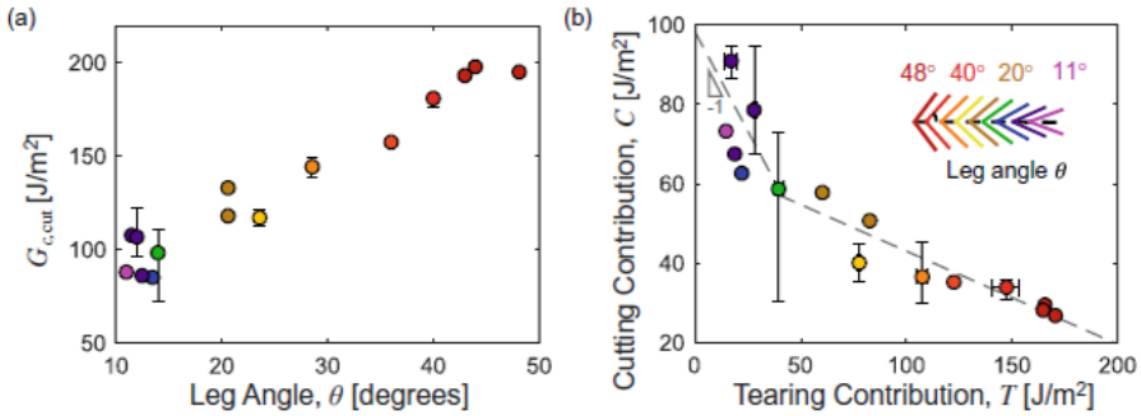

Figure 2.5: Test geometry variation for control of cutting and tearing contributions. (a) G_{cut} increases monotonically with leg angle. (b) The variation in C as a function of T transitions between two regimes. The fit (dashed line) on the left has a fixed slope of -1, indicative of "true" cutting. A linear fit at higher T yields a slope of -0.23. Error bars represent maximum and minimum values of three or more samples [20].

Lake and Yeoh's earlier work identified a linear relationship between cutting and tearing contributions at low tearing energies, which they termed the "true" cutting regime, characterized by smooth cutting behavior. However, in subsequent studies with materials like 10:1 Sylgard 184, it was demonstrated that as tearing energy increases, this relationship can become nonlinear, as shown in Fig.2.5b, leading to a stick-slip response during cutting—a phenomenon where the cutting process alternates between periods of smooth movement and abrupt jerks [20]. This transition from smooth to stick-slip cutting suggests the onset of tearing events induced by material properties, which are crucial to understanding the fracture mechanics and optimizing cutting techniques.

Pure Shear Test The pure shear test is another fundamental method used to investigate the mechanical properties of soft materials under cutting conditions. This test involves applying a uniform shear stress to a rectangular specimen, creating a state of pure shear that allows for the study of material deformation and fracture under shear loading (Fig.2.6).

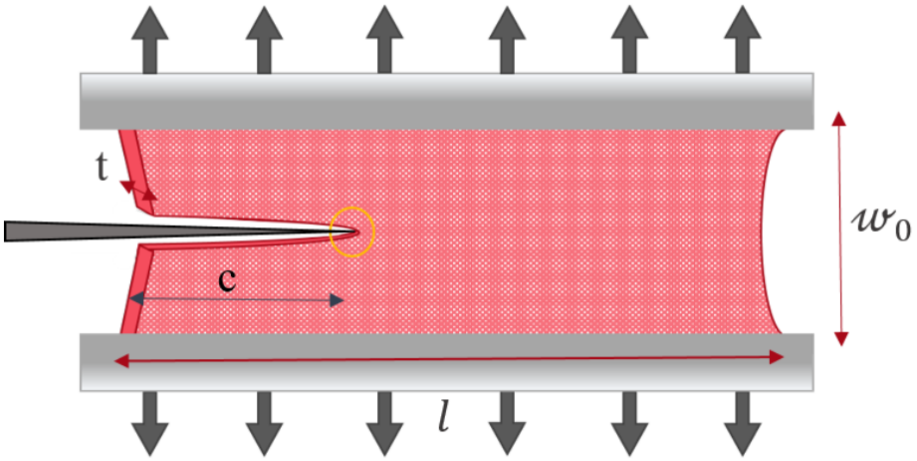

Figure 2.6: Cutting with a pure-shear geometry. The sample is characterized by length l, width w_0, thickness t, and crack length c.

In this test, a rectangular specimen of the soft material is prepared with dimensions that ensure shear deformation predominates over other deformation modes. The specimen is subjected to a uniform shear stress, typically achieved through specialized fixtures that apply shear forces while minimizing bending and axial stresses. The deformation and fracture processes are monitored using techniques such as strain gauges, digital image correlation (DIC), or other advanced measurement methods, enabling detailed analysis of strain distribution and failure mechanisms.

Although the pure shear test was initially developed for studying the cutting of rubber materials, much of the research has shifted toward examining fracture propagation [21, 22, 23]. This shift is due to the importance of understanding how materials behave under stress, predicting potential failure modes, and improving material designs to enhance durability and resilience. Fracture propagation studies often focus on crack growth in soft materials under varying stretch ratios. These studies have shown that as the stretch ratio increases, the crack tip shape transitions from a parabolic to a wedge-like form, which is indicative of dynamic crack growth, even at lower speeds [24, 25, 26]. When the stretch ratio exceeds 2 (Fig.2.7), the material exhibits out-of-plane displacements and buckling, significantly affecting crack propagation behavior.

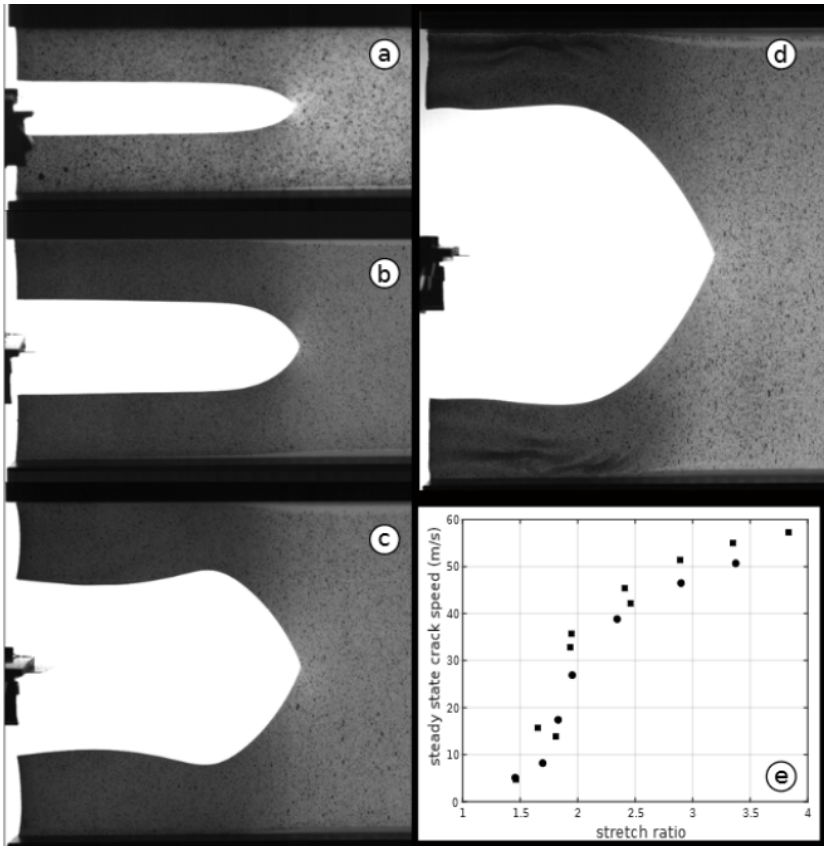

Figure 2.7: (a-d) Shape of the crack tip during steady state propagation. The initial stretch ratios are (a) 1.46, (b) 1.94, (c) 2.89 and (d) 3.84. The corresponding crack speeds are (a) 4.71, (b) 32.8, (c) 101, and (d) 175 cm/s.

2.4.3 Effect of Sharpness on Cutting Soft Materials

Sharpness is a critical parameter in cutting operations, although its precise definition remains elusive. Generally, sharpness is associated with the cross-sectional geometry of the cutting edge. Despite advancements in sharpening techniques, such as grinding, honing, and polishing, the cutting edge can never be reduced to a perfect line due to the finite size of atoms. This limitation results in a measurable thickness at the tip of the blade, often referred to as the effective radius of the nose between the sloping flanks of the tool, which is a key determinant of sharpness.

Sharpness is not solely characterized by a small included wedge angle; a thin blade

could still be blunt if its edge is truncated or rounded. However, tools with a small wedge angle generally exhibit greater sharpness. In metal-cutting tools, a balance must be struck between sharpness and durability. These tools often have large included angles to ensure stiffness and strength, particularly under high cutting forces or impact loading. Despite appearing more robust, the sharpness of these tools can still be comparable to that of knives.

Bluntness, in contrast, introduces unique instabilities when cutting soft materials. Unlike sharp tools, which produce clean cuts, blunt objects induce a range of mechanical responses due to increased resistance and friction during the cutting process. When a blunt object cuts through soft material, significant deformation occurs before fracture, leading to various instabilities, including:

Buckle Instability: The material may buckle or warp due to uneven stress distribution.

Plastic Deformation: Extended regions of the material may undergo plastic deformation, altering its mechanical properties.

Shear Band Formation: Localized shear bands may form, acting as precursors to cracks and leading to unpredictable fracture paths.

Additionally, blunt cutting involves higher energy dissipation compared to sharp cutting.

The sharpness of a blade significantly influences cutting operations, particularly when the edge is in constant contact with the material. In cutting soft materials or food, sharp blades concentrate stresses and strains at the tip, leading to localized deformation and eventual material separation. Sharp blades facilitate smooth and precise cuts, reducing the required force and minimizing damage to the material. This underscores the importance of sharpness in achieving efficient, clean, and effective cuts, which is essential in both industrial food processing and surgical applications.

The pursuit of optimal sharpness aims to minimize energy loss during cutting operations. Atkins' research highlights this objective. McCarthy et al.[27] critiqued existing sharpness evaluation methods and developed the Blade Sharpness Index (BSI), a dimensionless measure that relates the energy required to initiate a cut to the product of cut initiation depth, thickness, and fracture toughness of the material. The BSI provides a standardized, objective measure of sharpness, with BSI = 0 indicating ideal sharpness. This index has been

tested on thin sheets of polymer materials, such as polyurethane and silicone, demonstrating its applicability to surgical tools.

$$\mathrm{BSI} = \frac{W_{\mathrm{CI}}}{\mathrm{CI} \times x}$$

Further studies [28] using finite element models showed that increases in blade tip radius and wedge angle significantly raise the BSI, indicating decreased sharpness. This research also highlighted practical challenges, such as buckling and wrinkling of materials when using blunted blades. While the BSI offers a theoretical framework for evaluating knife sharpness, it has limitations in continuous industrial food processing, where blade stability and wear resistance are crucial.

The Blade Sharpness Index is particularly suited for characterizing blades in food processing, being independent of cutting velocity and wedge angle, and primarily depending on the blade tip radius. CI and FCI provide measures of sharpness equivalent to the BSI for specific substrates and velocities. However, BSI alone may not suffice to evaluate cutting performance in all applications, particularly due to the viscoelastic behavior of some materials. Future research should explore the effects of high cutting velocities on differently blunted blades to better understand and predict cutting performance in various contexts.

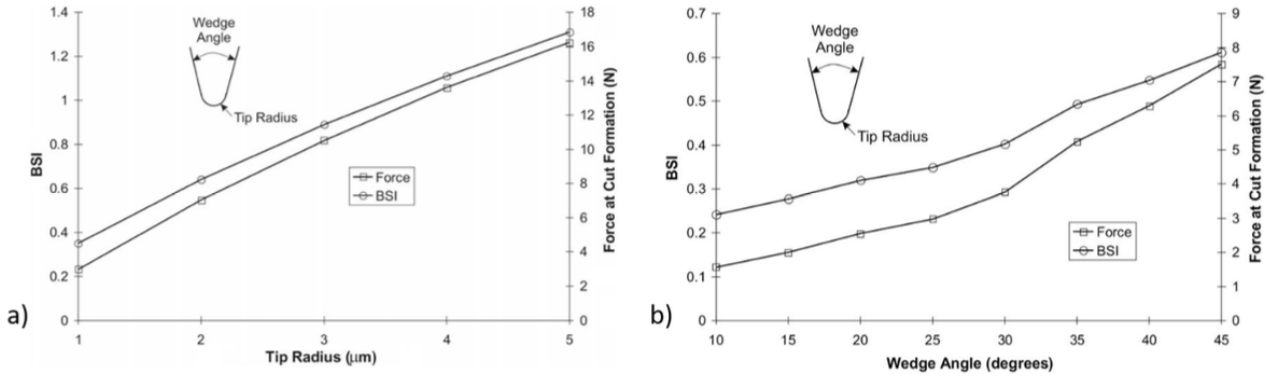

Figure 2.8: Blade sharpness index (BSI) as a function of (a) blade tip radius and (b) blade wedge angle [28].

In many applications involving soft materials [29, 30], such as food processing, blade

sharpness significantly affects cutting forces and parameters, particularly when the fracture energy substantially contributes to the total cutting energy. Blade sharpness is crucial for achieving efficient cuts, as it influences the quality of the surface finish after cutting. For isotropic materials like cheese, sharpness only partially affects the cutting forces, indicating that other factors, such as material properties and friction forces, also play a role.

Friction forces can impact the validity of the Blade Sharpness Index (BSI), suggesting that sharpness alone may not fully determine cutting performance for every application. For instance, when cutting fibrous products perpendicular to the fiber orientation, blade sharpness has a more pronounced effect on the cutting forces and parameters due to the higher contribution of fracture energy. However, for isotropic materials, the impact of sharpness is less significant, and other factors like friction become more prominent.

Recent investigations have explored how the sharpness and stiffness of blades impact the cutting process of rubber materials [27, 29]. A notable finding is the existence of a ”threshold” cutting regime that occurs when the blade tip is reduced below a certain critical length scale. In this regime, the energy required for cutting levels off, regardless of using a sharper blade. This is contrary to the usual expectation that sharper blades create higher stress concentrations and thus facilitate earlier material failure.

The specific length scale at which this transition happens is still not clearly understood. It was suggested that sharper tools may not lower the energy needed for crack propagation because they concentrate stress in a very small volume [3]. This volume is too tiny to engage the material’s microstructural features that govern fracture. Therefore, a sufficient cutting force is necessary to expand the deformed volume to a significant level before effective cutting can proceed. Additionally, the interaction between the blade and the material at the contact point might significantly influence this process. The contact dynamics, including friction and adhesion, need further investigation to fully understand their role in the cutting regime transition.

2.5 Contact Mechanics in Cutting Soft Materials

Understanding the interaction between the blade and the cutting surface is crucial during the cutting process. On the microscopic scale, the blade's pressure alters the contact area. If the material is too soft, it can adhere to the blade entirely. This interaction needs to be visualized to better grasp the process.

In Fig.2.9, a soft material being indented by a blade is depicted, resulting in an elastic contact where the area of contact depends on the loading. This contact area is variable, influenced by friction and adhesion, and plays a significant role in the cutting process, ultimately coupling with fracture to initiate a crack. A fundamental understanding of the mechanics of contact during cutting involves comprehending how a crack is initiated [31, 32].

In the undeformed configuration of the body with no opening (Fig.2.9), crack initiation is driven by an object penetrating the material and pushing through, which literally means contact mechanics. Unlike classical contact mechanics involving flat surfaces, cutting involves a crack-opening process. The blade is inserted into the material until it reaches the bottom, then pushed, experiencing an elastic phase before the crack propagates.

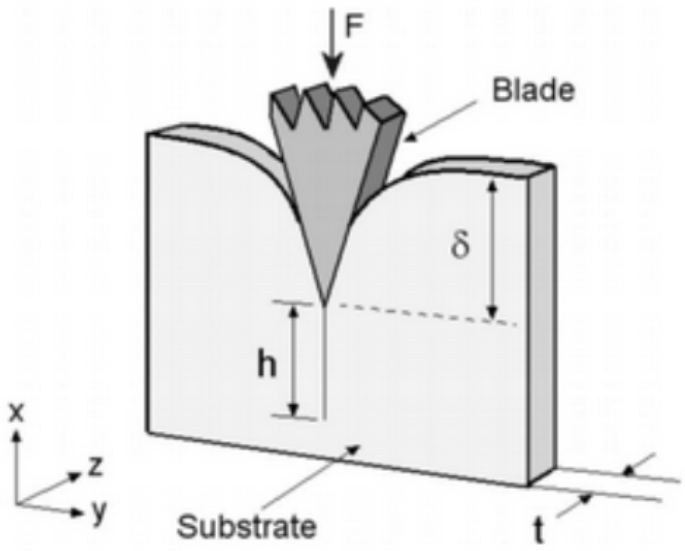

Figure 2.9: An idealization of the indentation-type cutting process [27].

This interaction leads to crack initiation and subsequent propagation within the material. Initially, the blade must overcome static friction to initiate movement. According to [27], loading curves indicate that cracks often begin before the cutting starts due to frictional stiction. This scenario resembles an indentation problem, with the transition from indentation to cutting occurring once the blade overcomes stiction. Thus, indentation mechanics significantly influence the cutting process.

In the work of [27], it was shown that after the cut initiates, the stiffness curves remain relatively constant up to a longer length than the blade displacement. This constant region represents the newly created cut surface moving over the blade's side, as shown in Fig.2.10. The stiffness curves start to decrease in this regime, indicating the onset of steady-state cutting. This phase requires stabilization as the initial cut surface fully passes over the blade and recontacts above its back, as illustrated in Fig.2.10c. After approximately double the length of blade displacement, the stiffness curves approach zero, marking the fully established steady-state cutting, where the cutting forces become constant, reaching an equilibrium state as depicted in Fig.2.10d.

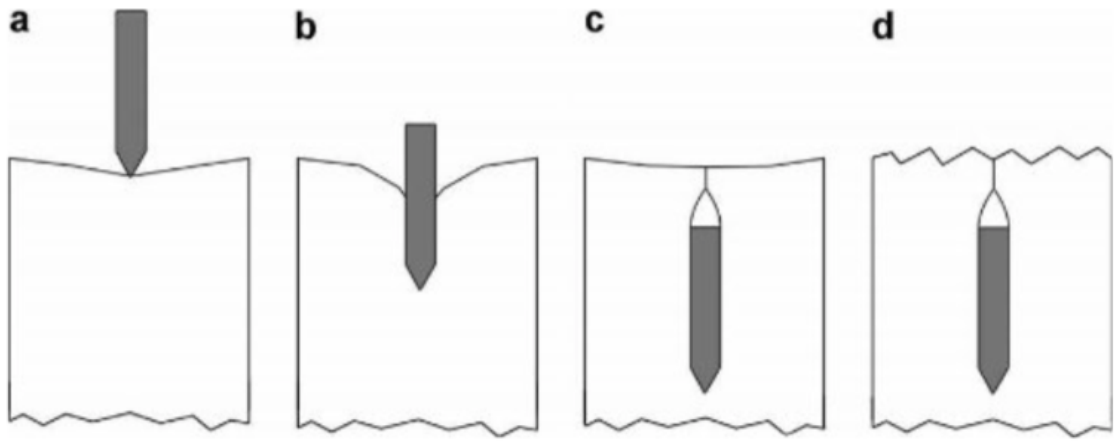

Figure 2.10: Different stages of the indentation cutting process. (a) Initial indentation at the point of cut formation. (b) Intermediate cutting where the cut material travels up the side of the blade. (c) Onset of steady-state cutting where the substrate material re-contacts above the back of the blade. (d) Steady-state cutting [27].

It is widely understood that a longer blade insertion increases resistance, implying signif-

icant energy loss due to friction during steady-state cutting. Thus, understanding the impact of friction on cutting is essential.

2.6 Effect of Friction on Cutting Soft Materials

Cutting soft materials presents unique challenges due to their deformable nature and susceptibility to frictional forces. Friction plays a pivotal role in determining both the efficiency of the cutting process and the quality of the resulting surface. A comprehensive understanding of the complex interplay between frictional forces, material properties, and cutting parameters is crucial for optimizing cutting operations and enhancing manufacturing outcomes.

Characterizing friction during the cutting of soft materials remains a challenging area of research. The inherent roughness of the blade and the soft material's tendency to maintain a real contact area close to the nominal area create conditions where Coulomb friction is imperfect. Consequently, the contact area does not strictly correspond to the nominal value, placing this scenario in a transitional frictional regime.

2.6.1 Steady-State Friction

Steady-state friction can be categorized based on the nature of the contact surface: rough contact and smooth contact.

2.6.1.1 Rough Contact

For stiff or plastic materials, Coulomb friction is both applicable and effective. The contact area between these materials is minimal due to their inherent stiffness and roughness, and it is proportional to the normal load. The real area of contact is significantly smaller than the nominal area, meaning the tangential force is also proportional to the normal load. When surface roughness is significant, contact occurs over a statistical distribution of microasperities, forming a multi-contact interface. Greenwood and Williamson's model [33] suggests that the real contact area is much smaller than the apparent contact area and is

proportional to the applied load, thereby justifying Coulomb's friction law in rough contacts.

Grosch [34] and Persson [35] further explained that friction in rough contacts primarily arises from viscoelastic losses at the micro-asperity scale. Nguyen et al. [36] observed that shear stress in rough contacts saturates at high pressures, leading to a plateau in the shear stress distribution. This indicates non-linear behavior where frictional force becomes pressure-independent at high contact pressures.

However, with very soft materials, a competition exists between Young's modulus and surface roughness. If the roughness is low, even a Young's modulus in the MPa range can classify a material as soft. In these materials, spontaneous contact occurs across the surface, akin to wetting, leading to a saturated contact area. Applying force does not change the contact area, resulting in constant stress as the nominal and real contact areas become equal. Here, friction depends on the total contact area rather than the normal force.

When roughness is smaller than a nanometer, materials tend to deform rather than adhere during contact. When roughness exceeds a millimeter, materials resist deformation, and roughness persists, leading to adhesion. For roughness scales between these extremes, erratic behavior can occur, influenced by specific material properties and the details of the frictional experiment.

2.6.1.2 Smooth Contact

In smooth contact conditions, frictional behavior is influenced by molecular-level interactions between the blade and the material. Vorvolakos and Chaudhury [37] observed that shear stress between smooth PDMS and a SAM-covered Si wafer varies with velocity and temperature. In this scenario, friction can be described by Schallamach's molecular model, where interfacial sliding involves the formation and breakage of molecular bonds [38].

Chateauminois and Fretigny [39] demonstrated that the shear stress distribution within a smooth contact area remains nearly constant and independent of the applied pressure, indicating a non-Coulomb frictional behavior. This finding highlights that, for smooth contacts, friction primarily depends on the molecular interactions at the interface rather than on the macroscopic contact pressure.

2.6.2 Unsteady-State Friction

Unsteady-state friction involves phenomena such as stick-slip and stiction, which significantly affect the cutting process of soft materials.

2.6.2.1 Stick-Slip Phenomenon

Stick-slip occurs when there are oscillations in the sliding friction force, characterized by alternating stick and slip phases. This phenomenon can be modeled using a mass-spring system, where the transition between stick and slip is influenced by the system dynamics and the local friction law [40]. The friction force oscillates due to the dynamic interaction between the applied load and the system's inertia.

By imposing the dynamic equilibrium of the system during sliding,

$$m\frac{d^2x}{dt^2} - F_d = -kx$$

and the boundary conditions, the displacement of the body during stick-slip is found to be:

$$x(t) \approx \left[\frac{(F_s - F_d)\cos(\omega t) + F_d}{k}\right]$$

where F_s is the static friction force measured before sliding, F_d is the dynamic friction force during sliding (assumed to be constant with velocity in the first approximation), and ω is the characteristic frequency of the system defined as $\omega = \sqrt{\frac{k}{m}}$. The characteristic time can also be defined as $T_i = \frac{2\pi}{\omega}$ as the slip period. The model described above is an oversimplification, as it assumes a constant dynamic force as a function of sliding velocity. Furthermore, the transition between stick and slip is assumed to be instantaneous, which experimental observations have shown to be inaccurate. Sliding heterogeneities appear within the contact area during the transition from static to dynamic situations, a phenomenon referred to as stiction.

2.6.2.2 Stiction

Stiction refers to the transition from rest to steady sliding and involves sliding heterogeneities within the contact area. This phenomenon is characterized by a division of the contact area into a slip zone and a stuck zone, as first theoretically addressed by Cattaneo and Mindlin (Fig.2.11) [41]. The friction force is proportional to the applied normal load, with slip occurring wherever the shear stress q reaches μp, where μ is the friction coefficient and p is the local pressure originating from the applied normal load. The adhesive zone remains limited by a circumference concentric to the initial area of contact at equilibrium. The slip zone is positioned adjacent to the edge of the contact area and ends at the boundary of the stuck zone. This slip zone increases over time while the stuck zone shrinks, relaxing the stress singularity at the edge of the contact area. This process continues until slip invades the entire contact area, initiating gross sliding.

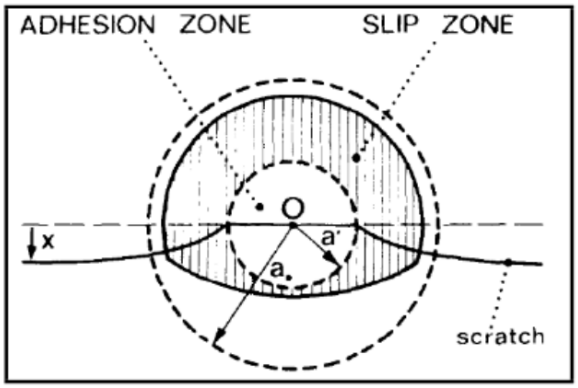

Figure 2.11: Contact area during stiction, showing slip and stuck zones as per the Cattaneo-Mindlin model [41].

Scheibert et al. [42] demonstrated that in rough contacts, stiction involves complex displacement fields that deviate from the classical Cattaneo-Mindlin model due to the finite compliance of the interface.

Characterizing friction during the cutting of soft materials remains a challenging area of research. The inherent roughness of the blade and the soft material's tendency to maintain a real contact area close to the nominal area create a situation where Coulomb friction is

imperfect. This places the cutting process in a transitional frictional regime. Studies reveal that frictional forces during the cutting of soft materials, akin to the interaction between silicone rubber and rigid probes, exhibit a unique stretch-dependence phenomenon [43]. This implies that frictional forces can vary with the material's deformation under cutting forces. As the material stretches or deforms under the cutting tool, frictional resistance at the tool-material interface may intensify.

2.7 Morphogenesis in Soft Materials

Morphogenesis refers to the process by which patterns and shapes are formed in materials, a phenomenon that becomes particularly intriguing in soft materials due to their ability to experience large deformations and nonlinear responses to external forces or environmental changes. In soft materials such as elastomers, gels, and biological tissues, morphogenesis is often driven by their inherent softness and capacity to undergo significant deformations. This nonlinearity, coupled with the material's ability to sustain large strains, enables the generation of complex shapes and structures that are not observed in stiffer materials.

The nonlinearity in soft materials is not only a consequence of their material properties but also a key factor in the formation of diverse morphologies. High strains in soft materials can induce various instabilities, such as necking or bulging, creating localized regions of high stress that serve as initiation points for cracks. The high stretchability of these materials can also cause cracks to branch or form secondary cracks, further complicating the fracture process [44, 45, 46, 47]. For example, in processes like soft coring [48], the material can undergo large-scale deformations that lead to the creation of unique shapes, such as clarinet-shaped objects (Fig.2.12). These shapes emerge as the material adapts to the applied forces, and in soft materials, this adaptation often results in features such as wrinkling, folding, or creasing.

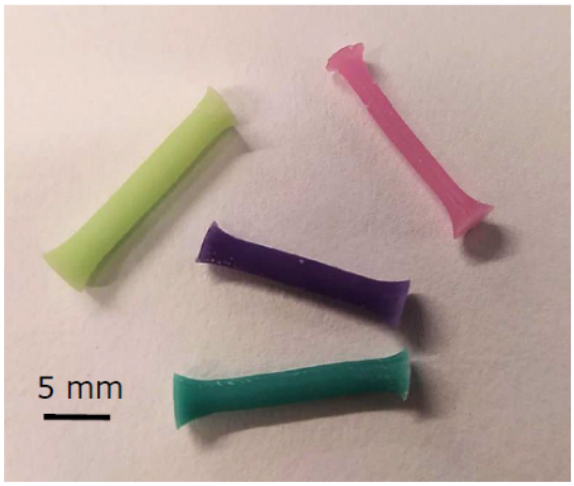

Figure 2.12: Some examples of clarinet-shaped cores obtained by cutting rubber with a cylindrical punch. In this case, the punch had a radius of 2mm, as witnessed by the similar size of the core extremities, but the core radius changes as the samples differ in stiffness [48].

Morphogenesis in soft materials can also arise not only from their nonlinear properties but from instabilities as well. When a soft material is subjected to external forces, it can reach a critical point where its response becomes unstable. This instability can manifest in various forms, depending on the geometry and boundary conditions of the material.

2.7.1 Instabilities Induced by Crack Propagation in Soft Materials

Fracture processes have been extensively studied, providing a solid foundation for understanding how materials fail under various conditions. Instabilities, such as sudden crack acceleration, oscillating crack paths, or branching, play a crucial role in predicting and controlling fracture behavior, which directly impacts the cutting of materials. Oscillations, defined as repetitive movements around a central equilibrium point, are prevalent in both natural and engineered systems. During crack propagation in soft materials, these oscillations can manifest as either stable or unstable phenomena, influencing the accuracy and effectiveness of the cutting process [49, 50, 51, 52].

Stable oscillations are characterized by the system's tendency to return to its equilib-

rium state after being perturbed. In these cases, small disturbances result in proportional responses that gradually diminish, allowing the system to revert to its original equilibrium. This damping effect ensures that deviations from the equilibrium point decrease over time, leading to predictable and bounded oscillations, bifurcations, or even fractal-like paths [53, 54, 55].

In contrast, unstable oscillations occur when small disturbances lead to exponentially increasing responses. In such systems, perturbations are amplified rather than attenuated, causing the oscillations to diverge from the equilibrium point, resulting in unpredictable and potentially uncontrollable behavior [56].

2.7.1.1 Mechanisms Driving Instabilities

The energy release rate, G, is a critical parameter in the fracture of soft materials, representing the amount of energy available for crack propagation per unit of newly created crack surface. In soft materials, G can be influenced by the material's viscoelastic properties, leading to time-dependent behaviors. Instabilities arise when fluctuations in the energy release rate occur due to changes in the material's response to stress, causing variations in crack speed and path [17].

Soft materials often exhibit nonlinear elastic behavior, meaning that the relationship between stress and strain is not linear [45]. This nonlinearity can cause the material to respond differently to stress concentrations near the crack tip, leading to instabilities in crack propagation. For instance, as the material stretches, the local stiffness around the crack tip can change, affecting the direction and speed of crack growth.

The viscoelastic nature of many soft materials adds further complexity to fracture behavior. Viscoelastic materials exhibit both elastic and viscous responses, resulting in time-dependent stress relaxation and creep. These properties can cause instabilities in crack growth as the material's resistance to crack propagation changes over time. Additionally, plastic deformation may occur in some soft materials, leading to permanent structural changes and further complicating the fracture process.

2.7.1.2 Oscillatory Crack Paths

Experimental studies have shown that cracks in soft materials can follow oscillatory paths, with the crack tip oscillating back and forth as it propagates (Fig.2.13) [57, 51, 58, 59, 60]. These oscillations can be influenced by factors such as the applied strain rate, material anisotropy, and environmental conditions. High-speed imaging techniques have revealed that these oscillations are often accompanied by dynamic changes in the stress field around the crack tip.

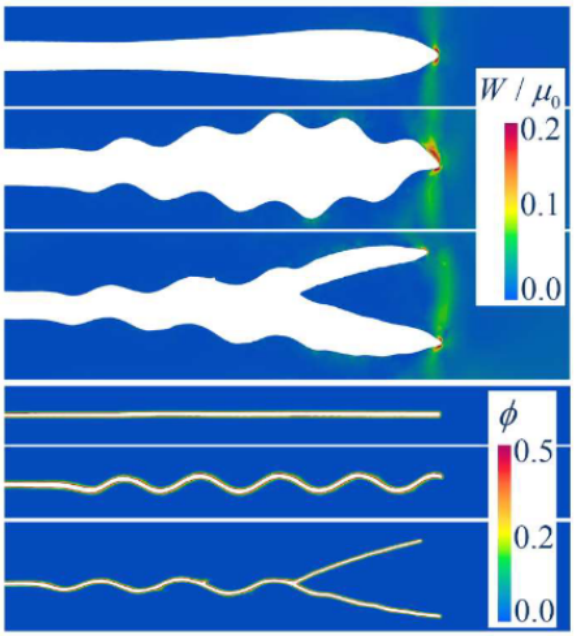

Figure 2.13: Effect of nonlinearity on crack dynamics. Three distinct crack morphologies observed in simulations: stable, oscillating, and branching cracks. The rendered colors correspond to the normalized strain energy density W/μ in the deformed (upper) and phase field ϕ in the undeformed (lower) configurations [51].

Another common observation in the fracture of soft materials is crack branching, where a single crack splits into multiple branches [47]. This phenomenon is frequently observed in materials with significant energy dissipation mechanisms, such as viscoelasticity. Secondary cracks may form parallel or perpendicular to the primary crack, adding to the complexity of the fracture process.

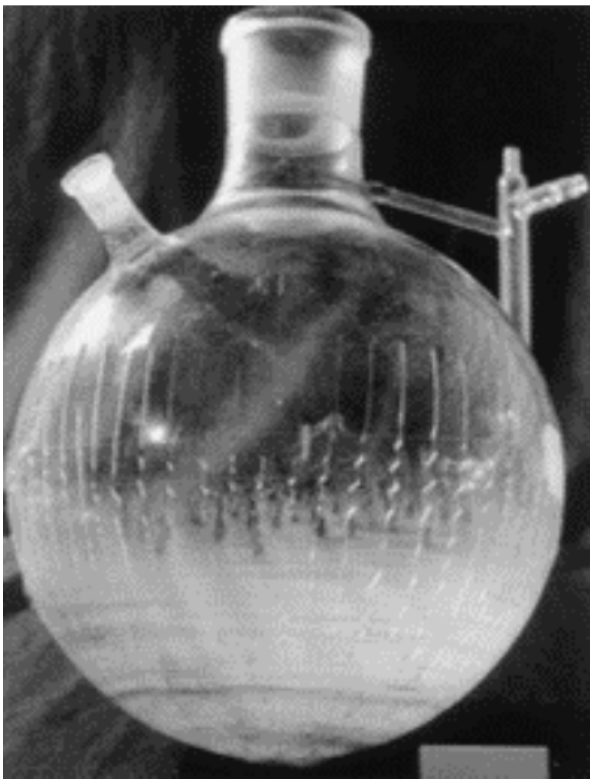

Figure 2.14: Oscillating cracks caused by differences in temperature along the length of the glass [61].

Another type of oscillatory fracture behavior involves thermocracks, which occur in materials subjected to thermal stresses arising from temperature gradients or rapid heating and cooling cycles (Fig.2.14) [61]. These cracks form when different regions of a material expand or contract unevenly, leading to internal stresses that exceed the material's fracture toughness.

Fractured surfaces of soft materials often display intricate patterns, such as ridges, waves, or more complex morphologies. These patterns can provide insights into the underlying mechanisms driving the fracture process. For instance, periodic ridges on the fracture surface may indicate oscillatory crack growth, while more chaotic patterns could suggest the presence of multiple interacting instabilities.

Fracture mechanics approaches, such as the Griffith criterion and the concept of stress intensity factors, have been adapted to study soft materials [62]. These approaches of-

fer insights into the conditions under which instabilities arise, such as the critical energy release rate necessary for crack propagation. However, the inherent nonlinearity and time-dependence of soft materials pose significant challenges for traditional fracture mechanics methods.

2.7.2 Instabilities Caused by Cutting in Soft Materials

Cutting soft materials introduces significant deformations and nonlinear behaviors under stress, leading to various instabilities during the cutting process. This section explores the different types of instabilities encountered during the cutting of soft materials and the mechanisms driving these instabilities.

2.7.2.1 Types of Instabilities in Cutting Soft Materials

One commonly observed instability during the cutting of soft materials is the formation of rough or wavy surfaces [63, 60, 53]. These surface instabilities can significantly impact the quality of the final product, making it essential to understand and control the factors contributing to their formation.

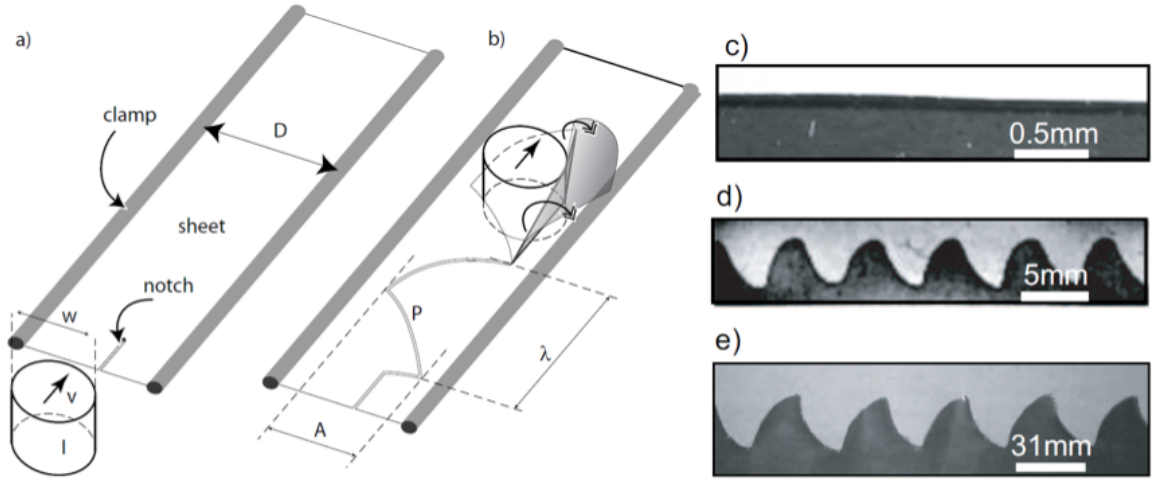

Figure 2.15: a) and b) Schematic diagram of the experimental setup. A cylindrical cutting tip is forced into a clamped thin polymer sheet with a notch, leading to an oscillatory crack path P. a) Initial configuration of the experiment. b) Typical configuration during fracture. The advance of the cutting tip through the sheet leads to out-of-plane deformations (double arrows and region in grey) along with mode III propagation at the crack tip. c–e) Edge of the sheet as seen from above (polypropylene 27µm thick) for three cutting tip widths: c) w = 0.15mm (straight path), d) w = 5mm (oscillatory path), e) w = 31mm (oscillatory path) [64].

One observed surface instability arises due to out-of-plane deformations that occur during cutting (Fig.2.15). As the cutting tool interacts with the soft material, out-of-plane motion can cause the material to bend or buckle, leading to irregular crack propagation paths. This effect is particularly pronounced when the material thickness is small compared to the size of the cutting tool, as the material tends to deform rather than resist the cutting force. These out-of-plane deformations couple with the fracture process, resulting in oscillatory crack paths, as observed in thin polymer sheets. The amplitude and wavelength of these oscillations are influenced by the width of the cutting tool and the material properties and can be highly reproducible under controlled conditions.

The sharpness of the cutting tool plays a crucial role in this process. A sharp tool ensures that cutting forces are concentrated along a well-defined edge, minimizing material deformation ahead of the crack tip. When the diameter of the cutting tool is relatively small, it reduces the tendency for out-of-plane deformations, resulting in no oscillations.

Despite significant advances in understanding the dynamics of cutting soft materials,

there remains a considerable gap in the development of comprehensive models that accurately predict cutting oscillations. While some studies have identified key factors contributing to oscillatory behavior during cutting—such as material properties, tool sharpness, and out-of-plane deformations—the complex interplay of these factors has yet to be fully captured in a predictive model.

Chapter 3

Cutting of thin elastomer sheets

3.1 Introduction

Cutting processes in soft materials present unique challenges due to their inherent properties, including high deformability, elasticity, and sensitivity to loading conditions. These factors create a complex interplay of mechanical behaviors that make the cutting process highly unpredictable. Unlike harder materials, where cutting mechanics are governed by well-established fracture and deformation models, soft materials exhibit behaviors that span ductile, brittle, and viscoelastic regimes—sometimes simultaneously. This complexity motivates the need for a specialized approach to simplify the cutting process, enabling researchers to isolate and understand the fundamental mechanics at play.

A key challenge in studying the cutting of soft materials is designing experiments that minimize extraneous variables, such as friction and irregular stress distributions, while allowing the material's intrinsic response to cutting to be observed. Such experiments are essential for advancing the theoretical understanding of cutting in soft materials and providing a foundation for optimizing industrial processes across applications, including biomedical engineering, food processing, and materials science.

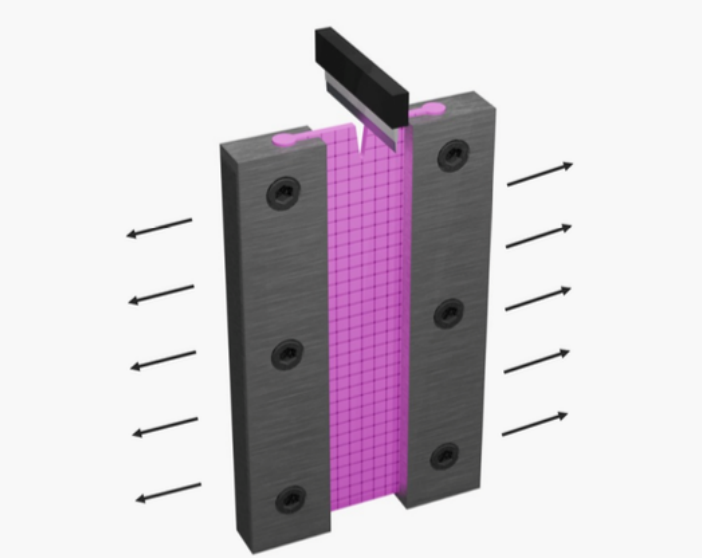

Figure 3.1: Pure-shear cutting on homogeneously stretched elastomer.

Inspired by the pioneering work of Lake and Yeoh [65], this study builds on their methodology by focusing on pure shear cutting as an experimental configuration. Lake and Yeoh demonstrated the importance of controlled cutting experiments, particularly in isolating the effects of fracture toughness under well-defined conditions. Pure shear cutting, with its ability to control the cutting path and blade position, provides a robust framework for observing the behavior of elastic materials during cutting.

The primary objective of this study is to explore the relationship between fracture toughness and propagation in cutting soft materials. This requires setting up experiments to minimize friction during cutting and to combine the stretching of samples with cutting in variable amounts (Fig.3.1). By refining the experimental setup and focusing on pure shear cutting, we aim to capture the interplay between elasticity and fracture toughness. This allows us to investigate critical factors, such as crack propagation, material deformation, and the influence of cutting parameters, which are essential for predicting cutting outcomes in soft elastic materials.

Elastomers were selected as the test material due to their widespread industrial use and mechanical properties, which make them ideal for exploring cutting mechanics. Elastomers are integral to various industries, including automotive, aerospace, and medical sectors,

where precision cutting is essential for manufacturing products such as seals, gaskets, and implants. Gaining insights into their cutting behavior can lead to improved manufacturing processes, reduced waste, and enhanced product performance.

This chapter aims to examine how cutting affects material toughness, control blade sharpness, and experimentally optimize the cutting setup. We measure fracture alone, compare it with fracture combined with cutting in varying amounts, and investigate the influence of geometrical parameters and blade sharpness. These investigations are crucial for understanding the mechanics of cutting soft elastic materials and developing predictive models for industrial applications.

Our experimental configuration was designed to study straight crack propagation under dual loading conditions, which were expected to favor a straight propagation path. However, it revealed instabilities. Predicting the crack path is challenging, especially when considering the instabilities that form regular patterns on surfaces after crack propagation. Therefore, the second part of this work focuses on the morphology of surfaces after cutting. Understanding what happens to the material involves predicting how and where one or multiple crack tips will propagate. This understanding is crucial in cutting material research and poses a significant challenge in the field of fracture mechanics, fundamentally tied to understanding material separation mechanisms [66, 67, 68, 69]. The second part of this chapter addresses how we deal with instabilities that perturb straight crack propagation. Specifically, we observed two types of instabilities: out-of-plane wrinkling and in-plane oscillations. We attempt to explain these in-plane oscillations by drawing analogies with other oscillatory phenomena observed in cutting or thermal oscillations.

3.2 Materials

3.2.1 Material characterization

In our study, commercial polydimethylsiloxane (PDMS) silicones obtained from Zhermack, specifically Double Elite and Ecoflex 0010. These silicones are supplied in both base and catalyst forms and are primarily intended for dental model replication applications. The

Shore A hardness of these materials ranges from 8 to 32, as detailed in table 3.1. These materials were chosen for their high elasticity. The chosen materials span a wide range of Shore A hardness values, which correspond to different Young's modulus values.

The materials were labeled by Shore hardness and color. Although we primarily use Young's modulus in our work.

	Shore A	Mixing time, s	Crosslinking time, min	Young's Modulus, kPa
E8(pink)	8	30	15	276
E16(violet)	16	30	20	559
E22(dark green)	22	45	20	709
E32(green)	32	45	20	938
Ecoflex (transparent)	0	30	30	94

Table 3.1: Mechanical properties of materials used in the experimental part.

The manufacturing process of the samples involved mixing the liquid base component with its corresponding crosslinker in equal proportions. This method ensures uniformity and consistency in the resulting elastomeric materials. All samples were prepared with a length of 100 mm, a width of 35 mm, and a thickness of 3 mm. The samples have cylindrical parts on the borders, which are fitted to the clamps to provide homogeneous stretching with applied strain. For certain experiments, the sample width was varied from 20 mm to 35 mm, and the thickness was adjusted from 1 mm to 3 mm.

The strain hardening behavior of the elastomers (Fig.3.3) was evaluated using a standard uniaxial tensile test, the results of which are presented in the corresponding (Fig.3.2). According to a custom model developed by Ciccotti and Lechenault [48], the behavior of elastomers under strain can be effectively described.

$$\frac{dW}{dI_1} = \frac{E}{6(1+a)}\left(1 + \frac{a}{1+b(I_1-3)^c}\right)$$

where $W(I_1)$ is the elastic energy potential, and E, a, b, and c are the material's parameters obtained by fitting the uniaxial curves. However, for applied strains less than 40%, the Neo-Hookean potential provides an accurate description of the elastomeric behavior.

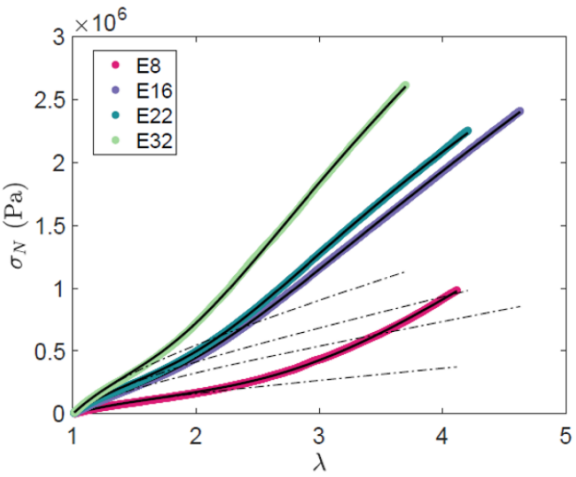

Figure 3.2: Uniaxial extension curves (nominal stress against stretch) for the four elastomers, and the corresponding fit with custom equation (lines), as well as with Neo-Hookean law (dash-dot).

The mixture solidifies within a time frame ranging from 20 to 180 minutes, depending on environmental conditions, at a standard room temperature of 20 ℃, in molds with the specified dimensions detailed in table 3.1. The corresponding elastic moduli are also reported in table 3.1. The hardness is provided on the Shore A scale. Shore hardness is quantitatively related to Young's modulus [70].

Figure 3.3: Sample shapes with corresponding Young's modulus.

3.2.2 Blades processing

Blade sharpness was assessed through three key parameters, as depicted in Fig.3.4: the radius of curvature, the angle of the blade, and the thickness of the wider section of the

blade. Each blade underwent characterization using scanning electron microscopy (SEM), enabling the acquisition of distinctive attributes such as tip curvature, tapering angle, blade width, and length.

To measure and control these three parameters, we utilized a Tormek T-8 sharpening machine and learned the technique for precise control. The shapes of the blades were chosen as optimal for cutting elastomer sheets with the dimensions we worked with. If the angle is too small, the blade becomes too brittle. Therefore, studying and presenting the optimal blade shapes was necessary. While we intended to add data on blade degradation during cutting, we did not measure this extensively.

Initially, we started with industrial blades due to their reproducibility, as sharpening is time-consuming. We changed the blade for each test to ensure consistency. However, these blades did not perform as well as expected due to variability. Consequently, we decided to fabricate our own blades. After this decision, we obtained data with processed blades, but the number of samples is limited because sharpening blades for each set of measurements is complex and time-consuming.

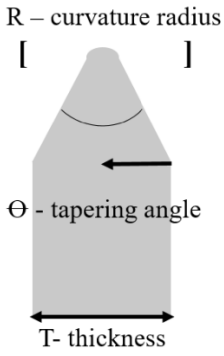

Figure 3.4: Blade Sketch with Noted Parameters for Sharpness.

The cutting procedures utilized three distinct commercially available blades, as illustrated in Fig.3.5 and table 3.2:

A paper razor blade (single-edge, steel, GEM).

A shaving razor blade (double-edge, steel, Gillette®).

A trapezoid razor blade (single-edge, steel, Martor).

For clarity, these blades will be referenced by their respective numbers henceforth.

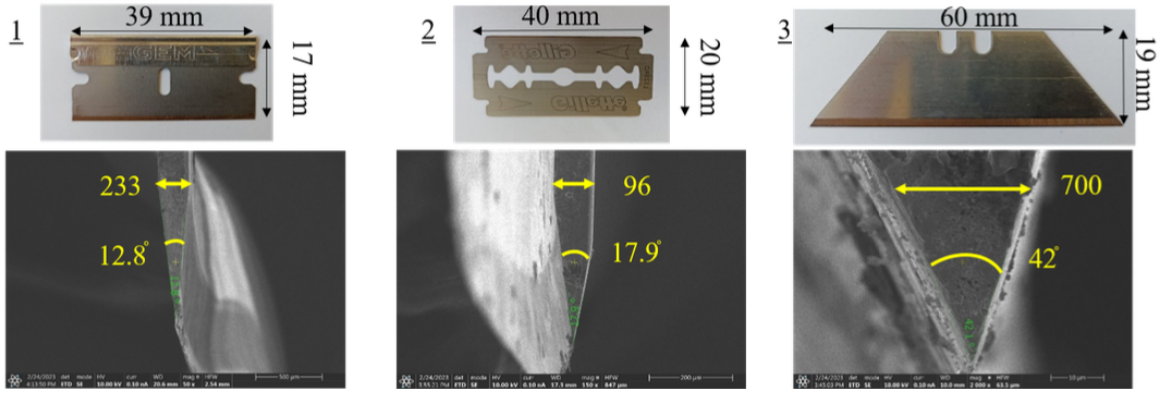

Figure 3.5: Comparison of different blades: photos and SEM measurements on tips of each blade.

	Tapering angle, °	Radius of curvature, nm	Thickness, mm
1	13	50	233
2	18	2	96
3	42	1	700

Table 3.2: Blade's characteristics.

SEM experiments revealed that the angles of commercial single-edge blades from GEM might vary within a range of 7 degrees, while for other blades, the variation was up to 5 degrees. To control the exact angles and remove large defects on the blade surfaces, they were further post-processed manually on a polishing machine, which allowed us to set any desired angle. Fig.3.6 shows the difference between the same blade before and after post-processing. The sharpening time was 1 minute per side, and the polishing time was 45 seconds per side. SEM images were provided for both the unprocessed and post-processed blades, illustrating that the blade surfaces became smoother and cleaner after processing.

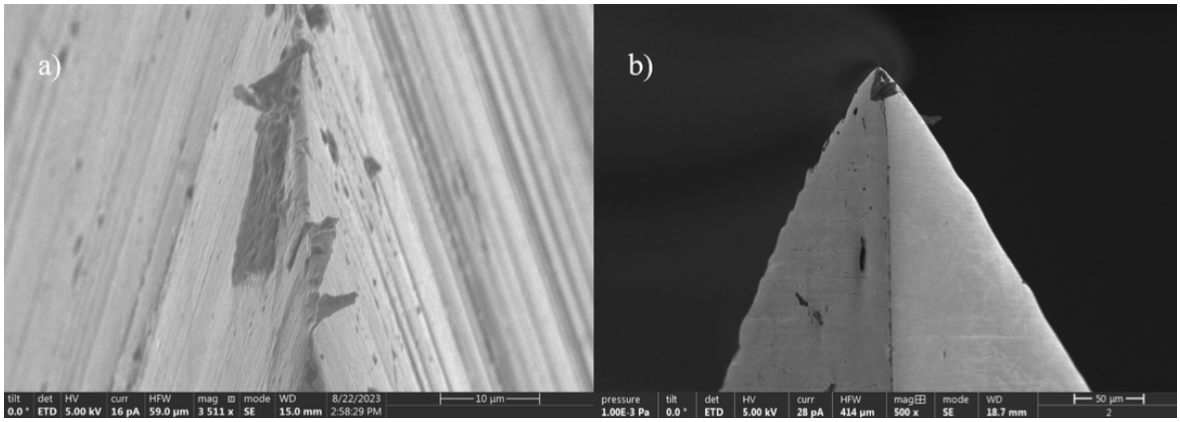

Figure 3.6: SEM measurements of Blade 1: (a) Commercial blade after post-processing (scan conducted in front of the sharp part of the blade), (b) Commercial blade before post-processing (scan performed from the side of the sharp part).

3.3 Methods

3.3.1 The cutting setup

The PDMS samples were characterized using the pure shear cutting test. The new loading fixture, designed by Ludovic Olanier in the ESPIC workshop (Fig.3.7), securely clamped the sample with a metallic holder within the Instron machine. Two clips grip the cylindrical part of the sample and secure it with screws, mechanically applying a predetermined strain. This setup allows the sample to be stretched up to 200%, with experimental stretches varying from 0% to 60%.

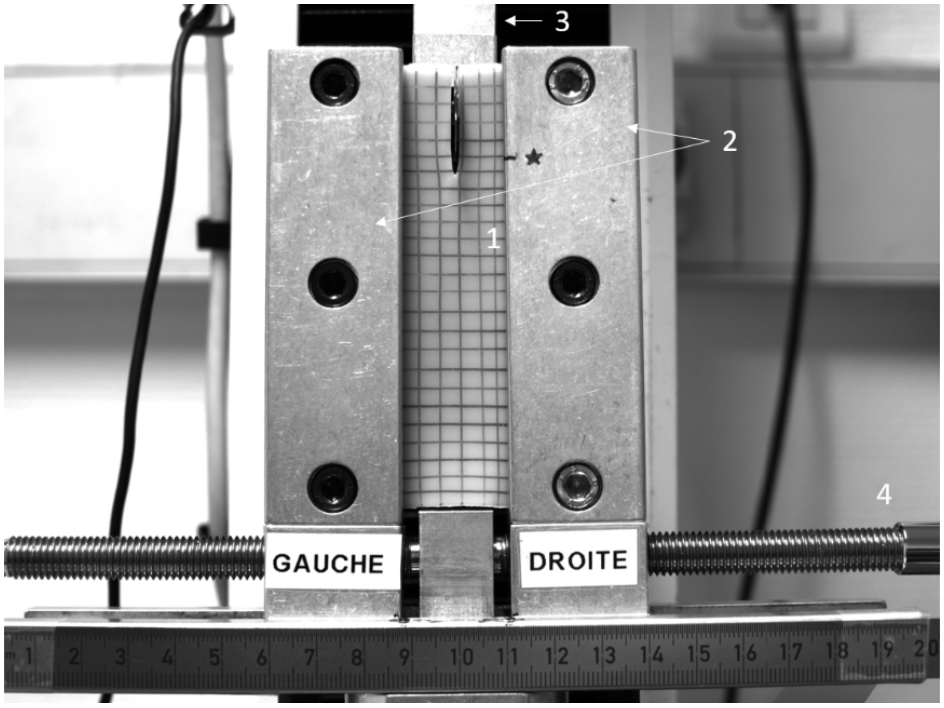

Figure 3.7: Loading fixture used for the pure shear cutting test: 1) a sample, 2) two clips grip the cylindrical part of the sample and secure it with screws, 3) blade in holder, 4) screws to move clips over it.

This custom-built experimental fixture is integrated into an Instron machine, ensuring that the blade passes through the middle of the sample width during the cutting experiment. The stretch was measured manually, while the Instron machine measured the force. The cutting edge of the blade was positioned orthogonally to the thickness of the sample. The experimental arrangement was devised to conduct cutting tests with applied stretching to the sample, minimizing friction impact on the large scale of crack rims by utilizing a razor blade. We experimentally validated that the samples were homogeneously stretched due to the geometry of the specimens.

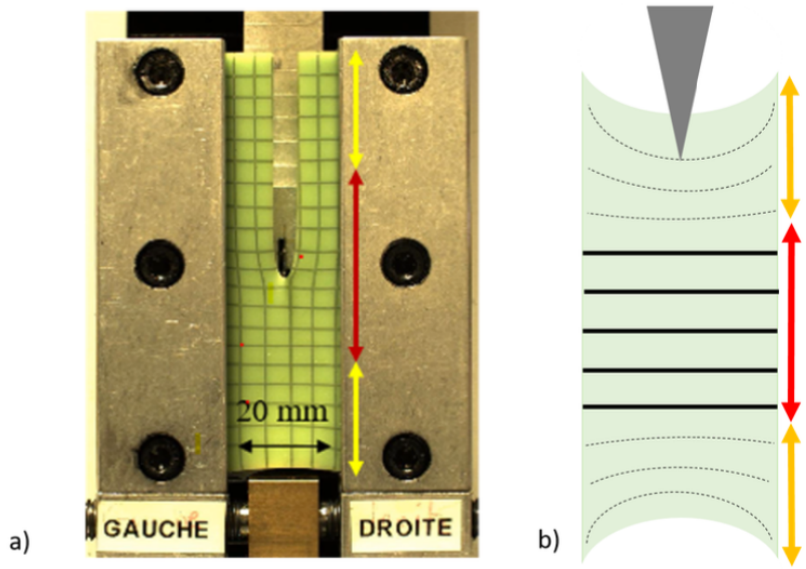

Figure 3.8: The cutting experiment of E32 was conducted at a speed of 1 mm/s under a 20% applied strain. The experimental setup included a) photo of the setup and b) schema to show the edge effect near the borders of the sample. Regions exhibiting edge effects, indicated by yellow arrows (scales like width), were excluded from each experimental measurement set. The red arrow denotes the specific region where the applied stretch is homogeneous, from which data were collected (scales like height).

When the cutting of the sample was executed, the cutting force was measured by the Instron machine load cell, which sampled at 80 points per second. This stationary load cell, with a nominal force of 100 N, had a cutting blade fixed to it. The apparatus regulates the motion of the upper grip, which drives the blade. A load sensor in series between the blade and the fixture provides the force/distance curve. Force calculations were taken in the region where there was no edge effect influence (indicated by the red arrow in Fig.3.8) and calculated as an average within this range.

Most cutting tests were carried out at a constant displacement rate of 1 mm/s ± 0.01 mm/s. It should be noted that if we apply a strain over 4%, the edges of the blade will not be in contact over the length and will become independent of the length and thickness of the blade. While there is still contact in a tapered region in the small vicinity of the crack, this allows us to neglect the friction between the rims of the crack and the large parts of the blade.

$$G_{tot} = G_{tear} + G_{cut}$$

It means we need to measure the energy stored for the pure shear test, which is why we perform it. We will provide the energy computation G.

The motion during each test examination was captured by a Baumer camera with an acquisition frequency ranging from 1 to 30 fps.

3.3.2 Measurements of fracture toughness

A tensile test was conducted to calculate the calibration of the energy density under real conditions for pure shear. During the test, the two sample holders were fixed by custom-built experimental grips on the Instron machine (Fig.3.9). Tension was applied to the sample by the moving part of the machine with a well-determined opening, where stretch was applied at a constant speed of 1 mm/s ± 0.01 mm/s to an upper grid and stopped at a certain controlled strain.

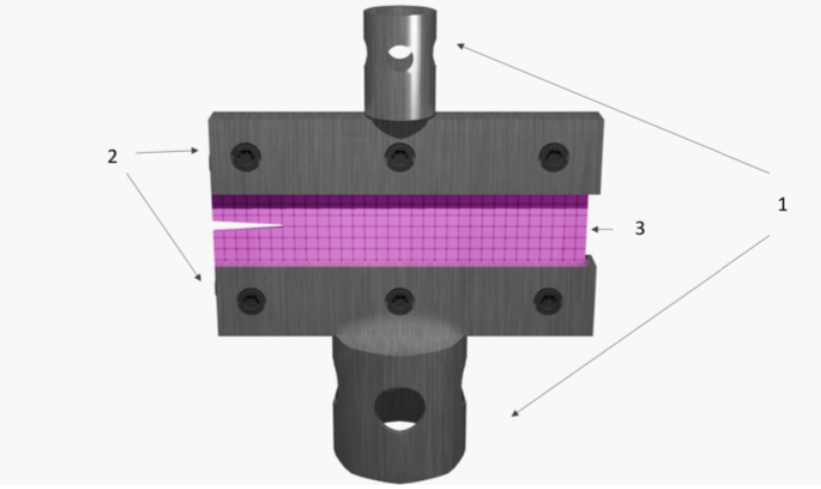

Figure 3.9: Experimental fixture of tearing test: 1) clamps to set the fixture to the Instron machine, moves only the upper part, 2) clamps that hold the sample, 3) sample.

To calculate fracture energy, changes in force during crack propagation were recorded. A camera device was used to measure the strain of a grid. Prior to the experimental tests,

a V-shaped notch was made in the center of the sample, 25 mm from the edge, to initiate crack propagation in an area with minimal edge effects.

The sample was held under the same conditions as in the cutting experiments. The Instron machine provided displacement data, while the camera measured strain.

3.3.3 Determination of Cutting Energy

As discussed in the introduction, the concept of fracture energy G_{tear} has been extended to various materials. In elastomers, Rivlin and Thomas [71] termed it tearing energy, represented as:

$$G_{tear} = \frac{\Delta U_{el}}{\Delta A} = \frac{W(\lambda) w_0 b \Delta c}{b \Delta c} = W(\lambda) w_0$$

where U_{el} - energy cost during a tearing material, A - the surface area of applied force during tearing, w_0- the width of the sample, $\lambda = 1 + \varepsilon$ - elongation of the sample, σ - Cauchy stress tensor, b- the crack width, c - crack length and the strain energy is given by Zhu [72]:

$$W(\lambda) = \int_1^{\lambda} \sigma \, d\lambda$$

Neo-Hookean 's model function is a function allowing to estimate the strain energy related to elongation:

$$W(\lambda) = \frac{\mu}{2}(I_1 - 3)$$

where I_1 is the first invariant of the Cauchy strain tensor:

$$I_1 = \lambda_1^2 + \lambda_2^2 + \lambda_3^2$$

$$\lambda_1 * \lambda_2 * \lambda_3 = 1$$

In the pure shear case $\lambda_3 = 1, \lambda_1 = \frac{1}{\lambda_2}$ Using this equation, we can determine

$$W(\lambda) = \frac{E}{6}(\lambda^2 + \frac{1}{\lambda^2} - 2)$$

$$G_{tear} = w_0 \frac{E}{6}(\lambda^2 + \frac{1}{\lambda^2} - 2)$$

Lake and Yeoh [65] introduced a pure-shear test geometry and derived a simple expression to extract the strain energy release rate following energy arguments in the cutting process:

$$G_{tot} = G_{tear} + G_{cut}$$

where

$$G_{cut} = \frac{\Delta U_w}{\Delta A}$$

, where U_w - is applied work of the blade, A - is the contact area with the blade.

$$G_{cut} = \frac{Fdx}{tdx} = \frac{F}{t}$$

, t - the thickness of a pure -shear sample.

$$G_{tot} = w_0 \frac{E}{6}(\lambda^2 + \frac{1}{\lambda^2} - 2) + \frac{F}{t}$$

3.3.4 Optical and mechanical profilometry

These methods will be used only in the second part of the chapter corresponding to morphological investigations. We used an optical profilometer, the Bruker Contour GT-K, to obtain topographical data from the surfaces of our samples after cutting, ensuring no mechanical contact was made. The working principle of this machine involves obtaining the optical path difference between light reflected from the two arms of the profilometer (reference and sample). This difference yields a spatial interference pattern (interferograms) that contains information about the surface topology of the sample. The software then processes this data to generate a 3D map of the scanned surface.

For our surface scans, we used a green light laser to scan areas of 50 mm in length with a 0.1 mm width. These scans were then stitched together. The final resolution of the scan was 1 nm. To process these measurements, we took an average of all profiles in the

horizontal direction and detrended the data afterwards.

We switched to a mechanical profilometer, the Dektak, due to its faster measurement capabilities. Mechanical profilometry differs from optical profilometry as it involves the physical contact of a microscopic tip with the surface, which moves along the sample length. The vertical movement of the tip, caused by the surface relief, is captured and amplified. The traverse unit moves the stylus along the X axis (length of the sample), perpendicular to the Z axis. The granite base serves as a reference plane and as a support for the parts to be measured. The radius of the tip is 2.5 microns, with a conical stylus (90-degree cone angle). The stylus contact force is adjustable from 10 to 400 microNewtons, allowing the instrument to measure a wide variety of materials without damaging them.

The data from both methods showed a discrepancy of no more than 5% for a set of 15 measurements.

3.4 Results and Discussions

3.4.1 Fracture toughness measurements

Tearing tests, as depicted in Fig.3.10, were conducted to obtain the fracture energy as a parameter representing the material's crack resistance for different PDMS samples.

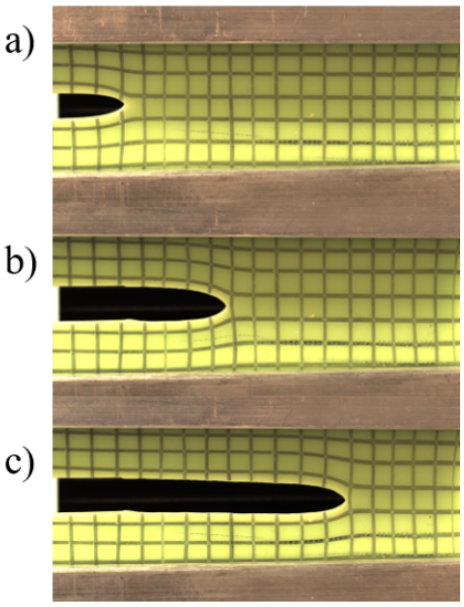

Figure 3.10: Crack propagation process during a pure shear test with 10% applied strain.

The results of these tests are presented in Fig.3.11a. It can be observed that the crack velocity increases with the applied strain.

The tests were conducted by a loading protocol: a notch is precut with a razor blade, with a length larger than the width w in order to avoid edge effect regions, with the following loading protocol, and then strain is applied as fast as possible to minimize crack propagation before reaching the target strain. We only consider the crack propagation after the stretch is fixed and measure only one velocity in this regime.

According to Griffith's crack propagation criterion, the crack propagates when the strain energy release rate equals the fracture energy of the material, which may depend on crack propagation velocity.

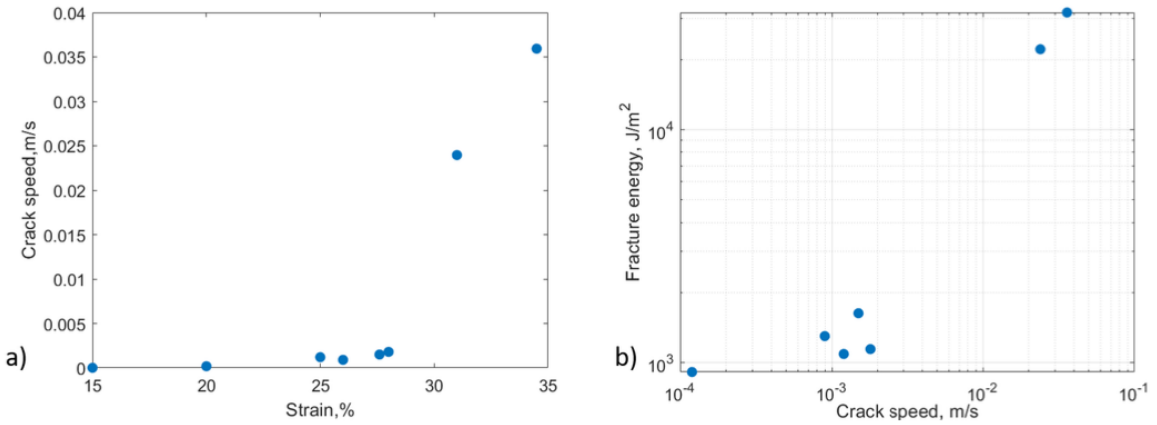

Figure 3.11: a) crack propagation speed as function of applied strain for E32 and b) fracture energy as the function of crack speed for E32.

We see that G is not a constant, but it changes with the crack propagation velocity $G = \Gamma(v)$. Even if the material is essentially elastic, we have crack propagation with a viscoelastic character. This means that for different λ, the crack propagates with different velocities, and there may be a threshold of crack propagation and a threshold for dynamic instability.

The pure shear test configuration facilitates the control of the energy release rate by adjusting the deformation imposed on the sample. Determining the curve Γ as a function of V, necessary for predicting crack growth, is considered a material parameter for a given elastomer [73]. table 3.3 presents the energy release rate corresponding to a crack propagation velocity of 1.1 $\pm$ 0.2 m/s. The strain energy release rate values were calculated using the approach outlined in the materials section.

Elastomers	$\Gamma, J/m^2$
E16	740±60
E22	750±40
E32	910±40
Ecoflex	$>$ 2200

Table 3.3: Fracture energy of different elastomers.

3.4.2 Cutting tests

The pure-shear cutting test geometry offers the advantage of studying cutting with minimal friction between the long side walls of the blade and the rims of the crack, particularly when the crack opening caused by the applied strain is larger than the blade thickness. For all of our blades, this condition was met with strains greater than 2%.

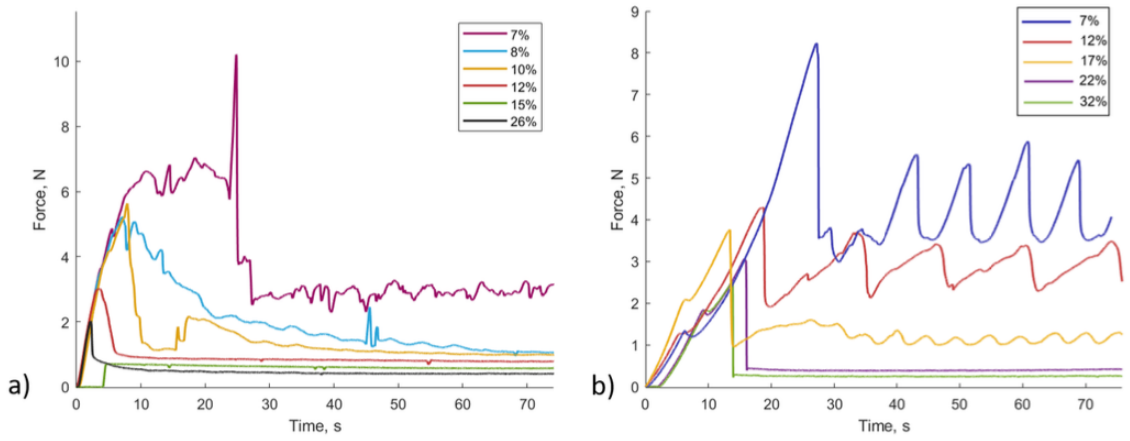

Figure 3.12: Variation of typical experimental force-displacement curves during cutting a) E32 elastomers and b) E8 elastomers by a razor blade 1 at different nominal strain with insertion velocity of 1 mm/s.

During cutting with varying applied strain, the variation of the cutting force (F_{cut}) was measured as a function of the deformation rate at an insertion velocity of 1 mm/s, with applied strain (from 0 to 50%). In each test, a prominent peak of the cutting force was

observed (Fig.3.12) corresponding to the indentation of the blade and the initiation of a crack. Subsequently, different regimes of the cut were discerned (Fig.3.12, cf. table 3.4) for the ranges specific to each material:

When the applied strain is small, sawtooth force with sharp peaks is obtained.

For a middle range of applied strains, sinusoidal-shaped force curves were obtained.

For large applied strains, the curve reached a stable plateau state.

Moreover, for the elastomer E8 with a smaller Young's modulus, stick-slip behavior was observed where the crack ran ahead of the blade during the fast phases.

The average force after the indentation peak at the beginning was used to calculate the cutting energy.

Elastomers	Small strain	Middle strain	Large strain
E8	0 - 16%	17 - 22%	$>$ 22%
E16	0 - 10%	11 - 14%	$>$ 14%
E22	0 - 7%	8 - 12%	$>$ 12%
E32	0 - 7%	8 - 11%	$>$ 11%

Table 3.4: Different regimes of the cut corresponding to applied strain.

In cases where large sawtooth force oscillations force profiles are observed, the fracture surface exhibits regular transverse striations as shown in Fig.3.18. The number of striation cycles corresponds to the number of force peaks on the cutting path. The stick-slip cycles are constituted by the alternation of "stick" phases, where the fracture does not propagate and the sample is elastically loaded progressively over time, and "slip" phases, where the crack progresses rapidly and the sample is quickly unloaded. This aspect will be discussed further in the section about the morphology of surfaces after cutting.

Lake and Yeoh demonstrated that, in the case of vulcanized rubber, within a given range of moderate strains, a negative linear dependence of tearing energy on cutting energy can be observed [65]. The sum of the strain energy release rate contributions from stretching (stored elastic energy) and cutting (work done on the blade) is constant, which is consistent with the application of the Griffith fracture propagation criterion. However, when plotting the total energy release rate as a function of stretch, we can observe three distinct regions, like

in Lake and Yeoh paper (Fig.3.13).

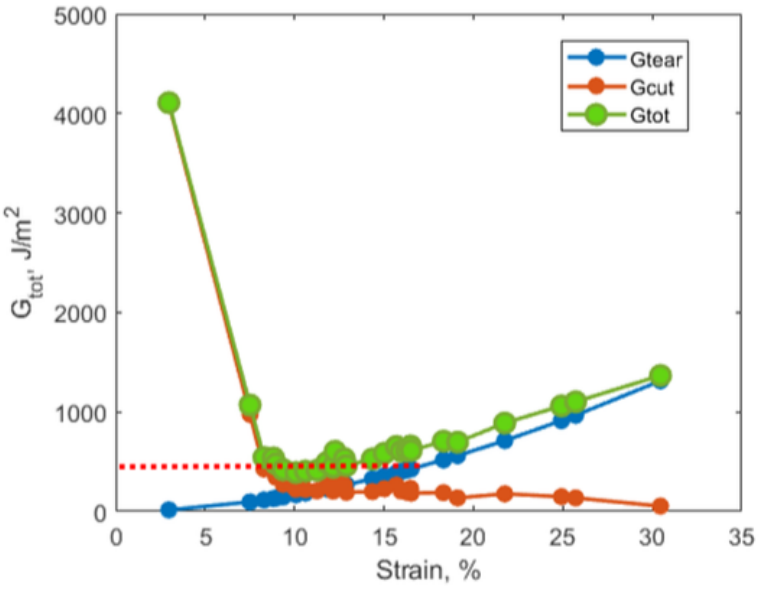

Figure 3.13: Total energy release rates expressed as the sum of cutting and tearing energies with changes of applied strain for elastomer E32.

We observed that in the strain region from 0 to 8%, the total strain energy release rate has a significant decrease with strain, followed by a plateau until 17%, where the sum of cutting and tearing energy remains constant. Subsequently, towards the end of the strain range, the total strain energy release rate slightly rises again.

In region (a) of Fig.3.14, where a small strain is applied, the applied stretch is not large enough to prevent friction on the two parallel side edges of the blade, resulting in elevated extrinsic work of friction being added to the work of cutting as argued in [48].

In region (b), the crack opening is wider due to a larger applied strain, and only the local tapered region of the blade comes into contact with the sample, thus reducing friction to the inevitable local intrinsic component, which we include in the work of cutting.

In region (c), the applied stretch keeps increasing, and we expect the friction to remain local. However, the total strain energy release rate for cutting keeps increasing with applied stretch, consistent with the observations of Lake and Yeoh. While Lake and Yeoh attributed this increase to the occurrence of stick-slip fracture, recent investigations by Donghao Zhao

have shown that the increase in the size of the blunted large strain region at the crack tip is responsible for the increase in the number of broken chains per unit area.

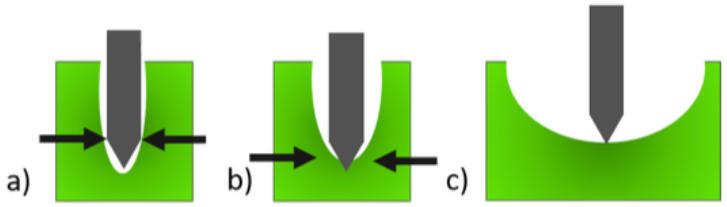

Figure 3.14: Different cutting regimes corresponding to applied strain: (a) 0% - 8% applied strain results in a significant impact of friction between the side walls of the blade and the sample due to insufficient crack opening by stretch, (b) 9% - 20% applied strain: the local tapered region of the blade contacts the sample, reducing friction to the inevitable local intrinsic component included in the work of cutting, (c) 21% and beyond: The increase in the blunted large strain region at the crack tip raises the number of broken chains per unit area, increasing the total strain energy release rate with applied stretch.

3.4.3 Variation of the Young modulus of the elastomers

To assess how the elastic modulus impacts the total energy release rate during combined stretching and cutting, we tested four different elastomers with varying Young's modulus values (table 3.1). All samples exhibited similar trends in their dependence on applied strain (Fig.3.15): significant friction impact in the small strain regions, followed by a plateau, and then a slight rise in the overall potential as discussed before. The average value of the plateaus was found to be proportional to the Young's modulus (table 3.5).

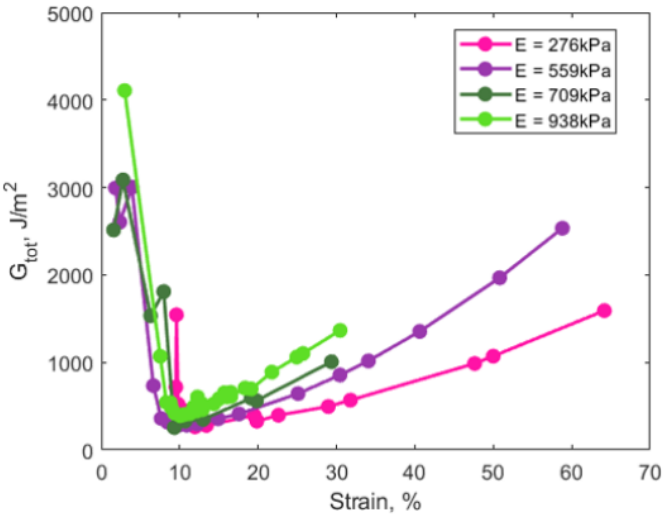

Figure 3.15: The total energy release rate, expressed as the sum of stretching and cutting contributions, is plotted as a function of the applied stretch for the four different elastomers considered in this study.

However, the cutting behavior for elastomers E22 and E32 differed in the region of high applied strain. Specifically, after 30% strain, the crack propagation rate was faster than the blade speed, leading to a loss of the force signal during the measurements.

Elastomers	1	2	3
E8	300 J/m^2	250 J/m^2	480 J/m^2
E16	300 J/m^2	270 J/m^2	500 J/m^2
E22	320 J/m^2	-	-
E32	400 J/m^2	300 J/m^2	500 J/m^2

Table 3.5: Values of total energy release rate plateaus for different elastomers as measured with three different blades named 1,2,3 and described in the Section 3.4.4.

3.4.4 Variation of the blade sharpness

To evaluate the influence of blade sharpness on the total energy release rate for combined stretching and cutting (Fig.3.16), we conducted experiments using three different blades labelled 1,2,3. The characteristics of the three blades are reported in table 3.2 in terms of the three characteristic parameters affecting sharpness: the blade thickness, the tapering

angle, the terminal edge radius. For the blades with the large thickness, region (a) is found to be larger, since larger applied stretches are required to avoid friction on the lateral walls of the blade.

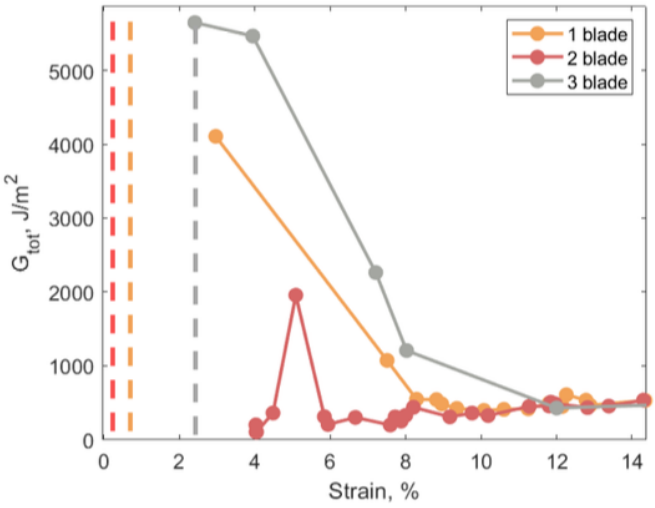

Figure 3.16: Total energy release rate with changes of applied strain for elastomer E32 by different blade types. Dashed lines correspond to thicknesses of different blades.

3.4.5 Morphology

In this study, we focus on the instabilities that arise during the combined stretching and cutting of rubbers. Two major instabilities have been identified in this system: large out-of-plane wrinkling with a sawtooth force signal, and small in-plane sinusoidal oscillations.

The first type of instability, large out-of-plane wrinkling, occurs when the blade is blunter and the applied strain is small. These wrinkles significantly affect the cutting process and the resulting material surface. The planar configuration of the sample is unstable, causing the system to move out of plane. This leads to wrinkling out instead of cutting, which increases elastic deformation and force up to a point when cutting is initiated, rapidly unloading the elastic energy and starting the same process by wrinkling on the other side.

The second type of instability, small in-plane sinusoidal oscillations, seems to occur almost always when the applied stretch exceeds a certain threshold. These oscillations are more subtle but still influence the precision and quality of the cut.

For small oscillations, the system is found to be stable with respect to out-of-plane motions, but it is found to be unstable with respect to in-plane motions of the crack front. Yet, the oscillations are small and sinusoidal, making the whole perturbation a weak oscillating perturbation of the force. The system is always cutting, with no real stick-slip, but this instability leads to an oscillation in the direction of propagation, which is the point of interest. This is not an instability of the propagation, but rather an instability of the direction.

We have observed differences in the behavior of specific samples under varying conditions. By understanding the mechanisms behind these instabilities, we aim to improve the efficiency and accuracy of cutting processes in elastomeric materials.

3.4.5.1 Out-of-plane wrinkling

Previously, it was noted that the behavior of elastomer E8 on the force curve was different compared to the other samples (fig. 3.12b), with special shapes of a sawtooth force signal. Additionally, we observed that under small applied strain, this elastomer exhibited out-of-plane motion, symmetrically repeatable as shown in Fig.3.17.

In all experiments, the blade moves downward at a constant speed of 1 mm/s. In phase (a) of Fig.3.17, the sample wrinkles out of plane, causing elastic deformation of the sample and it loads without cutting. In phase (b), it starts to cut more rapidly and unloads, while wrinkling goes back. In phase (c), we observe a symmetrical situation similar to phase (a), but the motion occurs in the opposite direction.

We suggest that the out-of-plane motion occurs due to the comparison of costs between bending and cutting in the elastic deformation of the sample. The sample on the cutting border wrinkles to its maximum extent while the energy cost of cutting becomes equal to the energy cost of bending. Then, the cutting process starts and wrinkling goes back as the material returns to its original state.

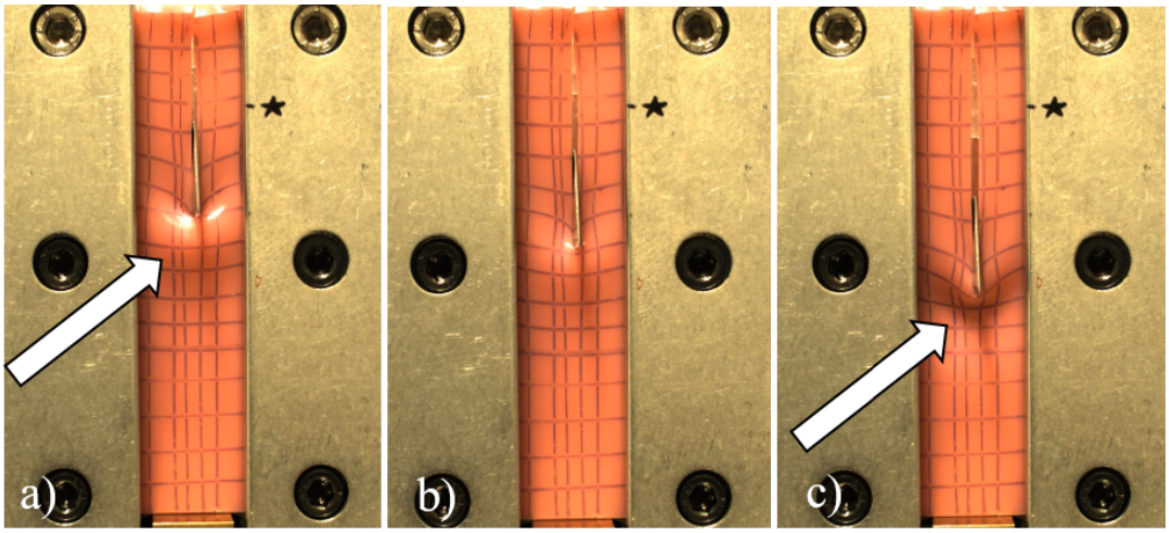

Figure 3.17: Pure-shear cutting experiment with 3% applied strain for elastomer E8 using blade 3 at a cutting speed of 1 mm/s. Arrows show different out of plane motion of the elastomer: a) sample wrinkles out of plane, b) cutting starts, wrinkling goes back, c) sample wrinkles in the opposite direction.

Our observables to study this instability are combinations of measuring the force signal, taking pictures from the side in real-time, and then analyzing images of the post-mortem fractography. We observed zigzag lines (Fig.3.18), where the spatial periodicity corresponds to the time duration of each full oscillation. The force peaks also correspond to the out-of-plane wrinkling, with the maximum of each peak linked to the maximum of the bending part.

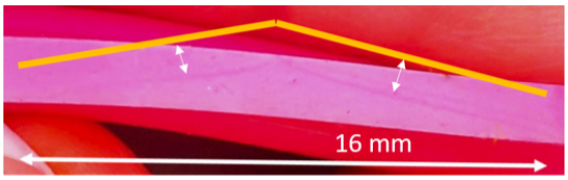

Figure 3.18: Patterns on the surface elastomer E8 with applied strain 3% after cutting by blade 3 with speed 1mm/s. The orange traces represent the average slopes, which follow patterns.

Due to defects on the blade, cutting scratches the cut surfaces, and this motion corresponds to the out-of-plane motion observed in the videos. We clearly see zig-zag patterns on the surface with a characteristic length of 16 mm for the sample (Fig.3.18).

To eliminate this instability, we decided to work with applied strains greater than 10% for this elastomer.

3.4.5.2 In-plane Sinusoidal Oscillations

First, we present the result: we see topographic oscillations on the fractography of post-mortem surfaces. This observation is original and interesting, yet we must demonstrate whether this is an intrinsic instability of the cutting process or if it originates from the machine, the blade fixture, or the bending of the blade. Below, we outline the measurements we conducted to exclude each of these hypotheses.

We initially used light deflection to observe patterns on the cut surfaces when viewed under bright light (Fig.3.19a). For samples with barely visible light deflection were used black inks to obtain those patterns (Fig.3.19b). This phenomenon occurred for all types of elastomers across almost every strain.

Figure 3.19: Patterns on the surface of elastomers a) E8 and b) E32 with an applied strain of 20% after cutting by blade 3 at a speed of 1 mm/s.

To investigate these original and interesting patterns, we must understand their origin.

In order to exclude the possibility that these patterns originated from the Instron machine, we recorded the force while freely displacing the blade without the sample. Moreover, we repeated the experiments on two different Instron machines in ESPCI and ENS. The aim is to evaluate the wavelength and amplitude of the force oscillation as a function of the material and loading parameters. Fig.3.20 shows the Fourier transformation of force signals during the blade motion without samples. The results are markedly different: without a sample, We see a flat spectrum in the region corresponding to the oscillation wavelength. The largest and most energetic peak corresponds to a wavelength of 5 mm, which is the same as the observed oscillation.

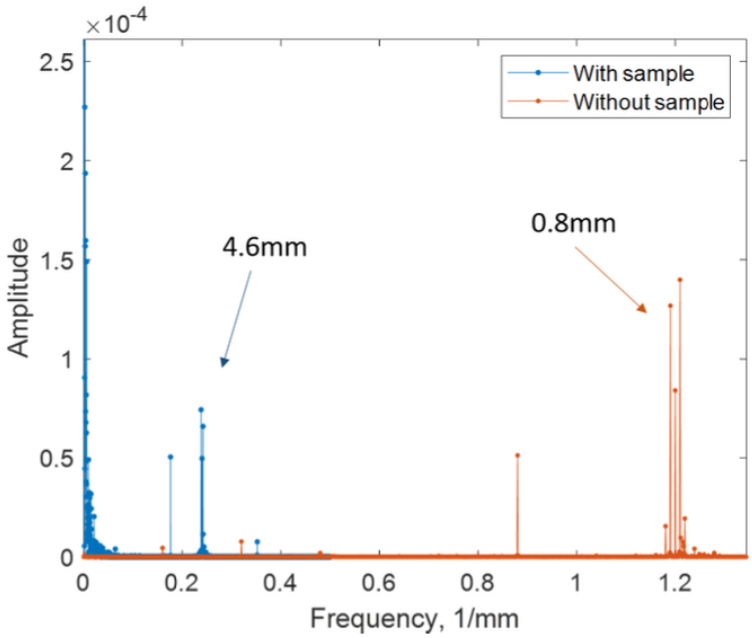

Figure 3.20: Fourier transformation of force signals during blade motion with and without a sample.

We can thus conclude that the oscillation is not originated by the Instron machine, but rather from the cutting process itself.

To investigate if these oscillations could be originated by bending of the blade during cutting, we measured blade deflection during cutting using a sensor reacting to its touch. This hypothesis was also excluded as we did not find any detectable blade displacement

during cutting.

Therefore, we can conclude that these oscillations are originated by an intrinsic phenomenon regarding combined stretching and cutting, which should be further investigated. To provide a more quantitative metrological investigation of the oscillating profiles, we used profilometry to scan topography of the oscillations over the whole length of the samples (Fig.3.21). The aim is to evaluate the wavelength and amplitude of the oscillation as a function of the material and loading parameters.

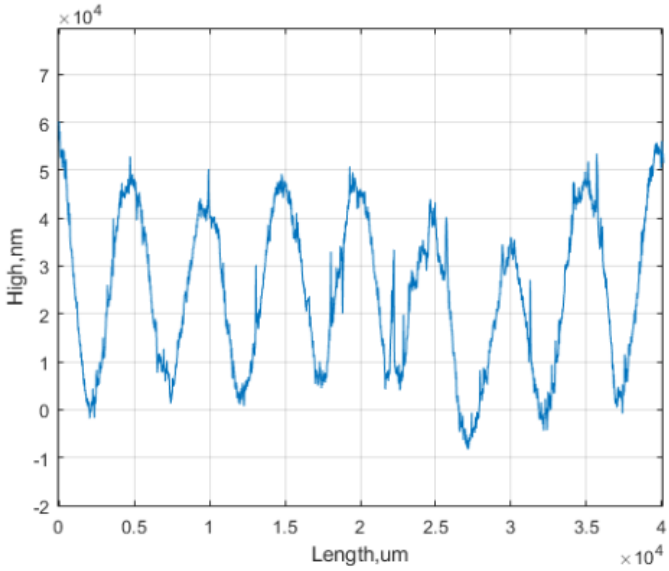

Figure 3.21: Surface scan of elastomer E16 on the applied strain 8% by mechanical profilometer.

To understand how these oscillations originated, we tested how different cutting conditions influenced them. All samples exhibited the same trend as in Fig.3.22. The amplitude is vanishing below a threshold and then increasing with applied strain while the wave-lenght in our experiments were constant 5.0 mm ± 0.4 mm with applied strain for each elastomer.

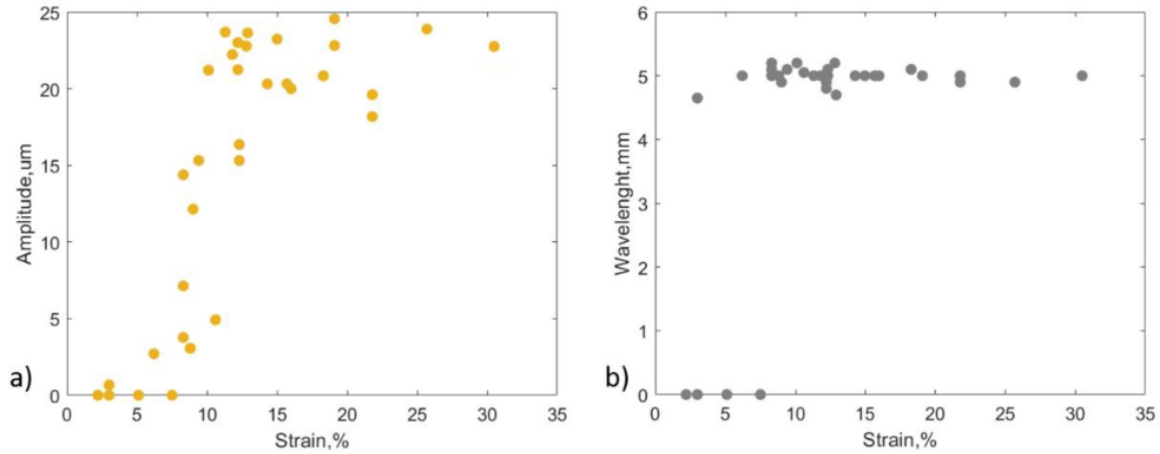

Figure 3.22: Mechanical profilometer data: a) amplitude of oscillations on the surfaces after cutting E32 with varying applied strain. A threshold indicating the appearance of oscillations after 5% of applied strain, b) wavelength of oscillations on the surfaces after cutting elastomer E32 with different applied strain.

To investigate how blade sharpness might affect the oscillations, we repeated the cutting tests for three different blades (Fig.3.23). The dependence of oscillations on the sharpness of the blade shows that for blades 1 and 2, a slight rising trend in the amplitude of the oscillations was observed with applied strain greater than 5%. However, for the third blade, the threshold for the plateau is higher compared to the first two blades. We observed the blade tapering angle and strain dependence of the amplitude of the oscillations for each elastomer table 3.6. For the wavelength of all samples, we did not find any changes with various factors.

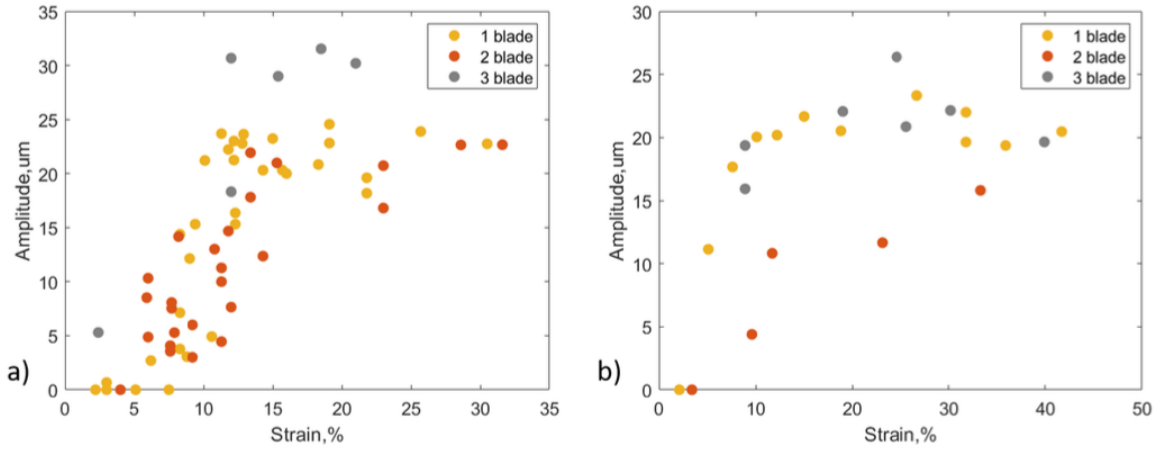

Figure 3.23: Amplitude of oscillations on the surfaces after cutting with varying applied strain for elastomers: a) E32 and b) E16.

Elastomers	1 blade	2 blade	3 blade
E8	17 μm	16 μm	20 μm
E16	20 μm	12 μm	21 μm
E22	21 μm	-	-
E32	23 μm	23 μm	30 μm

Table 3.6: Values of amplitude plateaus for different elastomers as measured with three different blades named 1,2,3 and described in the text.

Our modeling strategy aims to identify the factors that determine the scaling of the wavelength and amplitude. Therefore, we need to investigate which parameters can cause the wavelength to change. Reasonable choices include changing the thickness and width of the sample, altering the ratio between toughness and stiffness (Γ/E), as well as varying the cutting speed or blade geometry.

To determine how we could affect the wavelength in our measurements, we examined the dependence in the region from 10% to 12% applied strain, cutting at different speeds. As shown in Fig.3.24, varying the cutting speed from 0.5 to 3 times did not yield a significant change in the measured wavelength. We assume that the large scatter in the amplitude's values was due to the shifting threshold for each cutting speed, while the wavelength did not show significant changes.

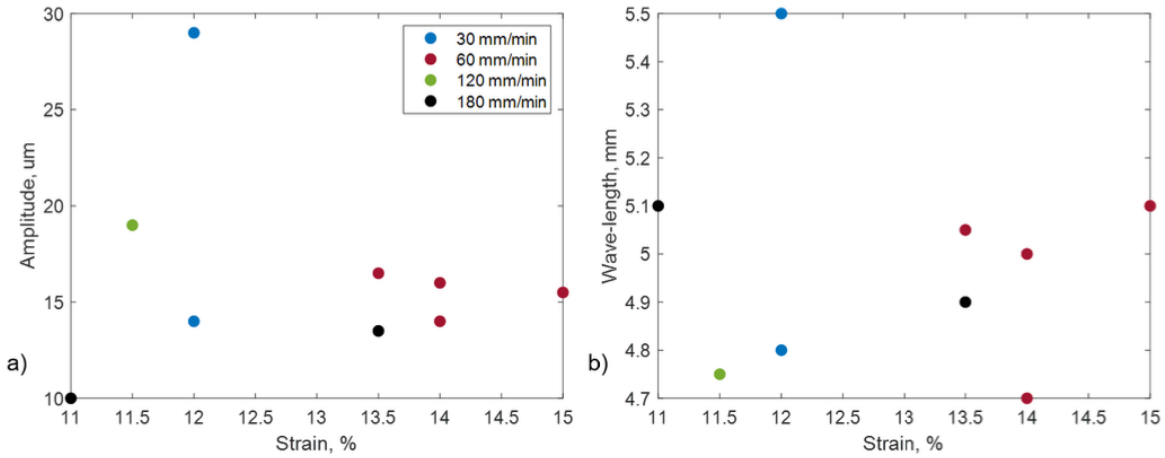

Figure 3.24: Mechanical profilometer data on the surfaces after cutting elastomer E32 with varying cutting rate: a) amplitude of oscillations , b) wavelength of oscillations.

Referring to the literature about other oscillations in fracture, we could expect changes in the wavelength of the oscillations as a result of alterations in the sample geometry during the pure shear test[64]. We changed the thickness of the samples from 3 mm to 1.5 mm (the minimum thickness we could work with in our setup). As shown in Fig.3.25, changes in geometry also did not much affect the wavelength of oscillations for our elastomers.

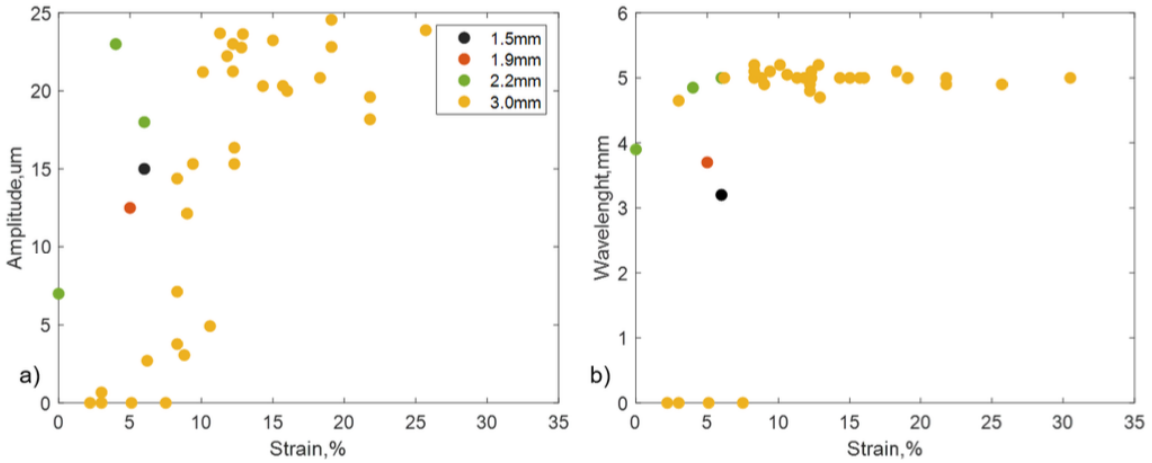

Figure 3.25: Mechanical profilometer data: a) amplitude of oscillations on the surfaces after cutting elastomer E32 with varying thicknesses of samples, b) wavelength of oscillations on the surfaces after cutting E32 with varying thicknesses of samples

Meanwhile, in our laboratory, Donghao Zhao is working with pure shear tests on synthesized PDMS samples with dimensions of 10 mm by 10 mm. Using confocal microscopy on PDMS samples with mechanophores, he observed the surface profile of the samples. Depending on the applied strain, he identified two regimes: one with no oscillations and one with a wavelength equal to 0.2 mm (Fig.3.26). This suggests that the constant wavelength observed in our measurements arises from the material properties and the geometrical conditions of the pure shear test.

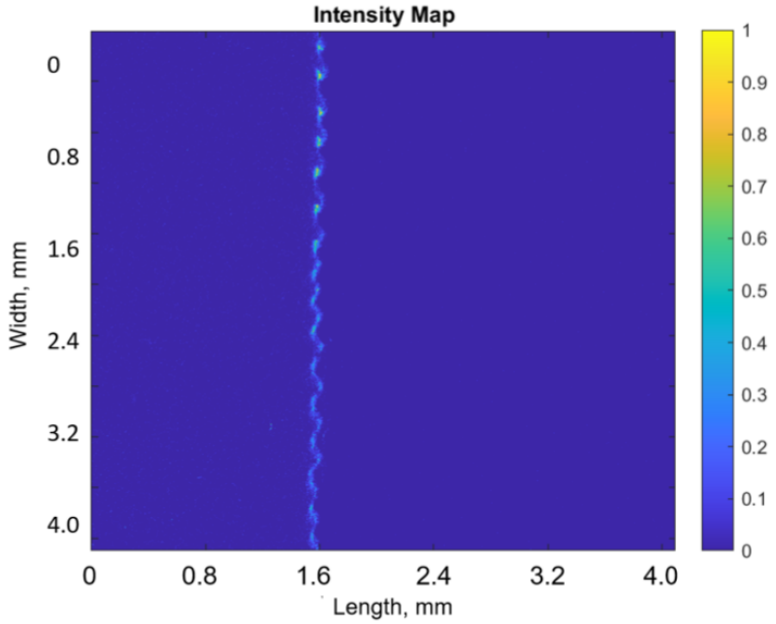

Figure 3.26: Confocal image of intensity map during cutting of PDMS with mechanophores. The colour bar corresponds to the volume density of broken bonds.

However, we can not be sure that this oscillation comes from the same instability mechanism as for our samples. For example, there could be some stick-slip dynamics, which seems to be the case, but this is close to the optical resolution.

Previously, Ciccotti and Lechenault introduced [48] the concept of the tomo-elastic length in the literature. This length is characteristic of a material's ratio between the cutting energy (that includes friction) and the elastic modulus. It provides a physical length scale below which expects to have large strains during a cutting process. When cutting chips smaller

than the tomoelastic shape, we expect to have strong morphogenetic effects. This could also drive the mechanics of this oscillation, which is related to the competition between elastic strain and cutting.

$$l = \frac{\Gamma}{E}$$

For materials from E8 to E32 this parameter typically has a scale of millimeters. Given that the amplitude of the observed oscillations during cutting with an applied strain over 5% has been found to be around 5 mm, a significant morphogenetic effect has been observed. However, the exact mechanism behind the origin of these oscillations still requires further discussion.

3.4.6 Origin of oscillating instabilities

In literature already were investigated different oscillating cracks in brittle and soft materials [74, 53, 62, 75]. To study the instabilities in this work here will be introduced different approaches to study oscillations during crack propagation:

3.4.6.1 Oscillations in Rapid Fracture

In the literature [74] was pioneered an innovative approach to exploring dynamic instabilities in brittle materials using the high strain method without pre-existing cuts. This method involves subjecting thin sheets of brittle materials, such as polyacrylamide gels, to high strain rates, driving crack propagation without the need for pre-existing notches or cuts. By avoiding pre-existing cuts, these experiments closely mimic natural fracture processes with natural initiation, allowing for the observation of dynamic phenomena that emerge only at high velocities.

It was shown that when a crack reaches a critical velocity, the crack path transitions from straight propagation to oscillatory modes (Fig.3.27). This critical velocity, approximately 0.87 times the shear wave speed (CS) of the material, marks the onset of a new dynamic instability. Below this threshold, crack dynamics can be described by linear elastic fracture

mechanics (LEFM). However, as the velocity increases and reaches the critical point, the crack path begins to oscillate in a sinusoidal pattern. These oscillations are intrinsic to the material and are independent of the sample's macroscopic dimensions, suggesting a fundamental microscopic scale governing the behavior.

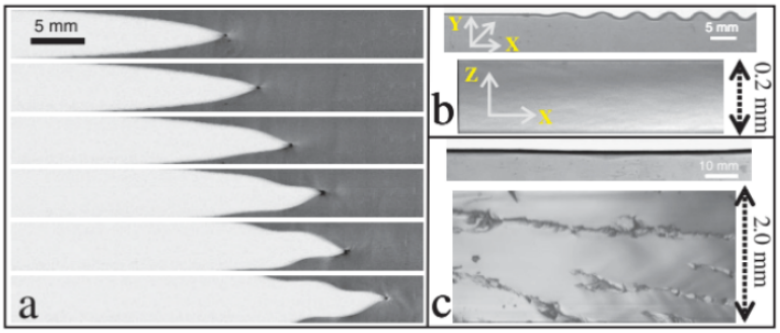

Figure 3.27: A sequence of photographs, shown at 0.69 ms intervals, of a propagating crack undergoing a transition from linear (top two pictures) to oscillatory motion. Photographs of XY profile (top) and (XZ) fracture surface (bottom) of (b) a 0.2 mm thick gel sample where oscillations developed and (c) a 2.0 mm thick gel where the crack retained its straight-line trajectory. In (c) the fracture surface is microbranch dominated, whereas in (b) the oscillating crack has a mirror surface. Propagation in (a), (b), and (c) was from left to right [74].

Fineberg's high strain method without pre-existing cuts is excellent for understanding rapid fracture dynamics and provides critical insights into how crack dynamics transition from straight propagation to oscillatory modes under rapid loading conditions. However, our instability occurs at much lower crack propagation velocity where the pure shear fracture propagation is stable. We can conclude that the reason for our instability must be related to a more complex interaction between the sample deformation and the action of the blade.

3.4.6.2 Oscillations in Thin Sheets Cut by Blunt Objects

A study by B. Roman en ect. [53])developed an insightful approach to exploring oscillating instabilities in brittle thin sheets when cut by blunt objects. This method involves driving a blunt tool through a clamped thin sheet.

The study revealed that when a critical value of a control parameter is reached, the

crack path transitions from straight propagation to oscillatory modes. This critical value, determined by the angle ψ (Fig.3.28), marks the onset of a dynamic instability. Below this threshold, the crack follows a straight path. However, as the angle increases and surpasses the critical value, the crack path begins to oscillate. These oscillations are intrinsic to the material, but their characteristics are strongly influenced by the size of the indenter, suggesting that the indenter dimensions govern the behavior.

The experiments demonstrated that the straight path becomes unstable, leading to an oscillatory pattern whose amplitude and wavelength increase with the control parameter which is the size of the cutting tool.

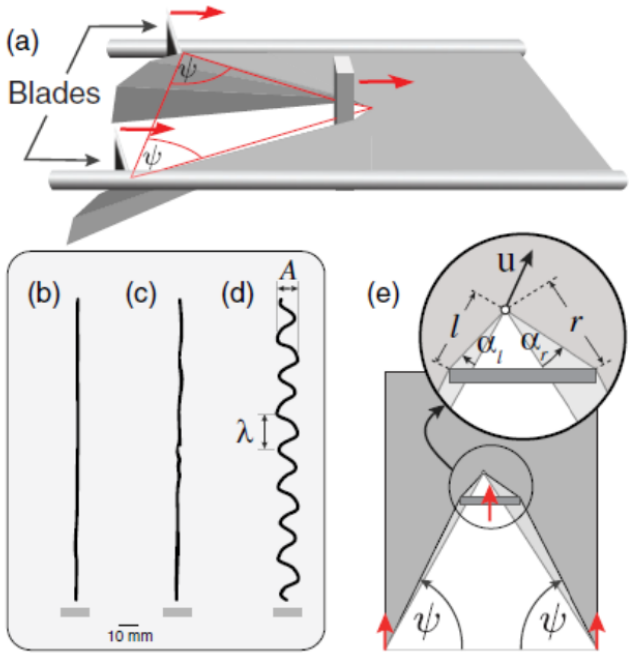

Figure 3.28: Modified setup for fixed ψ experiments. (a) Two lateral blades cut the sheet at the same speed as the tool. (b)–(d) Scanned experimental paths for different values of ψ : (b) ψ = $45°$—straight path, (c) ψ = $56°$, close to the transition—small humps, (d) ψ = $66°$—oscillating with measured amplitude (A) and wavelength (λ). Scale is the same in the three cases for comparison. (e) Geometrical parameters of the theoretical model (u is the propagation direction) [53].

This method is particularly useful for studying slow crack propagation and the detailed energy mechanics involved in the cutting process. When the tool penetrates the sheet, it

creates stresses that drive crack propagation. The energy release rate depends on the penetration angles and lengths on either side of the tool. As the tool moves, it induces periodic variations in stress, leading to a sinusoidal crack path. This dynamic instability causes the crack to alternate between different paths to release the stored elastic energy most efficiently.

However, this method does not replicate a pure shear test, as the samples are clamped rather than stretched. This difference arises because the film is stiff and not tensed; instead, the penetration of the large indenter leads to 1) the bending of some folds out of plane (with negligible energy contribution) and 2) in-plane stretching of the film due to the compression exerted by the blade.

3.4.6.3 Oscillations in thermocracks

In another example from the literature, the process of forming various morphologies during crack propagation in glass strips under thermal loading due to the slow immersion of a hot glass slab into a cold water bath (as in Fig.3.29) has been extensively documented [62, 75]. Thermal fracture, a phenomenon common in materials like glass, arises from temperature disparities that induce stress by inhomogeneous thermal dilation. For instance, in a glass strip, cracks exhibit different propagation behaviors depending on the magnitude of the temperature difference and the velocity of immersion in the cold bath. Researchers have shown that employing the Griffith criterion alongside the principle of local symmetry effectively characterizes the thermal crack propagation across different stable and oscillating regimes. Adda-Bedia et al. [62] demonstrated techniques to delineate the threshold separating these propagation regimes in glass strips. By slightly displacing a glass strip from a cold bath, they induced controlled thermal stresses, enabling the observation of distinct crack propagation behaviors (Fig.3.29).

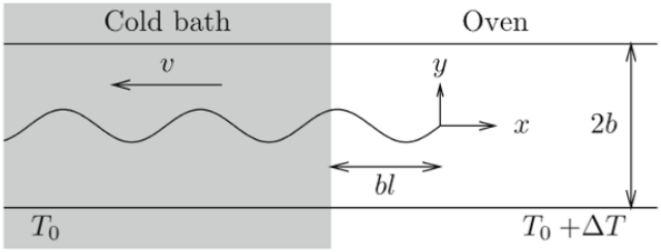

Figure 3.29: The experimental setup. A glass plate of width 2b is moved slowly at a constant velocity v from an oven maintained at temperature $T_0 + \delta T$ to a cold bath of fixed temperature T_0. The crack tip is steady in the laboratory frame (moving in the plate frame) and its position with respect to the cold bath (bl) is controlled by the temperature field [75].

They demonstrated that as long as the velocity of the plate is not too low, the temperature field, which is assumed not to be affected by the presence of the crack, can be described by the advection-diffusion equation.

$$\partial_{xx} T + P \partial_x T = 0$$

with the boundary conditions: $T(x) = 0$ in the cold bath and $T(x) = 1$ for $x \to \infty$ [76]. This approach allows for the precise control and observation of crack propagation behaviors under thermal stress conditions. The temperature field in such scenarios can be represented mathematically to predict the stress distribution and subsequent crack path in the material.

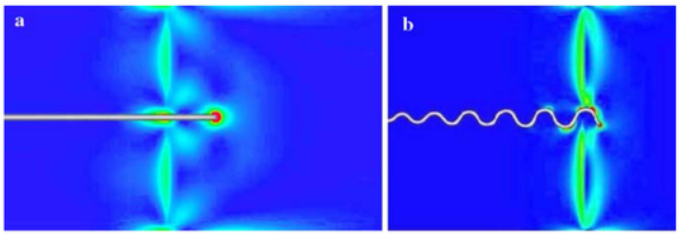

Figure 3.30: Typical crack paths obtained using the phase field model. The white region corresponds to the broken surface and the color code corresponds to the density of elastic energy in the material (red: high elastic energy density, blue: zero elastic energy). a) A straight centered propagating crack ,b) a wavy crack above the instability threshold. This picture shows that the crack width is much smaller than the wavelength of the observed oscillations [75].

Using the phase field model, they illustrate the various regimes of crack propagation, as demonstrated in the accompanying figures. This model offers a computational framework for simulating crack propagation and analyzing the associated morphological changes in materials. Through numerical simulations based on the phase field approach, researchers can visualize and characterize the behavior of cracks under different loading and environmental conditions. (Fig.3.30).

Although thermal loading seems very different from cutting, we think that this latter instabilities shares the strongest analogy with the novel oscillation observed in our combined stretching/cutting experiment. In both cases, the sample is a flat elongated slab, and the loading results in two regions with different elastic energy density ahead and behind the crack front. While in the thermal crack the change of stability was shown to be driven by the distance of the crack ahead of the thermal discontinuity, in the cutting experiment the action of the blade could have the similar role of pushing the crack front ahead of the stretching energy discontinuity. Although this analogy is very preliminary now, we are developing some more quantitative models that are very promising.

3.5 Conclusions

This chapter investigates the mechanics of cutting soft materials, with a specific focus on the interplay between stretching and fracture loading. Through detailed experimentation and analysis, several key findings have emerged:

The study identifies three distinct cutting regimes based on the applied strain. At low strains (0%-8%), friction between the blade and the crack rims significantly impacts the cutting process. At moderate strains (9%-20%), the blade tip predominantly drives the cutting, reducing frictional effects. At high strains (21% and beyond), the cutting process requires higher energy due to the increased curvature of the crack. Understanding these regimes is crucial for tailoring cutting techniques to specific material properties and desired outcomes.

The total energy release rate, which combines cutting and tearing energies, varies with applied strain and blade type. The energy plateaus observed for different types of elas-

tomers indicate a material-dependent threshold for efficient cutting. By eliminating most of the friction on the crack's sidewalls, we found that while the energy increased, the change in $\Gamma(v)$ with velocity indicated that Griffith's theory still holds, but with adjustments for velocity-dependent effects. We combined the work done by the blade with the strain energy release rate, which appears to be a suitable variable for characterizing material properties in elastic samples. The observed changes in Γ with strain suggest a coupling between fracture energy and the extent of stretching during cutting.

Applied stretching allowed us to observe and trigger directional stability in the cutting process, leading to the observed oscillations. Despite the blade's stiffness and predetermined path at a given velocity, it is the sample's deformation that generates these instabilities.

We highlight the presence of two novel instabilities observed during the combined stretching and cutting of elastomer sheets. The first instability is due to out-of-plane wrinkling during cutting, primarily observed with blunt blades or under conditions of low applied stretch. The second instability is an in-plane sinusoidal oscillation that occurs consistently when the applied stretch exceeds a threshold of around 5% strain. Profilometry measurements reveal that these patterns are consistent across different elastomer samples. The experiments demonstrate that the wavelength of these oscillations is approximately constant at 5 mm for PDMS materials from E8 to E32, attributed to the similar tomo-elastic length of these materials. This finding is critical for applications where surface finish and precision are paramount, as it provides insights into achieving the desired surface quality.

We have learned that the interplay between cutting speed, applied strain, and material properties is crucial for understanding and controlling the stability and quality of the cutting process. Although we have not yet developed a comprehensive model to describe these instabilities, our work has focused on observations that indicate these strain-induced oscillations. These findings lay the groundwork for future research and practical applications in optimizing cutting techniques.

Chapter 4

Wire-Cutting of Gelatin gels

4.1 Introduction

The study of crack propagation and directionality under combined loading conditions presents a compelling opportunity to deepen our understanding of material failure mechanics in soft materials. In earlier investigations, the cutting process was simplified by employing pure shear loading, where a blade was driven perpendicularly along a predefined path. This approach offered precise control and facilitated observations of fracture behavior. However, while insightful, such conditions would not provide answers about the blade's desired path during cutting processes in soft materials. To advance this understanding, we deliberately increase the complexity of the system by introducing mixed loading conditions that combine stretching and wire cutting.

This progression is motivated by the need to simulate conditions where cutting forces interact with pre-existing material stresses and geometrical constraints. Unlike the controlled trajectory of a blade, wire cutting introduces an additional degree of freedom, allowing the cutting tool to follow the path dictated by the material's internal stress distribution and external loading conditions. By intentionally misaligning these forces, we can create scenarios where the crack path and material behavior are not preordained but emerge from the interplay of competing factors. Such experiments are crucial for uncovering the fundamental principles that govern crack propagation and material failure in soft, elastic materials.

This research aims to investigate the interplay between stretching and wire loading by intentionally misaligning the driving forces to study the directionality of cutting (Fig.4.1). By employing wire cutting, we can minimize friction during the cutting process and allow the blade to move freely. This setup enables us to observe and track the trajectory of crack propagation. The primary reason for choosing wire cutting is that the wire provides a free path through the material, as its thin dimensions offer less resistance compared to the blade. This allows the wire to follow the path of least resistance, theoretically enabling it to go where it wants. Understanding these phenomena can provide insights into improving industrial cutting processes and material design, ensuring efficiency and precision.

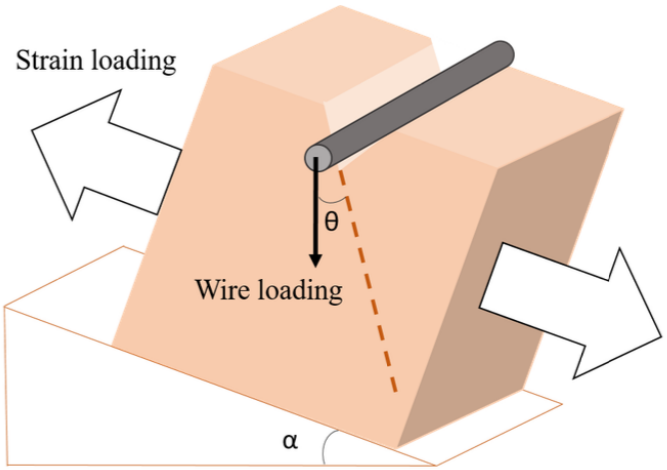

Figure 4.1: Schematic representation of double loadings on gelatin cube on a plane with angle θ (strain loading and wire loading). Crack path - dashed line appears at angle α.

The original experiment was designed in the laboratory, and due to its complexity, we will report all the work done on this project to explain the historical choices of the experimental modifications.

In our experiments, we utilize gelatin hydrogels as the primary material due to their robust elastic properties at room temperature and their well-documented behavior under stress. Gelatin, derived from porcine skin, is a non-toxic, biodegradable polymer that forms transparent, reversible gels capable of undergoing significant strains before failure. These properties make gelatin an excellent candidate for investigating the mechanics of fracture

and cutting in soft materials. By superimposing stretching and wire loading and intentionally misaligning them, we aim to observe the directional behavior of cutting and the associated instabilities.

Previous experiments have demonstrated that individual loading conditions—whether stretching or wire cutting—produce predictable crack paths. However, the combination of these loadings presents a more complex scenario, often resulting in an intermediate crack propagation direction influenced by both forces. Wire cutting, combined with remote traction, provides a unique approach to studying the fundamental concepts of fracture mechanics and crack directionality under dual loading conditions.

Our approach involves stretching a cube of gelatin with a precut and varying the angle of the applied strain and the mass of the cutting wire to explore the effects on crack directionality by the ratio between the two loadings. By conducting a series of controlled experiments, we aim to identify the direction of fracture propagation under mixed loading and the conditions under which the material exhibits stable or unstable crack propagation. These experiments are meticulously designed to minimize external variables and maximize the clarity of observed effects, providing a comprehensive understanding of the directional behavior of cracks under combined loading.

We employ advanced image analysis techniques to track the cutting trajectory, ensuring a detailed analysis of the crack propagation angles. This method allows for precise observation and measurement, facilitating a thorough investigation into the mechanics of crack directionality and the instabilities that may arise from combined loading conditions.

The ultimate goal of this research is to study the directionality of free-driving wire in cutting processes in soft materials, enhancing our ability to model and control material failure in practical applications. By systematically studying the directional tendencies of crack propagation and the resulting instabilities, we aim to contribute valuable insights to the field of material science and engineering.

One of the critical aspects of our study is understanding the intrinsic instability of the system. When the cutting wire is subjected to both stretching and its own weight, even a small deviation from the straight planar crack propagation condition can cause either a

spontaneous recovery toward the initial condition (stability) or a progressive amplification of the deviation (instability). In a symmetrical system, the vertical solution is stable. However, if the system is unstable, the two directions of twist are equally probable. If the system is tilted, one direction could be favored. Any deviation from symmetry can lead to increased instability. This phenomenon, likely related to Mode 3 twisting, suggests that the system is intrinsically unstable.

In addition to the primary focus on directionality and instability, our research also explores the morphological changes on the surface of the cut material. The surface textures observed during our experiments may result from global trajectory perturbations, adding another layer of complexity to the study. Understanding these textures and their formation mechanisms could provide further insights into the fracture processes in soft materials.

This is an original experiment and one of the most complicated, which is why the work of previous interns is reported here. We need all of the information to make it clear why we did the experiments. In previous studies, mixed loading was studied by compression, which seemed more stable in theory but was discarded due to the problems of friction between the two opposite lips after cutting. Consequently, we moved to traction.

4.2 Materials and Methods

4.2.1 Material Preparation

The material preparation technique was refined from the method previously employed by interns T. Chiez and C. Prat-Bernachot to enhance the reproducibility and stability of homogeneously crosslinked gelatin hydrogels. This modification aimed to achieve precise control over the concentration and improve adhesive properties, which are crucial for ensuring consistent attachment of the hydrogels to various testing surfaces and for maintaining the integrity of the mold components during the experimental procedures. By improving adhesive properties, we ensure that the hydrogels remain securely positioned throughout the tests, thus preserving the accuracy and reliability of the experimental results.

4.2.1.1 Gelatin Hydrogel Preparation

Gelatin hydrogels were synthesized using Sigma-Aldrich Type A gelatin, derived from porcine skin powder, with a gel strength of 300 Bloom. All samples were prepared in a closed glass container situated in a silicone oil bath, maintained at a temperature of 60℃ ± 2℃. This temperature range is optimal for dissolving the gelatin powder. The mixtures were continuously stirred using a magnetic stirrer set at 150 rpm to minimize bubble formation in the final solution. The mass concentration of all samples was consistently maintained at 3.2% ± 0.3%.

4.2.1.2 Mold Fabrication and Modification

Inspired by the work of Baumberger et al. [77], molds were constructed using silicone and plexiglass walls (Fig.4.2). In the initial technique, gelatin was crosslinked between two plexiglass molds, but this resulted in weak adhesion, with parts of the gel detaching from the plexiglass even after 2% deformation. To address this issue, Velcro strips were adhered to both sides of the plexiglass molds. The gelatin solution can penetrate into the loops and hooks of the Velcro, creating a more extensive and secure attachment when the solution is poured. This modification resulted in the first crack appearing only after 10% deformation, indicating a significant improvement in adhesive strength.

The molds were then clamped to the traction experimental setup. Subsequently, the samples were poured into cube-shaped molds featuring two silicone sides and two plexiglass sides with attached Velcro strips (Fig.4.2).

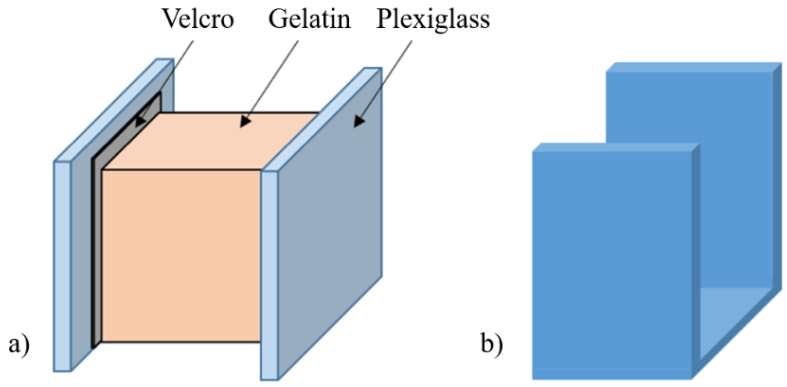

Figure 4.2: Schematic of the mold used to prepare gelatin cubes for tensile tests: a) plexiglass with Velcro showing how gelatin is attached after gelation, b) silicone mold.

The molds were sealed with a thick glass plate and covered with Parafilm to minimize evaporation and prevent solution leaks during gelation. The samples were then placed in a refrigerator at 6.5℃ for 12-15 hours to facilitate gelation.

4.2.2 Mechanical Characterization of Materials

The mechanical properties of the materials were assessed both at the initial preparation and after 12, 15, 18, and 24 hours of storage in the refrigerator. The error in mass concentration arose from the evaporation of a small amount of water during the drying of samples in the refrigerator. To control this evaporation rate, the mass was measured immediately after pouring into the mold and again 12 hours after the molds were taken out of the refrigerator. On average, the samples contained 96.8% water. A mass variation of approximately 4-6% was observed for all samples. These changes in mass are significant and have been taken into account in the calculations of concentration.

Consistent results were obtained, indicating a stable weight of the molds with gelatin between 12 and 24 hours of refrigeration. This allowed us to neglect water evaporation after the gels had been stored for more than 12 hours in the refrigerator. Additionally, the mass of three cubes was measured every 10 minutes over the course of one hour after being taken out of the refrigerator. These cubes were maintained at room temperature (20℃) between measurements. The observed mass variation was less than 0.1%, indicating

negligible evaporation and consistent sample concentration.

In this experiment, the room temperature was consistently maintained at 20℃. During the 30-minute testing period, the temperature variation in the middle of the cube was minimal, ranging only from 6.5℃ to 13.5℃. The internal temperature of the gelatin was measured at its core by a probe every 5 minutes during the 30 minutes. This short duration was insufficient for a significant temperature gradient to develop from the edge to the center of the cube. As observed in literature [78], the melting points for gelatin with high Bloom are much above the working temperature (Fig.4.3). Given that the total experimental duration did not exceed 30 minutes, it can be inferred that while the material was not at thermal equilibrium with the room, it retained its elastic and homogeneous properties throughout the experiment.

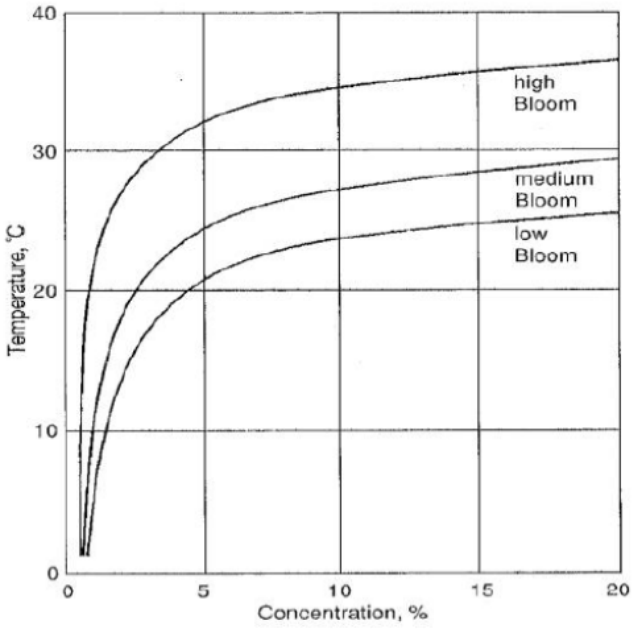

Figure 4.3: Variation in melting point as related to temperature and gel concentration for low, medium and high Bloom gelatins [78].

Compression tests conducted on samples immediately after refrigeration revealed a Young's modulus of 4500 ± 315 Pa. The Poisson's ratio was estimated to be 0.500 ± 0.004, indicating that the material is incompressible, which is consistent with the high water content

(96.8%) of the samples.

4.2.3 Experimental Setup

The system (Fig.4.4) for applying deformations was developed by previous interns T. Chiez and C. Prat-Bernachot. Holding and stretching fixtures were created, including a plane with angle control and adjustable holders, allowing for stretching distances from 20 mm to 70 mm. Several versions of the wire loading system were also developed. The wire was attached in a pendulum-like configuration, ensuring that the center of mass remained under the wire to maintain balance and prevent oscillations. Pre-tension was applied to the wire to prevent a bulging shape by applying force to the ”arms” of the pendulum during mounting, with the elastic return ensuring sufficient pre-tension. The wire used for this study was steel (piano wire) with a diameter of 0.2 mm. For the compression experiments, a metallic holder was made for the wire.

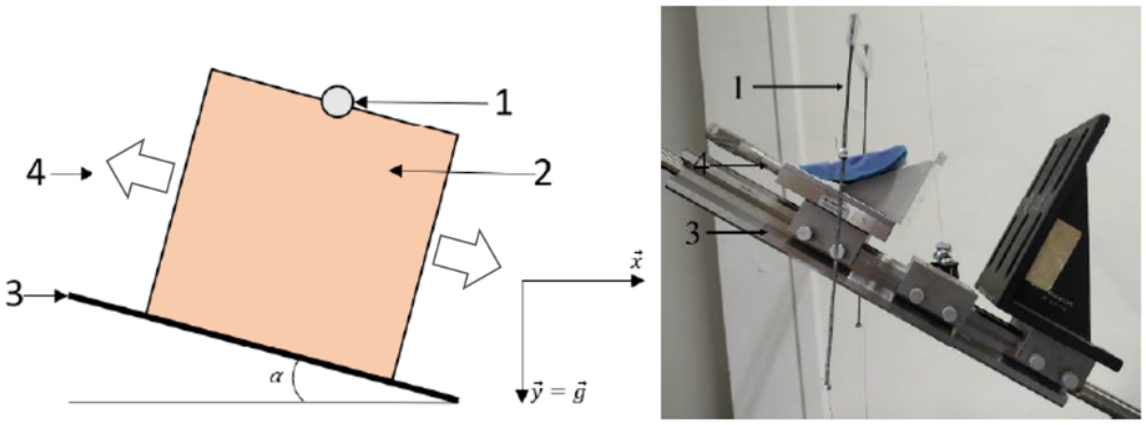

Figure 4.4: Experimental setup: a weighted wire (1) is placed in contact with a gelatin cube (2) which is placed on an inclined plane with angle control (3) and a wet Plexiglass substrate (4). The force is exerted by means of a micrometric screw allowing the left carriage to translate on the plane rail (3).

The system was later modified, an improved system for guiding and executing the wire in the gelatin was implemented (Fig.4.5). The holder was made from PMMA to keep the original weight of the wire system light. To avoid instabilities at the beginning of the experiment, the bottom part of the wire holder with metallic strips was equipped with a magnet. This

magnet was linked to a transmitter, enabling it to be turned on and off. When current was applied to the magnet, it held the wire holder in a controlled position. When the current was turned off, the holder with the wire fell under the influence of gravity. This allowed the wire to cut through the sample to avoid oscillations associated with positioning the pendulum on the assembly.

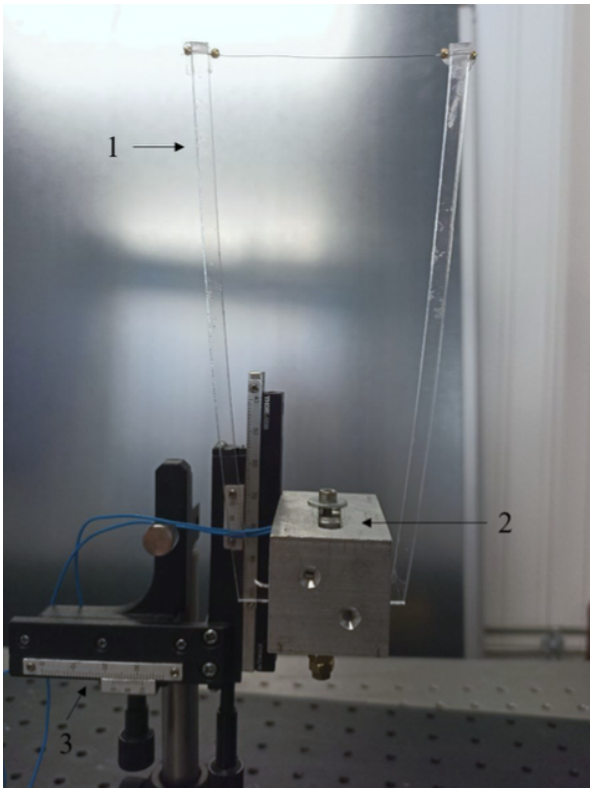

Figure 4.5: A weighted wire (1) is attached to a magnet (2) whose position is controlled by two rails (3).

This setup enabled precise control of the exact time to release the wire, ensuring it moved without external forces. The design aimed to enhance the stability of the experiments, manage the mass of the wire, ensure accurate wire positioning, and create conditions for the wire to move solely under gravitational force at the start of the experiment.

The mass applied to the wire during cutting was assumed to be equivalent to the mass of the pendulum. Additional weight could be added to the pendulum and controlled using metallic strips screwed to the bottom. The total mass of the weighted wire was adjustable

from 4.5g to 20g.

The wire cutting procedure began by creating an initial notch on the gelatin cube with a depth of 2-4 mm parallel to the Plexiglass sides. The bottom of the gelatin cube was placed on a wet Plexiglass substrate to reduce friction during stretching, and both Plexiglass sides were attached to the plane.

4.2.4 Methods

Measurements were acquired using ImageJ software. A Baumer camera, with an acquisition frequency ranging from 1 to 30 fps, was used to capture successive images of the cutting trajectory. The trajectory of the crack was manually reconstructed, and a linear regression was performed on all the points obtained. This produced a straight line whose slope corresponds to the tangent of the angle of the crack with the vertical (Fig.4.6).

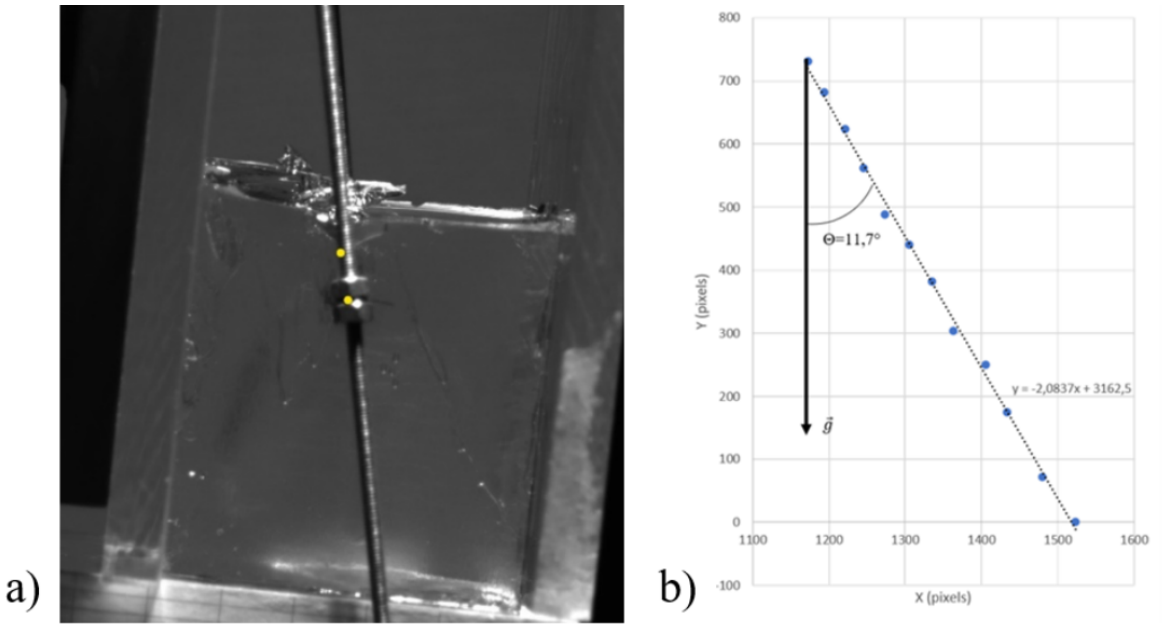

Figure 4.6: Cube of gelatin under 20% of compression with the mass of the wire 29.6g a) and measurement of the angle between the crack and the vertical b).

4.3 Results and Discussions

The first part of the work linked to compression experiments, tests without cutting wire, tests without deformation was made by T. Chiez and C. Prat-Bernachot. Improving the material characterisation, experimental setup and experiments corresponding to traction tests were obtained for this work and showing in the traction tests.

4.3.1 Tests Without Cutting Wire

According to the theoretical model [79], if the energy release rate associated with cutting is negligible compared to the energy release rate associated with crack propagation, then the crack propagates at an angle α corresponding to the inclination of the support. In other words, the crack will propagate perpendicularly to the tensile deformation stress(Fig.4.7). In cases of this straight crack propagation, we expect $K_{II} = 0$ and G to be at its maximum, indicating stable propagation. The tomoelastic length in this case is $l_{TE} = \frac{\Gamma}{E}$, with $\Gamma = 4.05\,\text{J/m}^2$, giving $l_{TE} = 0.0009$.

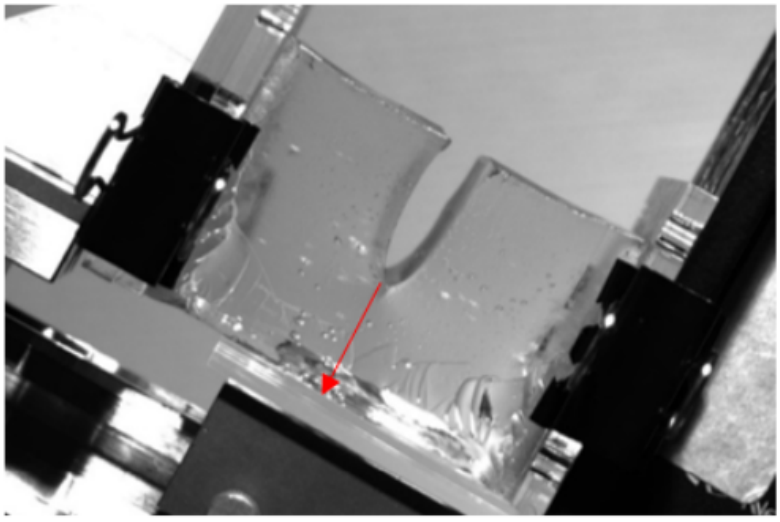

Figure 4.7: Sketch of traction test representing the possible angle interval, the dashed line represents the crack propagating perpendicular to the tensile deformation stress.

For the crack propagation tests without a cutting wire (referred to as ”empty” tests), the

deformation is gradually increased until crack initiation. Once crack propagation starts, the deformation is held constant. In these cases, the propagation is found to be stable: the crack continues to progress steadily while the deformation remains constant.

In these ”empty” tests, the direction of crack propagation is influenced by three key criteria: the initial alignment of the pre-cut, the distribution of the applied load, and the intrinsic properties of the material. Firstly, the initial alignment of the pre-cut significantly affects the trajectory of the crack, with any misalignment potentially leading to deviations from the intended path. Secondly, the distribution of the applied load can cause variations in stress intensity, influencing the crack direction as it propagates. Finally, the intrinsic properties of the gelatin hydrogel, such as its elasticity and fracture toughness, play a crucial role in determining the stability and directionality of the crack.

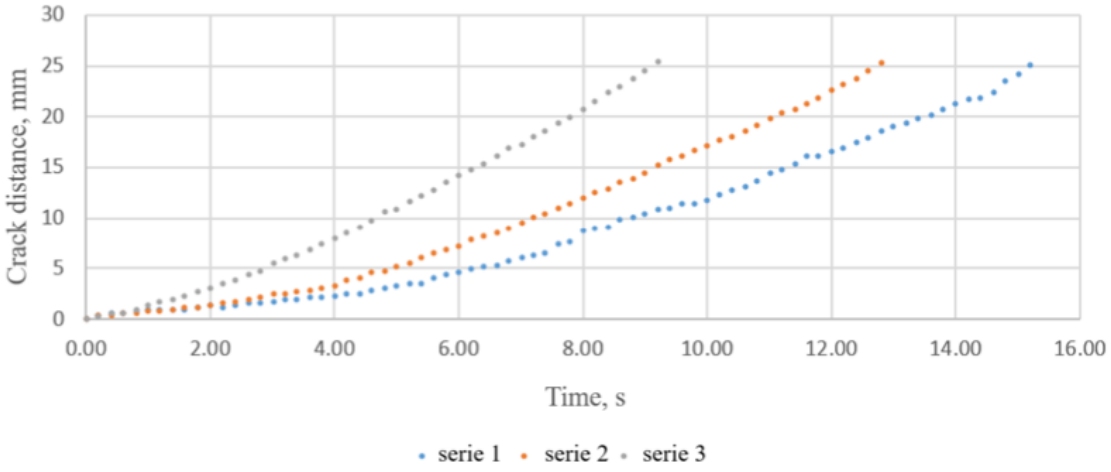

Figure 4.8: Crack propagation length under 14.2%, 15%, and 19.5% of applied strain.

Three tests are conducted under the same initial conditions: support inclination at an angle $\alpha = 34.5°$ and a pre-crack of 1 cm. The results show that the crack initiation does not occur at the same deformation in all three cases: the measured deformations allowing propagation are 14.2%, 15%, and 19.5% (Fig.4.8). However, it is noteworthy that the lips of the pre-crack adhere to each other, and this adhesion is sufficient to delay crack propagation, which may explain the variations in the deformation required for propagation.

4.3.2 Weight driven wire cutting

The experiments showed that the weighted wire moved at a non-zero angle during tests with no applied deformation. This will be discussed in more detail in the following sections. Theoretical model accurately describes the experimental data in extreme cases: deformation without cutting and cutting without deformation. However, it is now necessary to experimentally verify the case of combined cutting and deformation to fully understand the directional tendencies and stability of crack propagation. In the context of combined loading, the direction of crack propagation is influenced by several factors. The stress intensity factor K_{II} is not as well defined close to the wire, complicating the analysis of shear stresses near the cutting edge. Additionally, the maximum stress criterion presents a complex picture, with compressive stresses on the bottom side of the crack and tensile stresses elsewhere. This complexity is highlighted by Hui et al. [79], who demonstrate the intricate interplay between friction and deformation, making it challenging to achieve a clean cut under conditions that involve significant stress variations. Meanwhile, the maximum energy release rate, G_{max}, is a well-defined criterion that provides a clear direction for crack growth:

$G = \frac{F}{b}$

where G - energy release rate, F is the applied force and b is the thickness of the cut cube.

The system is assumed to be linear, and the direction of crack propagation remains vertical because any deviation would result in less work per unit area.

By conducting controlled experiments that combine cutting and deformation, we aim to observe the resulting crack trajectories and verify our theoretical predictions. These experiments will provide critical insights into the directional behavior of cracks under dual loading conditions, enhancing our understanding of material failure in soft materials.

4.3.3 Combination of Deformation and Cutting Effort

4.3.3.1 Compression Tests and Theoretical Model

Under the assumption that the crack propagates at an angle θ that maximizes the energy release rate G, this is the value that must be determined. The detailed equations are found in the appendix.

$G = \frac{\pi\sigma^2}{4E}\sin^2(2\theta) + \frac{F\cos(\theta-\alpha)}{b} = G_G + G_c,$

Energy release rate for a wire propagating in a cube of gelatin subjected to uniaxial compression, where σ, E, F, b, G_G, and G_c are the applied stress, Young's modulus, the force applied at the wire, the sample width, the energy release rate related to fracture, and the energy release rate related to cutting, respectively.

Assuming the system is linear, which allows for superposition, the total energy release rate G is the sum of G_G and G_c. Therefore, a global maximization of G is performed to determine the angle θ that nullifies $\frac{dG}{d\theta}$.

In the case where the energy release rate related to cutting is negligible, i.e., G_c is negligible compared to G_G,

$\frac{dG}{d\theta} = \frac{\sigma^2\pi c}{2E}\sin(4\theta)$

This nullifies for $\theta = 0$ (minimum of $G(\theta)$) or $\theta = \frac{\pi}{4}$ (maximum of $G(\theta)$). In this case, the crack should propagate at an angle of $45°$ relative to the normal of the force application (i.e., an angle of $45° - \alpha$ relative to the vertical) (Fig.4.9).

When the energy release rate related to cutting predominates over the energy release rate related to fracture, i.e., $G_c \gg G_G$,

$\frac{dG}{d\theta} = \frac{F\sin(\alpha-\theta)}{b}$

This nullifies for $\theta = \alpha$. In this case, the crack should propagate at an angle α relative to the normal of the force application, which corresponds to the direction of gravity.

According to this model, increasing the compression rate enhances the energy release rate related to fracture, thereby increasing the angle θ. Conversely, increasing the mass of the cutting system increases the energy release rate related to cutting, thereby bringing the angle θ closer to the vertical. To maximize the range of possible values, the angle α should

be set to a relatively small value (here, it is set to 12°).

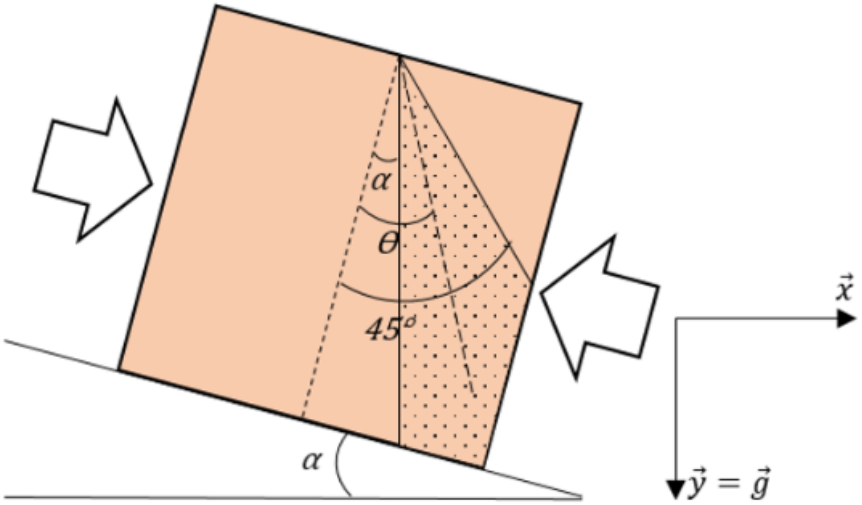

Figure 4.9: Compression setup, with the dotted area representing the interval of possible angles; the dotted line represents the crack propagating at an angle θ.

To understand the maximum energy release rate in this context, we start by calculating G as done in fracture mechanics. For instance, if compression is applied without considering fracture, no energy release would occur (i.e., $G = 0$ and $K = 0$). In a purely compressive and symmetric loading, no singular stress is induced on the crack. However, if misalignment occurs, shear forces could induce a crack, and combining compression with cutting allows us to examine this through the mode II fracture mechanics approach. This approach helps to explain the crack propagation direction when both compression and cutting forces are present.

As shown by [80] and [81], a greater force is required to initiate a crack in the wire compared to the force needed to propagate the crack. Therefore, it is beneficial to pre-crack the sample to work with smaller masses (and thus lower cutting forces). Initiating the crack in the sample also ensures the initial position of the wire, reducing variations between measurements. A device was constructed to ensure a consistent pre-crack depth: a blade is mounted on a shim, which slides along a fixed thickness plate, guaranteeing the depth.

This pre-crack also has the advantage of reducing fluctuations related to surface defects: during gelatinization, a glass plate is placed on the mold to reduce evaporation. However, this plate creates bubbles on the surface, and pre-cracking helps avoid these defects. Despite the pre-crack eliminating surface defects and ensuring the initial position of the wire, a specific case was observed in the results: measuring the angles is challenging, as shown in Fig.4.10 and detailed below, with instabilities appearing during cutting (”twist”). Therefore, further investigation into the origin of measurement fluctuations is required.

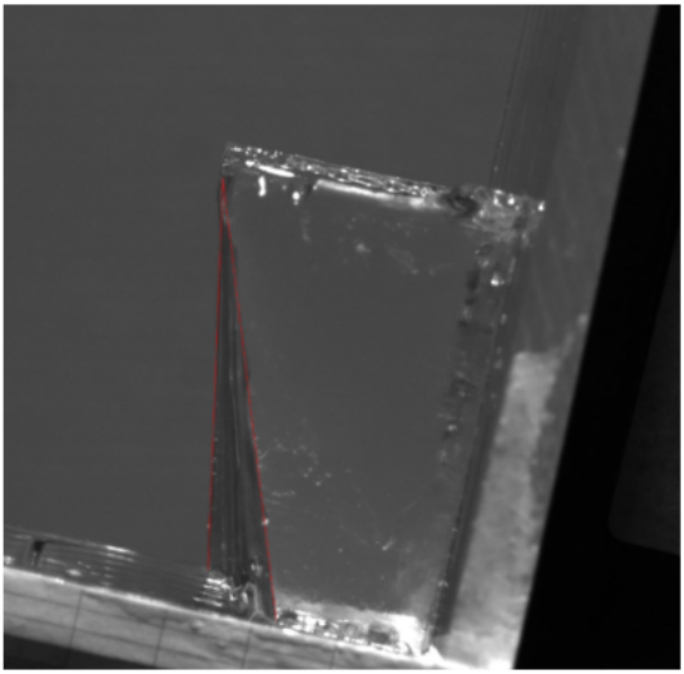

Figure 4.10: The angle variation between the front face and the rear face; cube subjected to 10% deformation with a cutting mass of 29.6g.

4.3.3.2 Compression Tests. Experimental Results

The results of the cutting tests are shown in Fig.4.11. This figure presents the relationship between the compression ratio of the cube (x-axis) and the cutting angle (y-axis) as measured from the acquired films.

An initial observation reveals that all data points are offset by 12° upwards. This is due to the wire intersecting the cube at an angle of 12° to the normal plane when it cuts vertically.

Therefore, at a compression ratio of 0%, the cutting angle is 12°. Additionally, the cutting angle increases with the compression ratio.

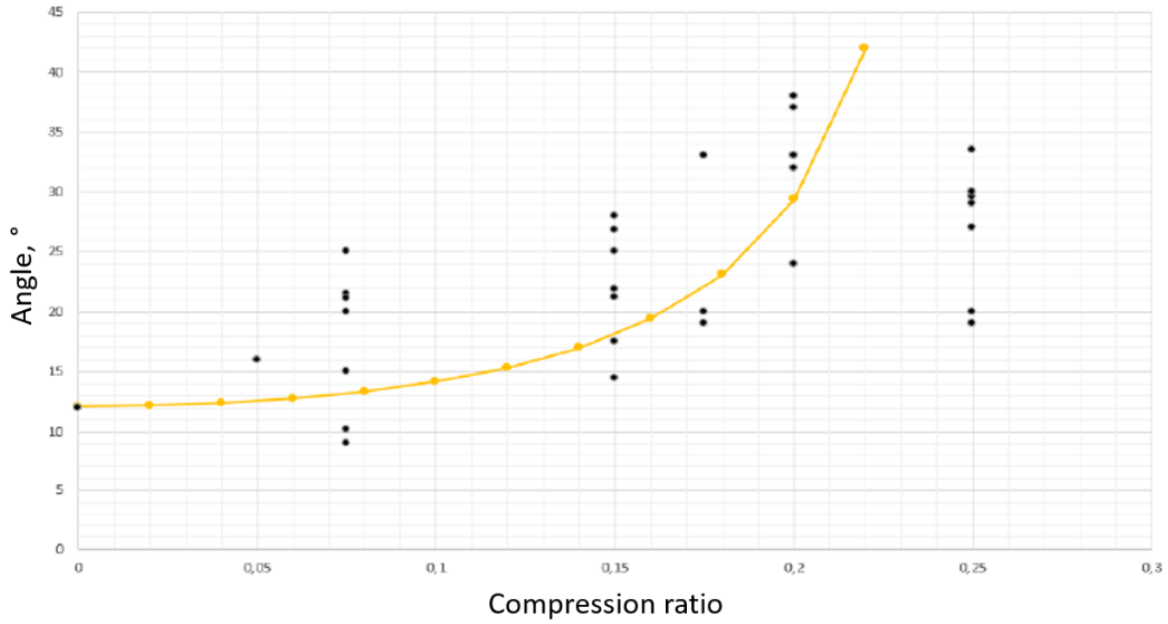

Figure 4.11: Cutting angle as a function of the compression ratio of the cube. The dashed line represents the theoretical trend.

However, the scatter plot does not exhibit a clear pattern. Significant variability is evident, even at similar compression ratios, with cutting angles varying by as much as a factor of two. For example, at a compression ratio of 7.5%, cutting angles range from 10° to 25°. This inconsistency persists across all compression ratios, suggesting that various curve shapes (linear, parabolic, or exponential) could potentially fit the data.

Despite the variability, an effort was made to align the scatter plot with the theoretical model, as depicted in Fig.4.11 by the yellow line. While the model appears to follow the general trend of the data, the points are too dispersed to draw definitive conclusions. Nonetheless, an intriguing observation can be made: at compression ratios between 20% and 25%, the cutting angle seems to peak. This is also indicated by the theoretical curve, which diverges at this interval. For compression ratios exceeding 25%, this divergence does not hold, suggesting that the model's assumptions may not be valid at higher compression

ratios.

The previous work was focused on compression tests, but due to the significant scatter in the data, it was decided to shift to traction tests. Even though the scatter is substantial, a theoretical trend can still be observed. The angle is positive and generally increases, indicating an effect consistent with the theoretical model. However, the model's reliability is compromised by the high degree of scatter in the data.

4.3.4 Friction

During the various cutting tests of a cube subjected to compression, it was observed that the two fracture surfaces could slide over one another during crack propagation, particularly at compression rates greater than 10%. This surface sliding introduces new, unwanted, and difficult-to-quantify parameters into the system, thus disturbing the crack propagation direction.

The objective is to estimate the gel-gel friction coefficient to determine if the friction between the two surfaces (right-left) can be neglected during cutting (Fig.4.12). For this purpose, the Coulomb model will be applied, even though it is not entirely applicable to soft matter. For many materials, the actual contact surface at the microscopic scale differs from the theoretical contact surface at the macroscopic scale. However, the aim here is to obtain an order of magnitude for the friction coefficient, rather than to conduct a precise study on gel-gel friction during the cutting of a gelatin cube subjected to compression. Therefore, the contact surface is assumed to be equal to the contact area between the support and the cube.

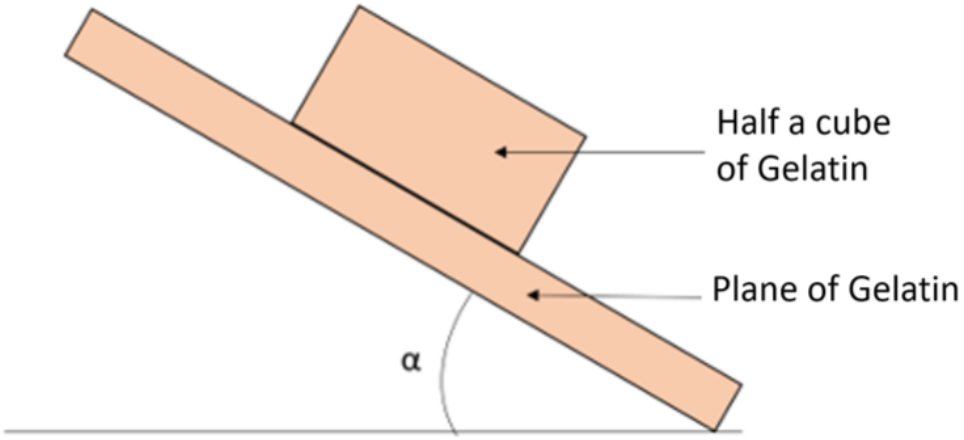

Figure 4.12: Friction of the two surfaces during a cutting test under compression (30%), inducing branching/tearing.

To determine the friction coefficient, tests were conducted on three samples of the same dimensions and concentration. For an angle $\alpha > 70°$, the samples toppled off the plate. Therefore, a smaller cube should be made to avoid this toppling. However, this value allows for an estimation of the friction coefficient: friction will occur for an angle greater than $70°$, and thus the friction coefficient is greater than $\tan(70°)$, which is greater than 2.75. Although this estimation is approximate, in comparison with other materials, it can be asserted that gel-gel friction is not negligible.

Another source of friction in this experimental setup occurs at the interface between the plexiglass plates that make up the jaws and the surfaces of the gelatin. This is problematic because the gelatin adheres to the plexiglass, which deforms the cube during compression: the final shape will be ”bulged” rather than prismatic. A solution was considered to address this friction: the plexiglass surfaces are lubricated. This solution seems sufficient because despite the high compression rates ($>$ 20%), the gelatin does not adhere to the plates that make up the jaws, thus remaining free from deformation.

4.3.5 Instabilities in compression tests

The results of the compression tests were not reproducible, prompting a study of the instabilities and fluctuations that occur during cutting. Initially, tests were performed on a series of cubes placed on a flat support (zero inclination angle) with the cutting wire laid on top. The results obtained (angle measurements) were scattered around 0°: in some tests, the angle was positive, in others, it was negative. The horizontal state appeared as an unstable equilibrium, justifying the addition of an angle $\alpha > 0$ at the support (arbitrarily chosen as 12° in this experiment).

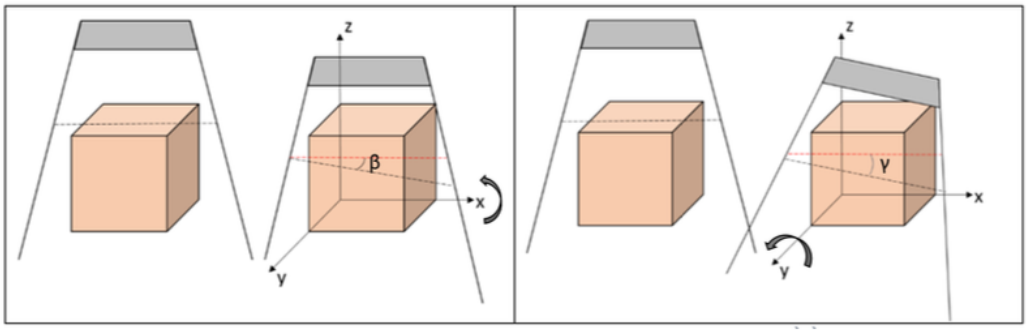

Figure 4.13: Instabilities during cutting: “twist”, rotation around the $\vec{x}$ axis while remaining in a plane parallel to the plane (left) and “tilt”, rotation around the $\vec{y}$ axis while remaining in a plane parallel to the plane (right).

However, other instabilities and fluctuations appeared during these tests: a rotation of the wire around the horizontal axis inducing a sliding of the wire (”tilt”) was observed, as well as a rotation around the vertical axis (”twist”) leading to an exit from the cutting plane (Fig.4.13). The initial hypothesis explaining the origin of these instabilities is the poor balance of the cutting system and the sample. Even if a pre-crack was made on the upper face of the cube, it remains soft and easily deformable: when the wire comes into contact to initiate the crack, it is possible that it locally accentuates the pre-crack. There are also defects related to the shape of the cube and the molding process (surface bubbles caused by the glass plate used to limit evaporation) as well as internal micro-defects. To limit the fluctuations related to these defects, the crack is initiated before the test with a blade mounted on a guide to

ensure a consistent pre-crack depth of 2 mm from one cube to another.

To study the ”tilt” and ”twist” phenomena, a new series of measurements was conducted. This time, an angle was imposed at the initial crack position (angle α_2 in Fig.4.14).

The measurement of the final cutting angle is sometimes uncertain: in the case of a crack with a straight profile, the measurement is simple, but it can be more complex if the crack is slightly curved. To obtain a more precise measurement, a series of points along the crack will be taken, and then an average of the measured angles will be calculated. Four angles will be measured: on the upper face, on the lower face, on the front lateral face, and on the rear lateral face.

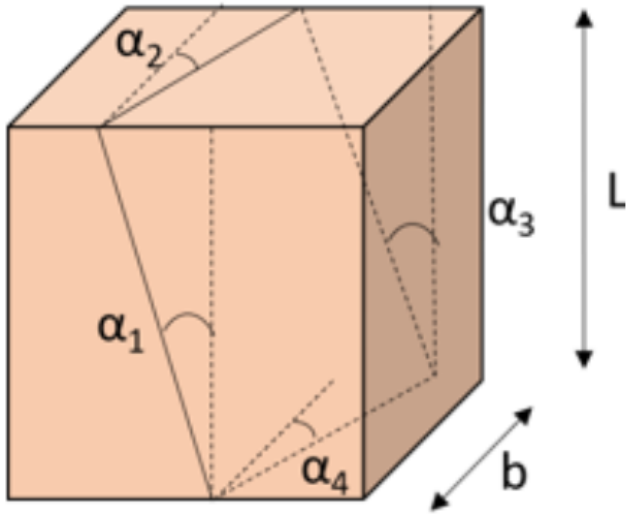

Figure 4.14: Sketch showing imposed angle α_2 and measured angles.

These angles are related by a trigonometric relation:

$\tan(\alpha_4) = \tan(\alpha_2) - \frac{L(\tan(\alpha_1)+\tan(\alpha_2))}{b}$

Thr relation between the imposed angle α_2 and the measured angles α_3, α_4, and α_1. The measurements are taken on the cubes after cutting, so the reference frame corresponds to an undeformed reference frame. However, since the cutting is performed under large deformations, the deformed and undeformed reference frames will not be the same, and the angle measurements will change. The observed defects (e.g., curvature of the crack)

will also be modified depending on the reference frame used. To ensure all results are in the same reference frame, it is necessary to know the relations linking these two reference frames.

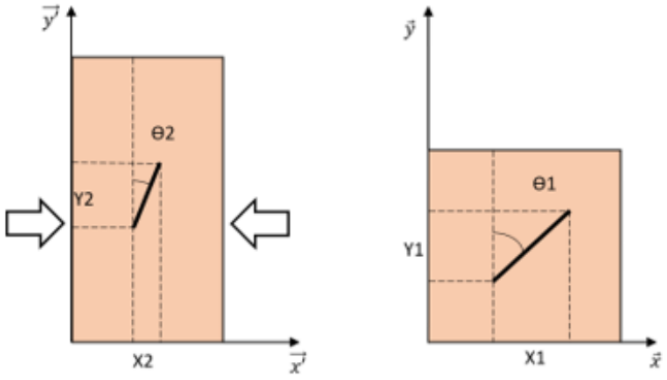

Figure 4.15: Reference frames and angles.

These two reference frames can be related by the following equation (see appendix for detailed calculation):

$\tan(\theta_1) = \tan(\theta_2)\frac{(1-\sigma/E)}{(1+\nu\sigma/E)}$

This relation represents the ratio between the deformed and undeformed reference frames.

It is now possible to know the value of the angle if the measurement had been taken under compression (i.e., if the angle had been measured according to the reference frame $(\vec{x}, \vec{y})$).

In the case of a "twist" instability, two angles are measured (one angle on the front face and one angle on the rear face (Fig.4.14). Fig.4.15 shows the percentage difference between these angles and the average angle in case of cuts with a "twist" instability calculated as follows:

$$\text{average angle} = \frac{\text{angle of the front face} + \text{angle of the rear face}}{2}$$

It appears that it is difficult to accurately estimate the angle made by the crack in the case of a "twist" instability. The positioning angle of the wire is at an unstable equilibrium. There is a variation in the front/rear angles without this variation being systematic. This pendulum

rotation occurs in an uncontrolled manner, so a solution must be found to eliminate this instability while having minimal influence on the rest of the setup (the wire must remain as ”free” as possible to propagate in the sample).

To avoid instabilities that could be caused by tilting and twisting of the blade, we improved the experimental setup(described in the section Materials and Methods) by changing wire holders to ensure the stability of the cut.

Our aim is to eliminate both ”tilt” and ”twist” instabilities. Initially, we strive to eliminate both, but the ”twist” could become a potential point of interest as it may indicate an underlying instability in the system. Therefore, understanding and controlling these phenomena is crucial for improving the reproducibility and accuracy of the cutting tests. As the wire makes initial contact to initiate the crack, it is plausible that this action locally accentuates the pre-existing crack, aiding in stabilizing the cutting process. To avoid the significant impact of friction between the gel-gel surfaces on the cutting and its possible influence on the instabilities, it was decided to continue with traction experiments.

4.3.5.1 Traction Tests: Theoretical Model

As with the analogy with compression experiment under the assumption that the crack propagates at an angle θ (Fig.4.16) that maximizes G, this value becomes critical to determine.

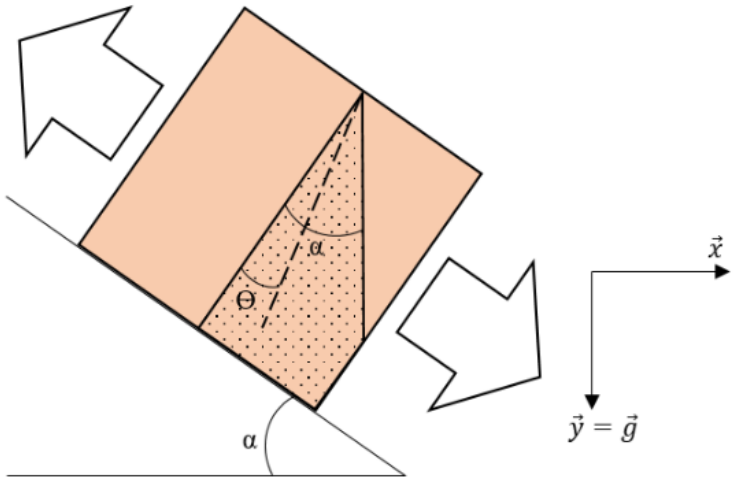

Figure 4.16: Sketch of traction test representing the possible angle interval, with the dashed line representing the crack propagating at an angle θ.

The angle θ is determined by the condition $\frac{dG}{d\theta} = 0$, corresponding to the direction in which the crack propagates most effectively by maximizing the energy restitution.

$G = \frac{\pi c \sigma^2}{E} \cos^4(\theta) + \frac{F \cos(\alpha - \theta)}{b} = G_g + G_c,$

where energy release rate for a wire propagating in a gelatin cube subjected to uniaxial tension, σ, E, F, b, G_g, and G_c are the applied stress, Young's modulus, the force applied at the wire, the sample width, the energy release rate related to fracture, and the energy release rate related to cutting, respectively.

The crack propagates in the direction that maximizes the energy release rate. Therefore, the angle θ that nullifies $\frac{dG}{d\theta}$ must be determined.

In the case where the energy release rate related to cutting is negligible, i.e., G_c is negligible compared to G_g,

$\frac{dG}{d\theta} = -\frac{\sigma^2 \pi c}{E} 4 \cos^3(\theta) \sin(\theta)$

This nullifies for $\theta = 0$ (maximum of $G(\theta)$) and for $\theta = \frac{\pi}{2}$ (minimum of $G(\theta)$). In this case, the crack should propagate at an angle of 0° relative to the normal of the force application (i.e., at an angle of α relative to the vertical).

In the case where the energy release rate related to cutting predominates over the energy

release rate related to fracture, i.e., $G_c \gg G_g$,

$\frac{dG}{d\theta} = \frac{F \sin(\alpha - \theta)}{b}$

This nullifies for $\theta = \alpha$. In this case, the crack should propagate at an angle α relative to the normal of the force application, which corresponds to the direction of gravity.

In the case of a tensile setup as schematized in Fig.4.4, the inclination angle of the support α must be maximized to have a wide range of possible measurements. In this study, the angle α is set to 34.5°. Beyond this limit, the pendulum comes into contact with the left jaw (the upper jaw). Thus, a different setup would need to be designed, but creating a mold suited to the situation is difficult, and modifying the setup should be avoided. Therefore, the value $\alpha = 34.5$ is retained as the maximum value (it is the only value used in this study since the objective is to have a large possible angle range for the advancement of the blade).

4.3.5.2 Traction Tests: Experimental Results

It was observed that different cutting regimes could be achieved depending on the applied strain. These regimes include guided cutting by the wire and branching. This bifurcation, which refers to the phenomenon where an initial crack splits into two or more separate cracks during the cutting process, was observed starting from 8% strain in the gelatin cube cuts. This typically occurs when the material experiences complex stress states, leading to multiple crack propagation paths; in this case, stresses are due to both the stretching deformation and the cutting action of the wire under gravity. Absolute branching occurred at strains exceeding 12%, while at 10% strain, both branching and non-branching cases were obtained.

Fig.4.17 shows the crack profiles in different applied strain regions. The crack tip position results are shown for each wire position at the start of the experiment with no applied strain (a*), b*), c*)), with applied strain before the beginning of the cut (b**), c**)), with the cut in the middle of the cube (a***), b***), c***)), and at the end of the cut (a****), b****), c****)).

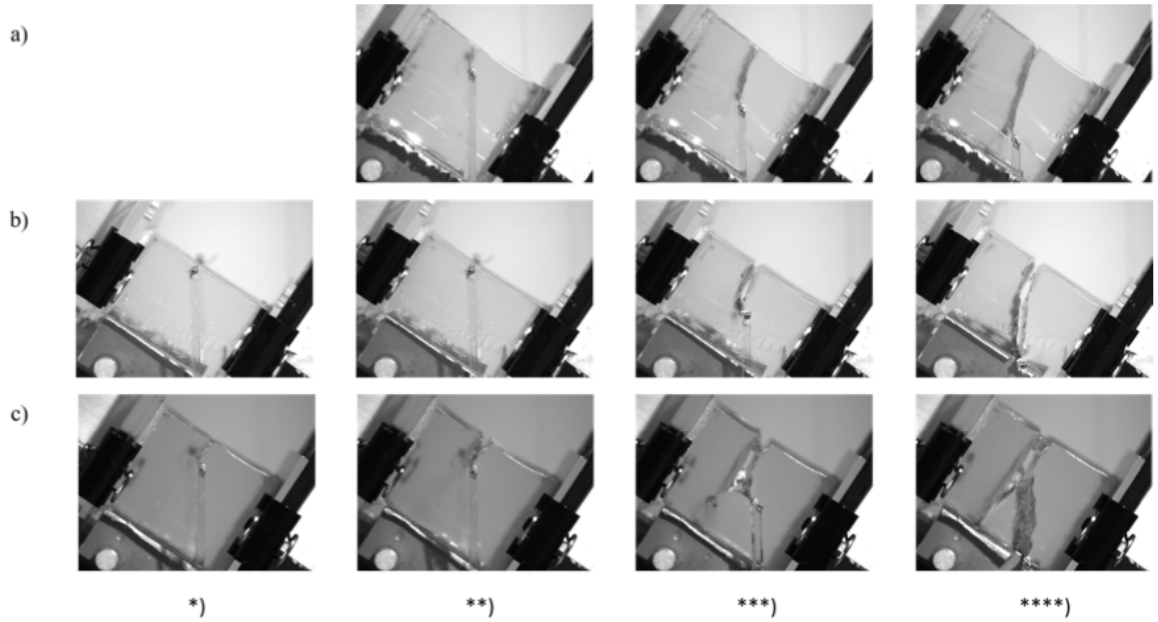

Figure 4.17: Crack profiles in different applied strain regions: a) 0%, b) 4%, c) 10% in different moments of crack propagation. *) Initial state with no applied strain, **) fixed applied strain, ***) propagation in the middle of the cube, ****) wire reaches the bottom of the sample. Bifurcation was observed in case c***-c****.

Profiles of the crack tip position were obtained using ImageJ software, with a resolution necessitating reporting results with an error no greater than 5%, corresponding to the pixel size. For each applied strain regime, a minimum of three measurements were acquired. In all measurements, the weighted wire cut at an angle to the gravitational force.

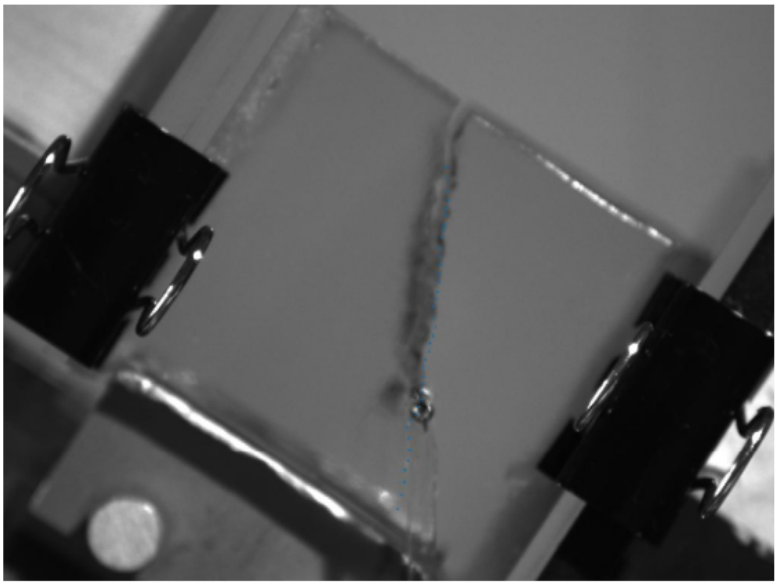

Figure 4.18: Propagation of the crack tip (dots) in gelatin gels subjected to a 2% applied strain using a 14g weighted wire, with approximation curves (lines).

In Fig.4.18, a gelatin cube subjected to 2% strain during the cutting experiment is presented. One of the two wire locations is tracked by blue dots, indicating the crack tip propagation. Based on this experimental technique, the angles of crack propagation were calculated for each experiment.

It was illustrated that the crack tip propagation tracks for gelatin gels under applied strains ranging from 0% to 8% follow different paths (Fig.4.19). A 14g weighted wire was used, and it shows the average angle as a red line on the graph as the approximations for each experiment.

The majority of experiments yielded positive angles relative to the vertical direction, while in the regime with no applied strain, negative angles were also observed. Specifically, in Fig.4.19, it is evident that for 2% strain, only positive angles were obtained, ranging from 5.2 to 16.5 degrees. Noise in the curves data (Fig.4.20) comes from the calculation of the position plus the instabilities during cutting, which might cause the path to deviate from being perfectly linear.

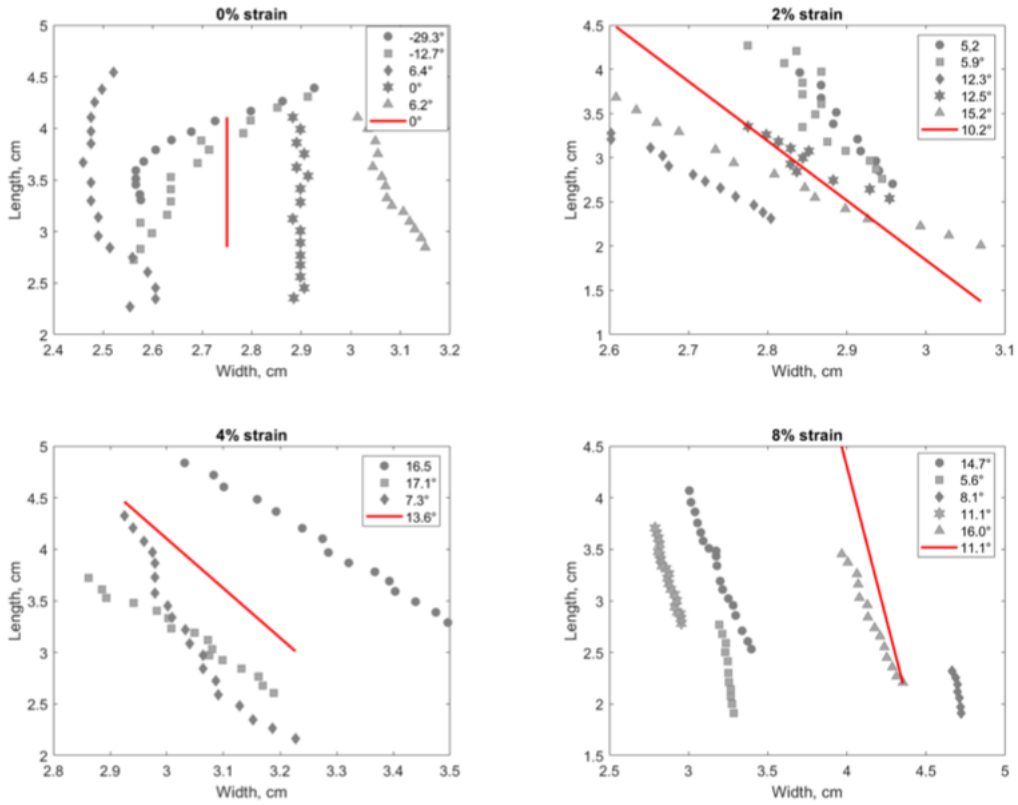

Figure 4.19: Propagation of the crack tip in gelatin gels subjected to a) 0%, b) 2%, c) 4%, and d) 8% applied strain using a 14g weighted wire, with an approximation curve of the average angle (lines).

Fig.4.23 compares angle changes for different strains, illustrating how they vary depending on the weight of the wire used. We can assume that increasing applied strain increases the value of the cut angle in traction tests as well. However, the data contains many scatters, making it challenging to plot a robust model for it.

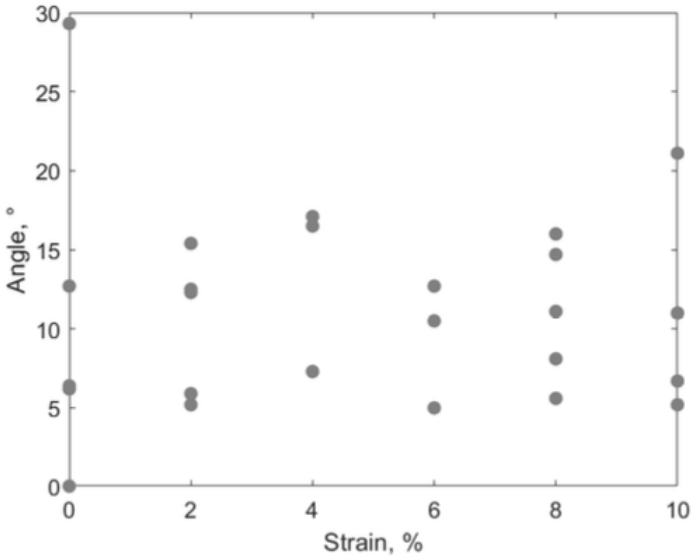

Figure 4.20: Propagation of the crack tip (dots) in gelatin gels subjected to a 2% applied strain using a 14g weighted wire, with approximation curves (lines).

In cases involving different wire weights, a wide range of angles was observed, indicating the occurrence of instability causing deviation from vertical crack propagation. In traction tests, the instabilities were influenced by the applied strain and the weight of the wire. For instance, with wire weights less than 10g, the wire often got stuck in the gelatin, whereas weights greater than 20g caused the wire to propagate predominantly in the direction of gravity (Fig.4.21).

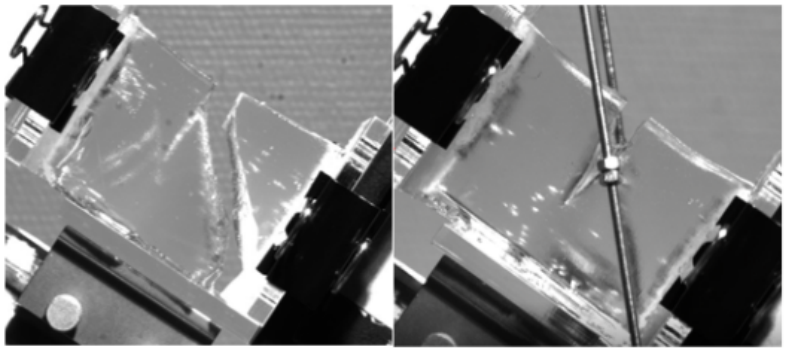

Figure 4.21: Branching: 12% strain and 11g mass (left); 10% strain and 4.5g mass (right).

The mass of the wire, including the holder, might significantly influence the cutting results. The case with no applied strain ($\theta = 0$) occurs when the energy release rate related to tension predominates. A test was conducted with total pendulum masses of 4.5g and 11g and a deformation rate of 12%, close to the values necessary for crack propagation in the absence of a cutting effort (see Fig.4.21). During cutting, the initial crack splits into two, with one crack following the direction perpendicular to the tension and another following gravity (an angle of approximately -5° relative to the vertical is observed). Locally, the material is no longer homogeneously stressed, rendering the assumptions used for the model calculation invalid. This specific case exceeds the scope of the current study, as branching is a complex domain. Therefore, deformation values ware chosen to be less than 12%. A test was also conducted with a mass of 4.5g and a strain of 10% to determine a lower limit of possible values. The results indicate that, for this mass, the wire struggles to propagate the crack in the gelatin, ultimately leading to branching, with the wire remaining immobile in the gelatin (Fig.4.22). Therefore, the mass value was chosen to be greater than 4.5g. When the mass increases, the angle decreases, and when the deformation increases, the angle increases. Around 10% deformation, the measured angle values decrease instead of increasing. However, this measurement zone is close to the branching zone observed at 12% deformation, which could affect the angle values.

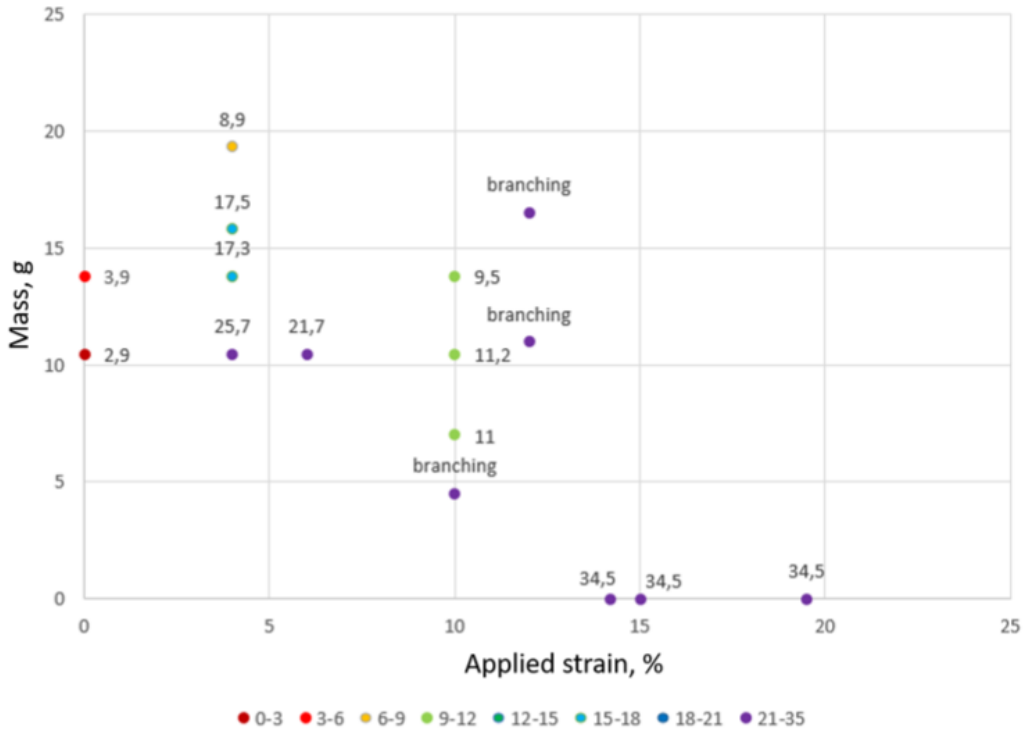

Figure 4.22: Sketch of traction test representing the possible angle interval, with the dashed line representing the crack propagating at an angle θ.

A test was also conducted with a mass of 4.5g and a strain of 10% to determine a lower limit of possible values. The results indicate that, for this mass, the wire struggles to propagate the crack in the gelatin, ultimately leading to branching, with the wire remaining immobile in the gelatin (Fig.**??**). Therefore, the mass values will be chosen to be greater than 4.5g. When the mass increases, the angle decreases, and when the deformation increases, the angle increases. Around 10% deformation, the measured angle values decrease instead of increasing. However, this measurement zone is close to the branching zone observed at 12% deformation, which could affect the angle values.

To find a balance for cutting by wires with different weights, wire weights between 13g and 17g were used. None of the angles measured were found to be 0 with applied strain, further affirming the presence of such a cutting effect. Different applied strain regions for two wires with different weights were obtained, where branching was observed in both cases with

applied strain over 8%. As shown in Fig.4.23, when comparing cutting angles, for a 17g wire with 2% and 4% applied strain, we observed larger angles compared to those with lighter weights.

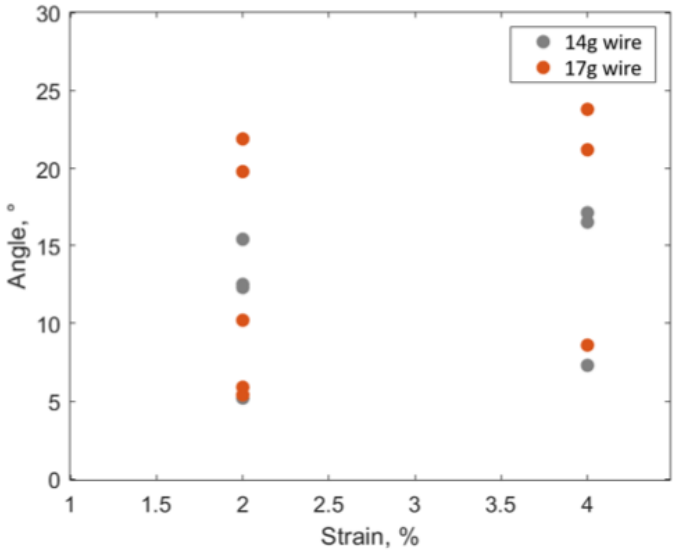

Figure 4.23: Propagation of the crack tip (dots) in gelatin gels subjected to a 2% applied strain using a 14g weighted wire, with approximation curves (lines).

4.3.5.3 Traction Tests: Instabilities

Similar instabilities to those observed in compression tests were present in the traction tests. During these tests, the wire cutting through the gelatin cube was influenced by the applied strain and the weight of the wire. Instabilities such as ”tilt” and ”twist” were observed even in a stabilized system before the beginning of the experiment. In certain experiments, as depicted in Fig.4.24, the wire exhibited bending from the center, as indicated by yellow and green arrows (Fig.4.24a and Fig.4.24b, respectively), further complicating the analysis. The mixing of Mode 1 (in-plane crack propagation) and Mode 3 (out-of-plane crack propagation) during these tests introduces additional variables that affect the stability and predictability of the cutting process.

The observed deviations in crack propagation were analyzed by measuring the angles at various points along the crack path. Measurements were taken on the upper and lower

faces, as well as the front and rear lateral faces of the cube. The relationship between these angles and the applied strain was studied to understand the instabilities better.

Determining the correct dependence of angle changes poses a significant challenge, largely due to the emergence of the third fracture mode (Mode 3) during cutting. Mode 3 appears when the crack propagates out of the primary plane of cutting, causing the wire to bend and twist, complicating the analysis. The considerable error in the angle range underscores the complexity of this phenomenon. We attribute this complexity to unknown instabilities within the gelatin cube and the imperfect toughness of the wire.

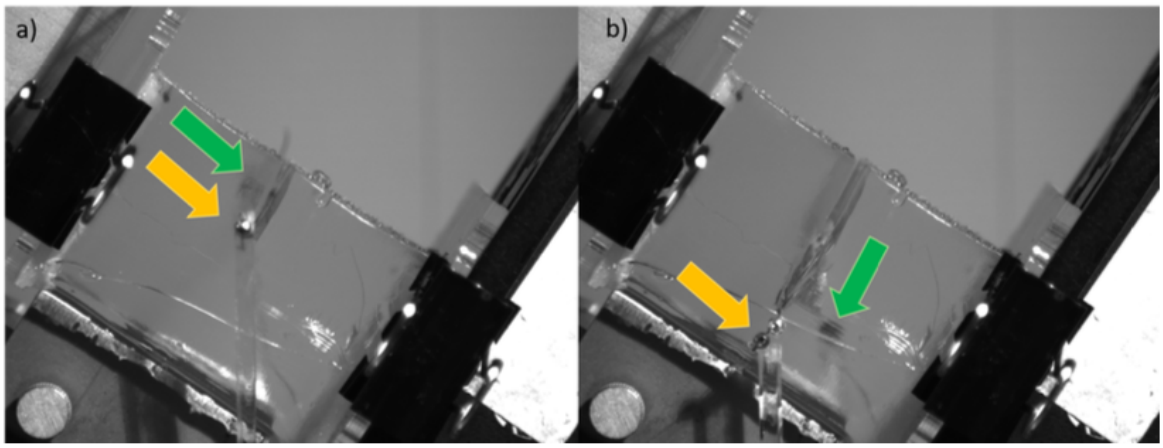

Figure 4.24: Crack profile showing a) cutting in Mode 1 and b) tilt indicating cutting in Mode 3.

The instabilities in both compression and traction tests highlight the complex nature of crack propagation in gelatin cubes under different loading conditions. By addressing these instabilities, the reliability and accuracy of the cutting process can be improved, paving the way for more precise characterization of mixed-mode behavior and the separation of the different fracture modes.

One possible effect of the appearance of these instabilities is the patterns created on the cut surfaces. The observed variation in surface patterns after cutting (Fig.4.25), depending on the applied strain, highlights an intriguing finding. Although the literature often attributes these patterns solely to the applied force on a hydrogel, our results suggest that they are

controlled by the applied strain regime. This implies that different applied strains correspond to distinct fracture propagation behaviors, aligning with investigations documented in the literature.

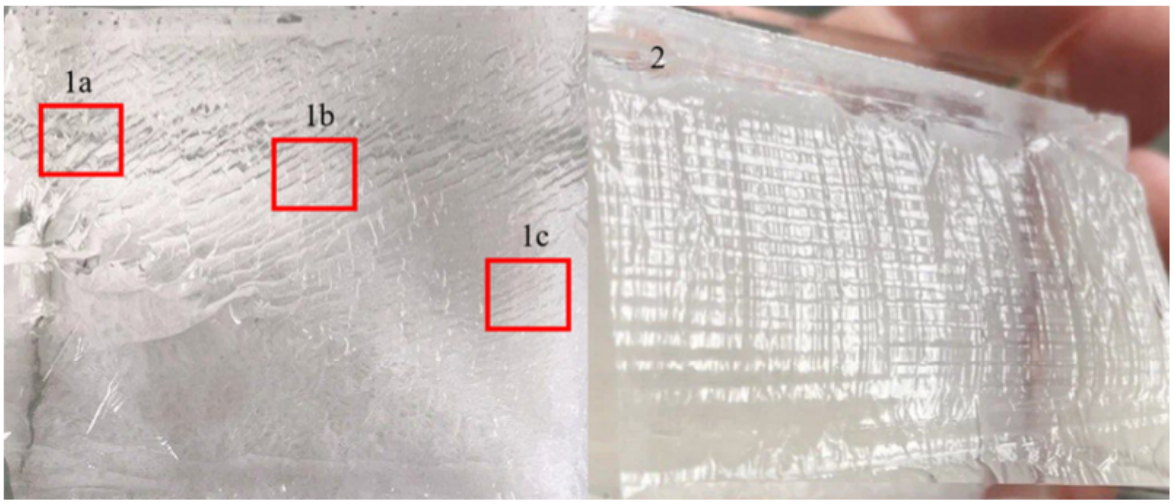

Figure 4.25: Photo of surface patterns after cut in different applied strains: 1a) - 1b) rhombus-like structures, 1c) - 2) straight lines oriented at an angle to the main cut direction.

It has been demonstrated that when wires of various diameters are inserted into the sample, the cutting action gradually stabilizes to a steady state. During this phase, fracture propagation, deformation, and friction occur simultaneously. Subsequent analysis of postmortem fracture surfaces has revealed the emergence of different macroscopic morphologies, which vary depending on factors such as gel sample formulation, cutting rate, and wire diameter [82]. Representative optical microscopy images illustrating each type of morphology are provided in Fig.4.26.

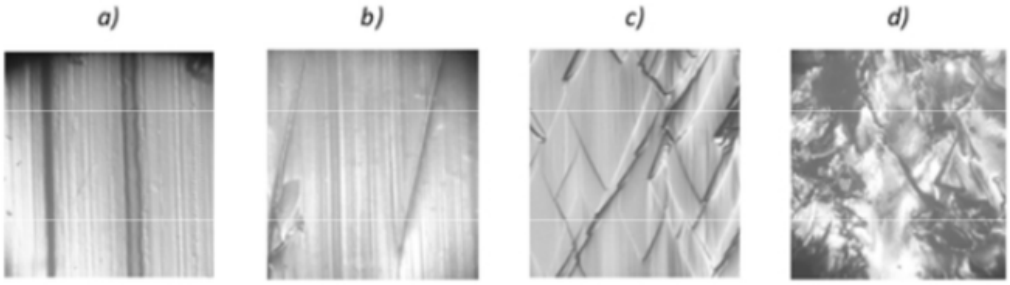

Figure 4.26: Optical microscopy images of the different fracture surface morphologies observed in different speed wire cutting experiments: a) V=25mm/min, b) V=100mm/min, c) V=5mm/min, d) V=25mm/min with another material.

These morphologies were classified according to four types that help to identify fracture propagation: 1. Wire-cut surfaces with straight lines aligned and parallel to its own direction (Figure 4.26a); 2. Surfaces after cutting have one or two straight lines oriented about 45° to the wire advance direction (Fig.4.26b); 3. Surfaces displaying regular rhombus-like structures, in which each quadrilateral figure is actually a step (Fig.4.26c); 4. Surfaces showing severe damage with material pull-out (Fig.4.26d).

The postmortem examination of the samples revealed two matching fracture surfaces that corresponded to morphologies of types 1, 2, and 3. Although the global fracture propagation direction aligned with the wire advance direction, the presence of steps on the surfaces indicated that crack propagation actually occurred with a non-planar crack front. Furthermore, in type 3 morphology, the crack front exhibited regular tilting and twisting, resulting in a crack path larger than the nominal one, as indicated by the roughness number (RN) exceeding unity. The type 4 morphology depicted in Fig.4.26d featured a mixed pattern formed by the combination of morphologies of type 1, 2, or 3 with highly stretched regions and pulled material. Interestingly, the pair of surfaces produced in one cut did not align perfectly. This phenomenon suggests that the formation of this morphology may be attributed to the adhesion between the wire and the sample materials.

The investigation of various fracture surface patterns has been extensively explored by researchers such as Tanaka et al. [83] and Baumberger et al. [84]. Tanaka initially described types 1 and 3 patterns observed in PAA hydrogels as a ”river-like pattern” and a ”scale pat-

tern," respectively. Building upon this, Baumberger et al. conducted a comprehensive study in gelatin hydrogels, revealing that crack velocities exceeding a critical threshold result in fracture surfaces appearing flat on the macroscale but exhibiting a microrough morphology. This microroughness is attributed to in-and out-of-plane deviations of the crack front line, stemming from the randomness of the network structure.

Similarly, Baldi et al. [85] reported a rhombus-like pattern for a series of PAA hydrogels. Their study demonstrated that the dimensions of the rhombus-like pattern increased with increasing wire diameter, while crack tortuosity decreased. This observation suggests that the magnitude of out-of-plane crack front deflection was lower or the heights of steps were shorter. Taken together, these findings underscore the importance of morphology studies in enhancing our understanding of the fracture process.

The stability of the system remains an open question, particularly in light of the demonstrated appearance of instability causing deflection of the crack propagation direction from the vertical gravity force direction. This finding underscores the complexity of the cutting process and highlights the need for further investigation to better understand and mitigate these uncontrolled factors.

4.4 Conclusions

This chapter has provided an investigation into the mechanics of wire-cutting in gelatin gels, focusing on the interplay between stretching and cutting loads. The experiment was designed by selecting a stiff blade, cutting under its own weight within soft gels, to ensure that only vertical friction would influence the cutting process, making it the sole factor deviating from pure cutting. Through a series of controlled experiments, several important observations have been made.

Firstly, while we expected the directionality of crack propagation to be stable, the experiments demonstrated that the cutting process in gelatin is highly sensitive to both the applied strain and the weight of the cutting wire. The experiments revealed that even small variations in these parameters could lead to significant changes in crack propagation direction

and cutting efficiency. This underscores the importance of precise control over experimental conditions when studying soft materials like gelatin.

Secondly, the study identified distinct cutting regimes depending on the strain applied to the gelatin samples. At higher strains, the wire tended to follow a more predictable path at certain angles, although it also introduced instabilities that resulted in more complex, often non-linear crack propagation. These findings enhance our understanding of the conditions under which stable versus unstable cutting occurs, which is crucial for applications where precision is critical.

Additionally, the work has highlighted the inherent challenges in predicting crack propagation paths when dual loading conditions—stretching and wire weight—are present. The findings suggest that the interaction between these forces can lead to competition between different crack propagation directions, further emphasizing the complexity of fracture mechanics in soft materials. These insights provide a foundation for developing predictive models that integrate mixed loading conditions, offering potential benefits for applications in industries such as biomedical engineering, where precise cutting of soft materials is essential.

The novel experimental design allowed for the observation of surface instabilities and trajectory perturbations, which are likely linked to fundamental material properties such as elasticity, toughness, and the interplay of strain and fracture dynamics. These observations could have implications for improving material design, optimizing cutting tools, and tailoring processes to achieve desired outcomes in industrial and medical applications.

Future research could build on these findings by exploring the influence of different material properties—such as viscoelasticity or heterogeneity—and environmental conditions, including temperature and humidity, on the cutting behavior of soft gels. Investigating additional cutting configurations, such as varying wire shapes, sizes, or loading angles, could further expand our understanding of fracture mechanics in soft materials. Furthermore, the development of computational models to simulate crack propagation under dual loading conditions would complement experimental work, enabling more precise control and prediction of cutting outcomes in soft materials.

By integrating these insights, the study contributes to advancing both the theoretical understanding and practical applications of cutting processes in soft materials, paving the way for innovations in material science and engineering.

Annexes

Annex 1: Crack Propagation in a Cube Subjected to Uniaxial Tensile/Compressive Stress

Case of Uniaxial Compressive Stress

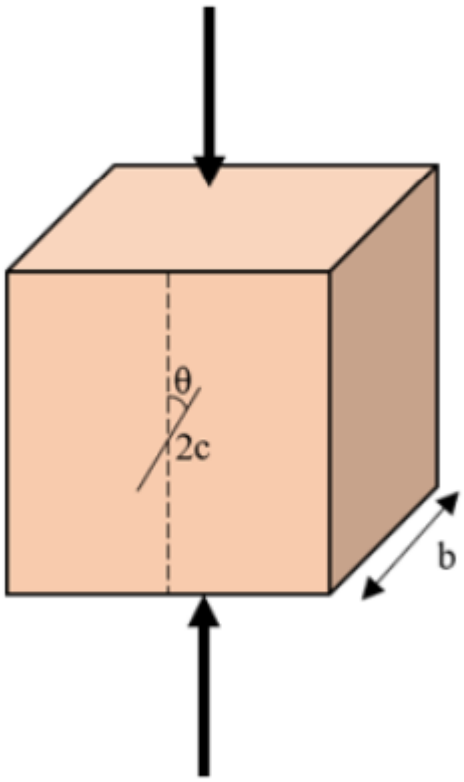

Figure 4.27: Sketch of traction test representing the possible angle interval, with the dashed line representing the crack propagating at an angle θ.

The stress tensor (in the absence of a crack) is given by:

$$\sigma = \begin{pmatrix} 0 & 0 \\ 0 & -\sigma \end{pmatrix}$$

The presence of a crack creates a free surface on the lips of the crack, making the tangential stress at that location zero, thereby locally relaxing the elastic energy.

The normal component to the crack is:

$$\sigma_{tn} = \begin{pmatrix} \cos\theta \\ \sin\theta \end{pmatrix} \cdot \sigma \cdot \begin{pmatrix} -\sin\theta \\ \cos\theta \end{pmatrix} = -\frac{\sigma}{2}\sin 2\theta$$

The elastic energy density is:

$$U_{el} \sim \frac{\sigma_{tn}^2}{E}$$

This elastic energy density is applied in a Saint-Venant zone with a diameter of $2c$ and a depth b, which gives:

$$\Delta U_{el} \sim -U_{el}\pi c^2 b$$

Since the work of external forces is zero, we have:

$$G = \frac{\Delta U_{el}}{bc}$$

Case of Uniaxial Tensile Stress

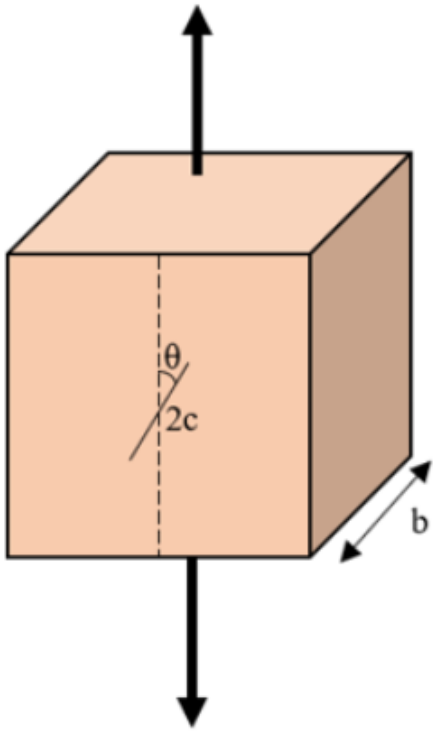

The stress tensor (in the absence of a crack) is given by:

$$\sigma = \begin{pmatrix} 0 & 0 \\ 0 & \sigma \end{pmatrix}$$

The presence of a crack creates a free surface on the lips of the crack, making the normal stress at that location zero, thereby locally relaxing the elastic energy.

The normal component to the crack is:

$$\sigma_{nn} = \begin{pmatrix} -\sin\theta \\ \cos\theta \end{pmatrix} \cdot \sigma \cdot \begin{pmatrix} -\sin\theta \\ \cos\theta \end{pmatrix} = \sigma \cos^2\theta$$

The elastic energy density is:

$$U_{el} \sim \frac{\sigma_{nn}^2}{E}$$

This elastic energy density is applied in a Saint-Venant zone with a diameter of $2c$ and a depth b, which gives:

$$\Delta U_{el} \sim -U_{el}\pi c^2 b$$

Since the work of external forces is zero, we have:

$$G = \frac{\Delta U_{el}}{bc}$$

Transition from an Angle in the Deformed Frame to an Angle in the Undeformed Frame

For all subsequent calculations, we consider linear material mechanics. Assume that the cracks in the cubes are straight lines inclined at an angle θ with the vertical. A compressive stress σ is applied along the horizontal direction $(\vec{x})$.

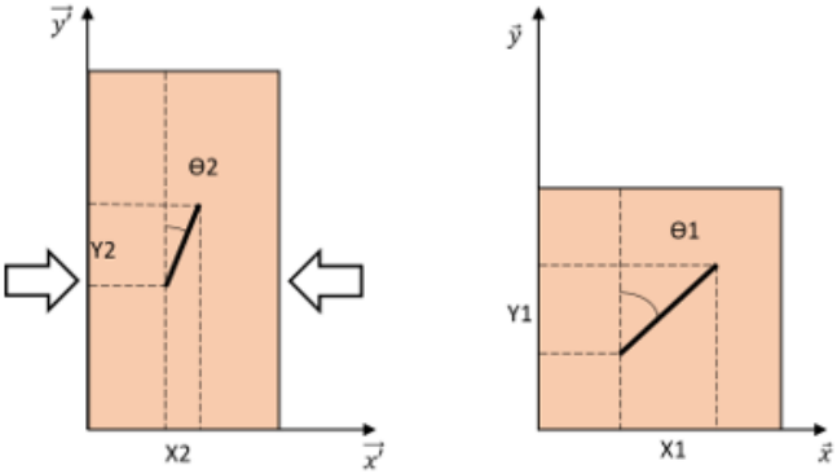

$$(\mathrm{d}\vec{x}) = \begin{pmatrix} x_1 \\ y_1 \end{pmatrix}$$

$$(\mathrm{d}\vec{x}') = \begin{pmatrix} x_2 \\ \\ y_2 \end{pmatrix}$$

We then have:

$$(\mathrm{d}\vec{x}') = (\mathrm{d}\vec{x}) + \epsilon(\mathrm{d}\vec{x}) + \theta(\mathrm{d}\vec{x})$$

Since there is no rotation, $\theta = 0$.

The strain tensor being:

$$\epsilon = \begin{pmatrix} \frac{\nu\sigma}{E} & 0 \\ 0 & -\frac{\sigma}{E} \end{pmatrix}$$

We obtain the relation:

$$\begin{pmatrix} x_2 \\ y_2 \end{pmatrix} = \begin{pmatrix} x_1\left(1 - \frac{\sigma}{E}\right) \\ y_1\left(1 + \frac{\nu\sigma}{E}\right) \end{pmatrix}$$

Hence the equation:

$$\tan(\theta_1) = \tan(\theta_2)\frac{1 - \frac{\sigma}{E}}{1 + \frac{\nu\sigma}{E}}$$

Chapter 5

Cutting elastomer's bar on the edge

5.1 Introduction

In the progression of this thesis, each chapter has incrementally advanced our understanding of cutting mechanics in soft materials, gradually introducing more complex experimental setups. Chapter 2 focused on pure shear cutting with a fixed blade path, providing insights into the interaction of fracture mechanics and cutting forces. Chapter 3 extended this concept by allowing the cutting wire to move freely under gravity, enabling it to choose its path through the material. This freedom revealed valuable insights into how soft materials like gelatin respond to mixed loading conditions and directional freedom during cutting.

Building on these foundations, this chapter introduces a new experimental approach, further increasing the complexity of the cutting process. Unlike previous setups, where the cutting element (blade or wire) followed a predefined or freely chosen trajectory, this chapter explores a scenario specific to elastic materials, such as PDMS, where the blade itself is given flexibility. However, this flexibility must be balanced with sufficient stiffness to ensure that the blade can still cut through the material effectively. The motivation for this experiment arises from the need to study how a flexible blade can respond to and adapt its cutting path in elastic materials, while still maintaining the ability to propagate a cut.

Inspired by everyday cutting experiences, such as slicing mozzarella or roast beef, we observe that achieving a straight, clean cut in soft materials is often challenging due to

deformation. These materials tend to deviate from the intended cutting path, leading to non-planar, irregular shapes. Translating these observations into a controlled experimental framework, this study aims to understand the interplay between the elastic deformation of the material and the blade's flexibility during cutting.

To investigate this phenomenon systematically, we developed we developed a series of controlled experiments using well-defined sample geometries and cutting fixtures (Fig.5.1). This configuration allows the blade to bend and adapt to the material's deformation, enabling it to choose its cutting path. We vary the cutting parameters and observe the resulting shapes.

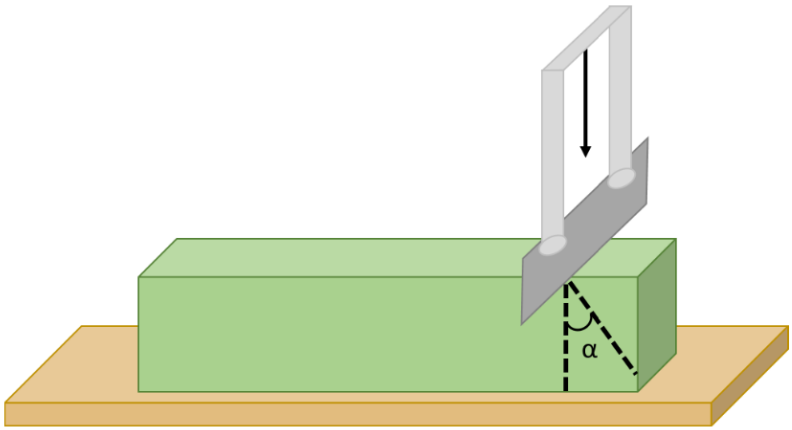

Figure 5.1: Schematic representation of blade cutting on an edge with a flexible blade fixture. The deformation of both the sample and the blade during the cut leads to a change of the cutting plane towards an angle α with respect to the vertical direction of actuation of the blade.

A central concept in our study is the comparison between the cutting distance d from the edge and angle α relative to the vertical axis of the blade's actuation. When in the text use in line equations such as $\frac{\Gamma}{E}$, where Γ represents the fracture energy of the material and E is the Young's modulus. This material's length scale, recently named the tomoelastic length (l_{TE}) [48], is crucial for understanding cutting behavior. Specifically, it defines a threshold length scale below which the chips undergo large strains during cutting, leading to significant morphogenesis—i.e., chip shapes that different from the target shape defined by the blade's

path. When $d < l_{TE}$, the energy cost for cutting becomes larger than the one for deforming the sample, leading to larger variations of the angle α defining the final shape of the chip (Fig.5.1). This scenario is of particular interest in the context of material cutting where precision and predictability of the chip shape are a fundamental target.

In this work, we aim to quantify this behavior, building on the findings from the "Soft Coring" study [48], which demonstrated that when coring a soft material with a stiff cylindrical blade, the shape of the resulting chip differs significantly from the target cylindrical shape due to large strains during cutting (Fig.5.2). We explore this morphogenetic effect in detail for a specific elastomer E22 (already characterized in previous chapters). By normalizing the data with d/l_{TE}, we hope to collapse these responses onto a master curve, providing a unified framework for understanding the cutting behavior across various materials.

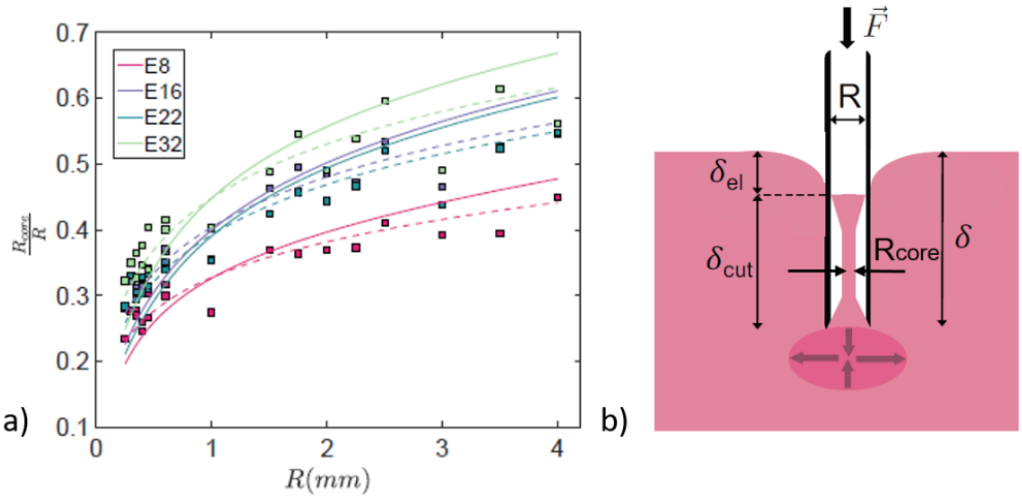

Figure 5.2: (a) Measured coring ratios plotted against the radius of the cylindrical blade. (b) A sketch illustrating the morphogenesis in the coring mechanism [48].

In this chapter, we also try to separate the morphogenetic effects induced by the sample deformation and by the blade deflection, by using two different blade fixtures with different bending stiffness. For stiff blades, the primary parameters of interest are d and l_{TE}, which govern the sample deformation during the cutting. In such cases, we expect a simpler relationship where d/l_{TE} serves as a universal parameter, allowing us to compare cutting

across different materials and conditions.

On the other hand, when dealing with flexible blades, an additional factor—the bending stiffness B of the blade fixture—must be considered. he bending stiffness can be approximated by $B = E_b I_b$, where E_b is the Young's modulus of the PMMA fixture and I_b is the second moment of area of the blade's cross-section, introduces a new length scale into the problem. This complicates the dimensional analysis and requires a more nuanced approach to understand the combined effects of blade and sample deformation.

One of the central questions in this chapter revolves around the origin of morphogenesis during cutting. Morphogenesis, in this context, refers to the complex shapes and surface patterns that emerge when cutting soft materials. A first basic approach for understanding morphogenesis is analyzing the symmetry of the problem. In an ideal symmetric system, like if we perform the vertical cut in the middle of the sample, one would expect a straight path of the cutting in both the deformed and undeformed reference frame (which sets the shape of the chip). However, experimental observations often reveal deviations from symmetry when cutting near an edge. These non-linearities are likely driven by the interaction between the elastic properties of the material and the fracture processes initiated by the blade. Even in the absence of a comprehensive model, we hypothesize that the interplay between these factors is responsible for the observed morphogenetic patterns.

While a global model describing the entire cutting process is beyond the scope of this chapter, fracture mechanics offers valuable tools for interpreting the observed phenomena. The crack path or cut can be influenced by factors such as the stress intensity factor, energy release rate, and the material's resistance to crack propagation. By applying these concepts, we can begin to describe the conditions under which the crack path deviates from the expected planar (or cylindrical in coring), leading to the emergence of complex cut profiles or chip shapes.

Understanding the role played by fracture mechanics in these processes is crucial for developing predictive models that can accurately describe cutting behavior and chip shapes in soft materials. Future work may involve developing a quantitative estimation of the hyperelastic deformation of the material, the bending stiffness of the blade, and the energy

considerations from fracture mechanics to fully capture the cutting dynamics.

5.2 Materials and Methods

5.2.1 Materials

5.2.1.1 Material Preparation

The first investigation of this cutting geometry was conducted using alginate ARTPRO. Young's modulus is 20 $\pm$ 4 kPa. The alginate powder was prepared by mixing it with water in a 1:3 weight ratio, followed by centrifugation to ensure homogeneity, employing mixing balls to enhance the uniformity of the solution. The resulting alginate mixture was then promptly poured into the designated mold with size 3.85 cm x 12.3 cm and adjustable height. This mixture transitions into a gel-like state within a matter of minutes and remains usable for up to six hours post-preparation, beyond which it begins to solidify, eventually drying out completely after approximately 24 hours. Throughout the six-hour window, no substantial changes in the material's consistency were observed, allowing for reliable experimentation within this timeframe.

In the second investigation, polydimethylsiloxane (PDMS) silicones were employed, specifically the Zhermack Double Elite with a Shore A hardness of 22, with the Young's modulus 709 kPa (Fig.5.3). The material was chosen for its suitability in precision molding applications and also to compare with other chapters and to have time independent samples. These silicone elastomers were thoroughly introduced and characterized in Chapter 1. The preparation of PDMS samples involved mixing the liquid base component with its corresponding crosslinker in a 1:1 ratio by weight, ensuring a consistent and uniform elastomeric material upon curing. The resultant samples were cast into rectangular blocks, each measuring 123 mm in length, 38.5 mm in width, with variable heights ranging from 19 mm to 50 mm.

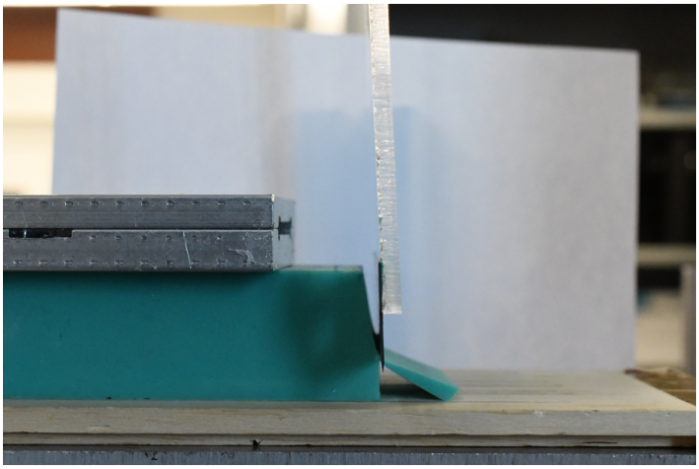

Figure 5.3: PDMS sample after testing.

5.2.1.2 Mold Fabrication

The molds used in the experiments were initially fabricated from polymethyl methacrylate (PMMA), designed as rectangular containers with base dimensions of 3.85 cm x 12.3 cm, while the height (H) was adjustable. However, with changing the materials to PDMS, this mold design encountered several significant challenges, particularly in demolding samples with heights exceeding 2 cm. Additionally, the interaction between the material and the mold during the crosslinking process led to the formation of a meniscus along the borders, adversely affecting the sample's surface geometry.

To mitigate these issues, a new mold was developed, also constructed from PMMA (Fig.5.4). This improved design comprised four laser-cut pieces, with dimensions of 8.5 cm x 13 cm and 4.5 cm x 13 cm, which were assembled by adhering the sides together to form two vertical corners. The mold surfaces were further lubricated by applying a thin layer of Vaseline to the inner surfaces, reducing friction and aiding in the demolding process. Additionally, the use of clamps allowed for manual adjustment of the mold height, offering greater flexibility in sample preparation. This design effectively eliminated the formation of menisci on the lateral surfaces, resulting in samples with flat, uniform surfaces and more consistent geometric properties.

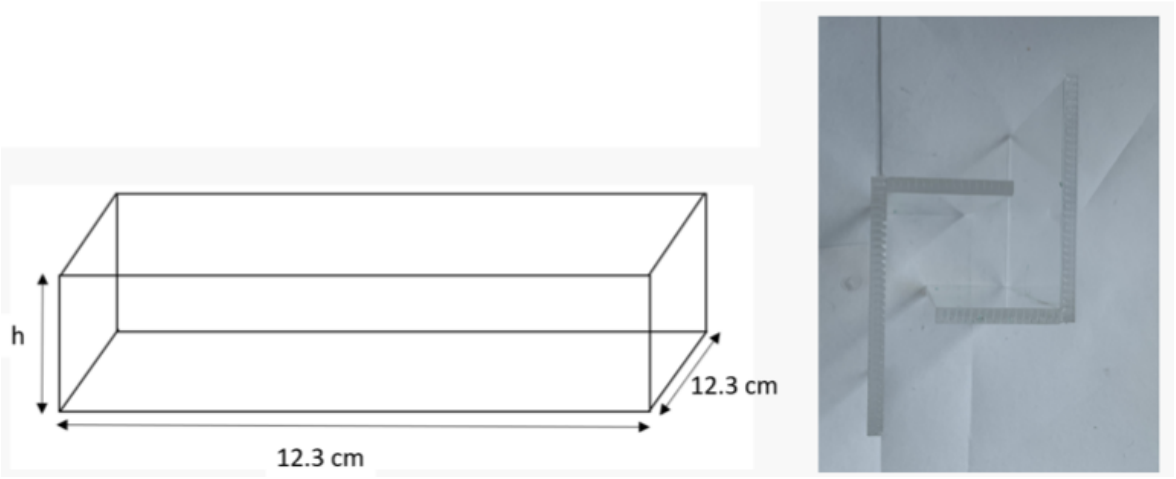

Figure 5.4: Mold for sample preparation.

This enhanced mold design not only facilitates easier demolding but also ensures precise control over sample geometry, thereby improving the reliability and reproducibility of the experimental results.

5.2.1.3 Blades with flexible fixture

Our initial idea was to have a vertical elongated blade that is stiff enough to cut when moved vertically against the sample, yet allowing for some lateral bending during the cutting. Since it was very difficult to achieve this with a single material, we developed a custom fixture made of a rectangular U shaped PMMA frame that is clamped on one side into an Instron machine grip and glued on the other side on a sharp steel blade (Fig.5.5a,b). The bottom side of the frame is missing to glue the blade, and to avoid encumbrance during the cutting of the sample.

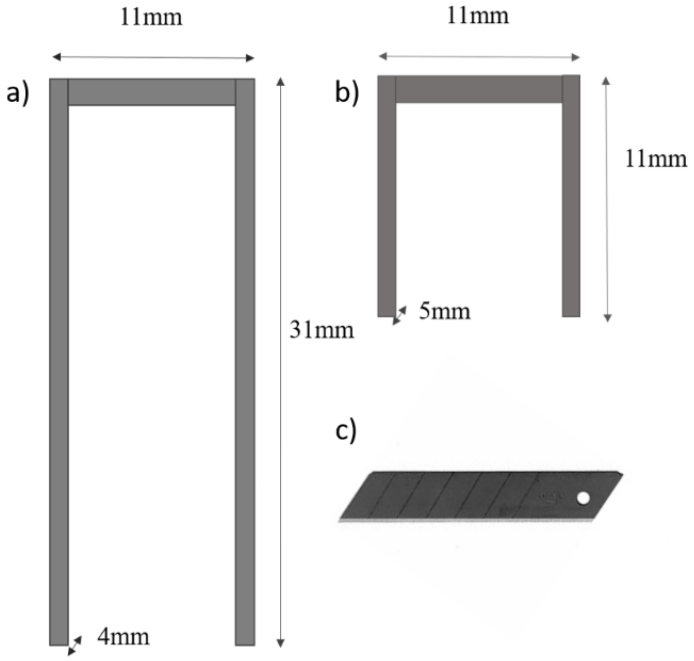

Figure 5.5: Blade fixtures representing (a) a softer holder, (b) a stiffer holder, and (c) the blade used for cutting tests.

We designed ”softer”(on the left Fig.5.6) or ”stiffer”(on the right Fig.5.7) fixtures based on their respective flexibilities. These blade holders, made via laser cutting, varied in length and thickness to control the flexibility of the blade.

A single type of blade was selected for all experiments—an alloy steel paper-cutting blade (LEDLUX) measuring 13 mm in length, 25 mm in width, and 0.7 mm in thickness, with a tapering angle of 30 (Fig.5.5c) and blunting radius $1\mu m$.

This setup permitted the study of how blade bending during cutting impacts the shape of the chips. It was observed that when cutting a soft material close to the edge, the resulting chip’s shape is not straight and varies depending on the distance d from the edge.

In the Fig.5.6, the softer blade holder is shown to bend during the experiment, causing the blade to cut at an angle relative to the vertical axis.

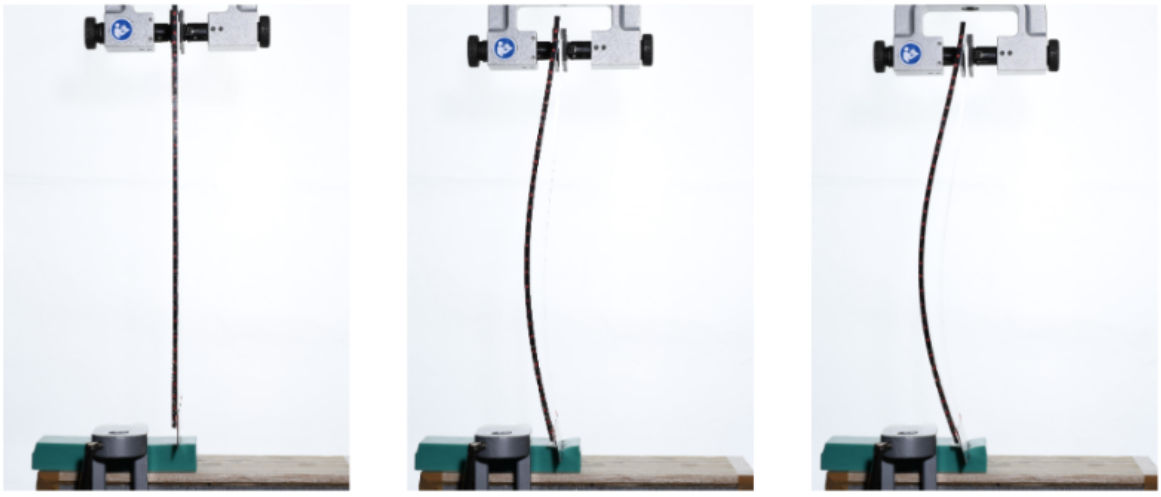

Figure 5.6: The softer holder bending during the experiment, leading to angled cuts. The sequence shows: 1) the position of the blade before contact with the sample surface, 2) initiation of the cutting, and 3) cutting in progress.

The following Fig.5.7 demonstrates the use of a stiffer mold, which minimizes deviation from the vertical axis throughout the cutting process, resulting in a less deformed chip.

Figure 5.7: The stiffer holder bending during the experiment, leading to angled cuts. The sequence shows: 1) the position of the blade before contact with the sample surface, 2) initiation of the cutting, and 3) cutting in progress. .

5.2.2 Methods

The experimental setup consisted of a blade with a holder and a cutting basement. The platform was constructed from stacked metal plates covered with plywood to prevent damage on the blade. To ensure the stability of the sample during cutting and prevent it from tipping, an additional clamp was designed to keep the remote part of the sample flat (Fig.5.6, 5.7).

This clamp did not exert any force on the sample when at rest, but effectively prevented one end of the sample from lifting off the platform during cutting, thereby maintaining stability without significantly affecting the forces applied to the sample.

Cutting tests were conducted using an Instron machine, with the sample secured between two stages. The sample was fixed to a plywood platform with the clamp described above, while the blade holder was attached to a 1 kN load cell, which applied a constant vertical displacement rate of 2 mm/min. The sample was positioned in such a way that the blade starts to cut at a distance d from the edge, that is analogous to the ”depth of cut” in orthogonal cutting of metals. This also sets the thickness of this chip/slice.. The experimental setup provided data on the force-distance curve within the sample, all along the cutting process through the sample.

Imaging during the experiments (Fig.5.6, 5.7) was carried out using a Nikon D300 camera equipped with a 55-200 mm lens. The camera was mounted on a tripod and connected to a computer, with LiveCam software facilitating image acquisition and time-lapse recording to thoroughly document the experimental procedures and to determine the shape of both the blade bending, the blade path and the sample deformation during the tape.

5.3 Results and Discussion

5.3.1 Cutting Tests

The initial results were obtained by Oriane Devigne during an internship. Typical force-displacement curves, measured using the Instron, are illustrated in Fig.5.8. Initially, the force-displacement curve $F\delta$ follows a power-law relationship $\delta^{1.2}$, as indicated by the red line in Fig.5.8.

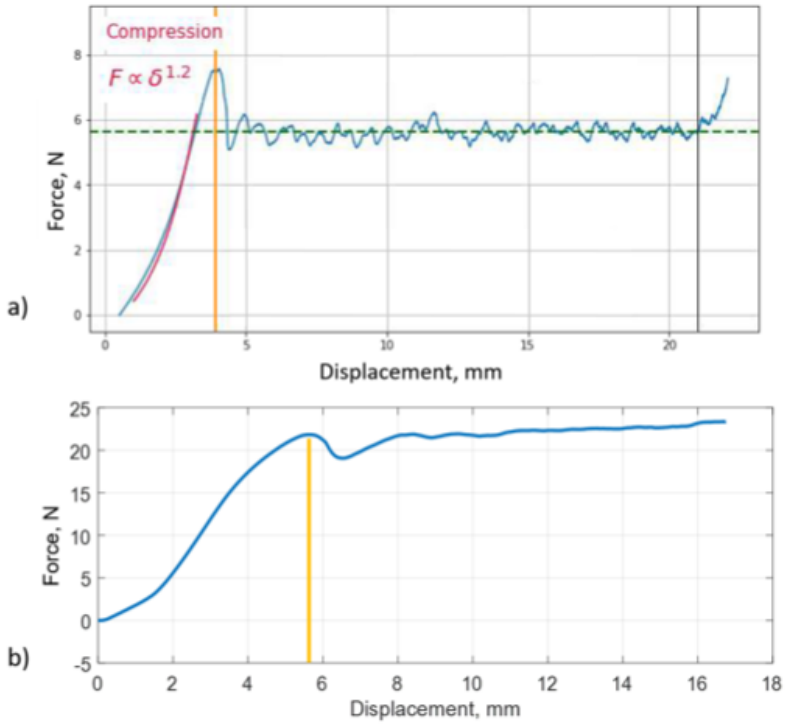

Figure 5.8: Force-displacement curve illustrating the phases of a) alginate cutting and b) PDMS cutting.

This phase corresponds to elastic indentation [27]. McCarthy reported partial cutting during this phase, where the stiction of the blade on the sample prevents smooth movement through the material. Initially, elastically deforming the sample requires less energy than cutting and overcoming friction. However, as deformation continues, it becomes more efficient to drive the blade through the sample. At the force peak, the blade penetrates the sample (indicated by the vertical yellow line in Fig.5.8). In case of alginate the cutting force then decreases and stabilizes to nearly constant values during cutting (shown in green in Fig.5.8a), while for PDMS cutting friction affects more the cutting and we see s small slope on the curve (Fig.5.8b). Slight oscillations in the force are observed due to the small amplitude stick-slip phenomenon in alginate cutting, while no stick-slip is observed in PDMS samples.

Even with a stiff, vertically moving blade, the deformation of the soft sample during the

cutting can lead to asymmetry in the cut surfaces. Remarkably, the cut surfaces are generally planar but tilted, and can be described by the angle α formed with the vertical axis after the end of the cutting process (Fig.5.9a). However, in approximately 15% of all cutting measurements, the cut surfaces deviate from planarity, sometimes exhibiting a parabolic trend (Fig.5.9b). Despite these deviations, a first-order fit of the angle α is used to explore its trend with the loading parameters.

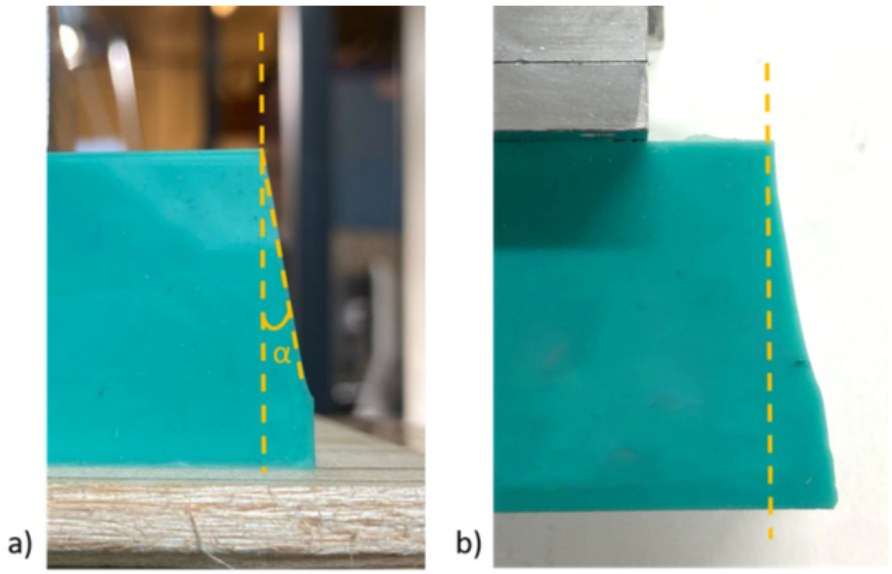

Figure 5.9: Illustration of (a) linear and (b) parabolic cutting profiles of samples at 5mm and 7mm of chip initial thickness, respectively.

The results may vary depending on the mounting orientation (left/right) or the shape of the sample. To assess the influence of blade asymmetry resulting from manufacturing, the experiment was conducted with both orientations (left/right). The data exhibit affine curves on the log-log scale (Fig.5.10). A power-law fit of the form:

$$\text{fit}(d) = \alpha$$

was applied to the data.

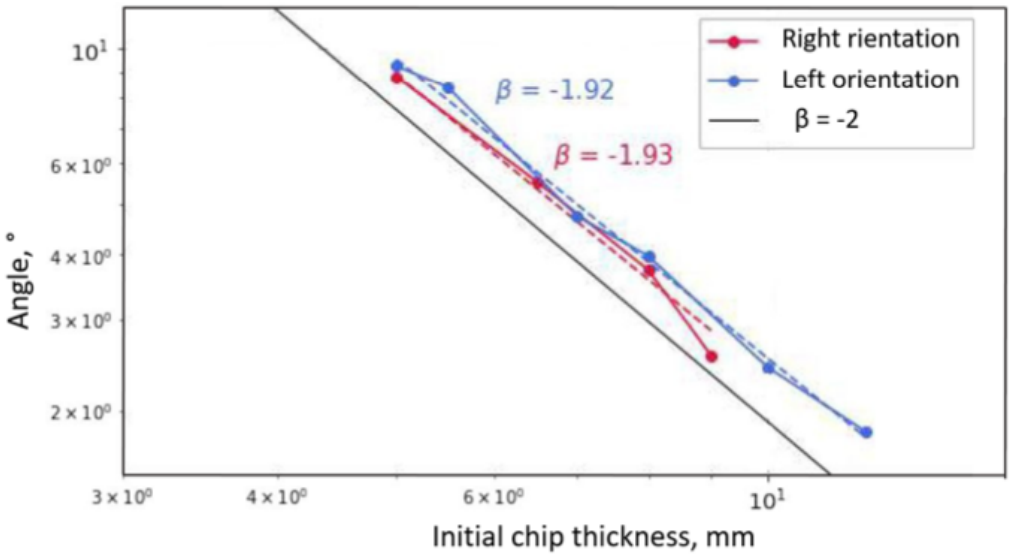

Figure 5.10: Results of alginate cutting experiments with different blade holder orientations using the softer holder.

In Fig.5.10, the power law exponent for cutting on the right side is -1.93, while on the left side, it is -1.92, resulting in a relative difference of 0.5%. Given the uncertainties involved, we can conclude that the direction of the experiment does not significantly affect the relationship between α and d.

The measurements on the PDMS samples were performed by an intern Adele Abada. To investigate the influence of blade flexibility on cutting angles, experiments were conducted using both softer and stiffer blade holders. The results show larger chip angles when using the softer blade at comparable distances d from the edge as depicted in Fig.5.11a and Fig.5.11b.

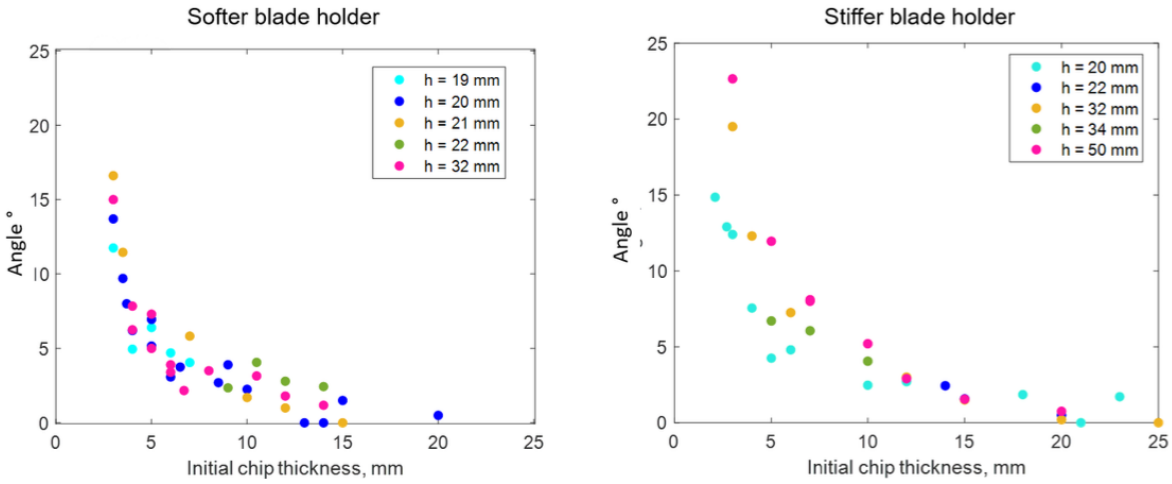

Figure 5.11: Different angles of chips observed after cutting samples E22 experiments with softer and stiffer blade holders as a function of the distance d from the edge.

Fig.5.11 also reports the data for samples of different heights h. The overall trend does not seem to be significantly affected by the variation of the sample height. However, for the stiffer blade, we can observe a weak tendency to increase the chip angle with the sample height.

The results of the cutting experiments with softer and stiffer holders are plotted on a log-log scale in Fig.5.12. The power-law exponent for cutting with the softer blade is -1.6 ± 0.3, while for the stiffer blade it is -1.1 ± 0.2.

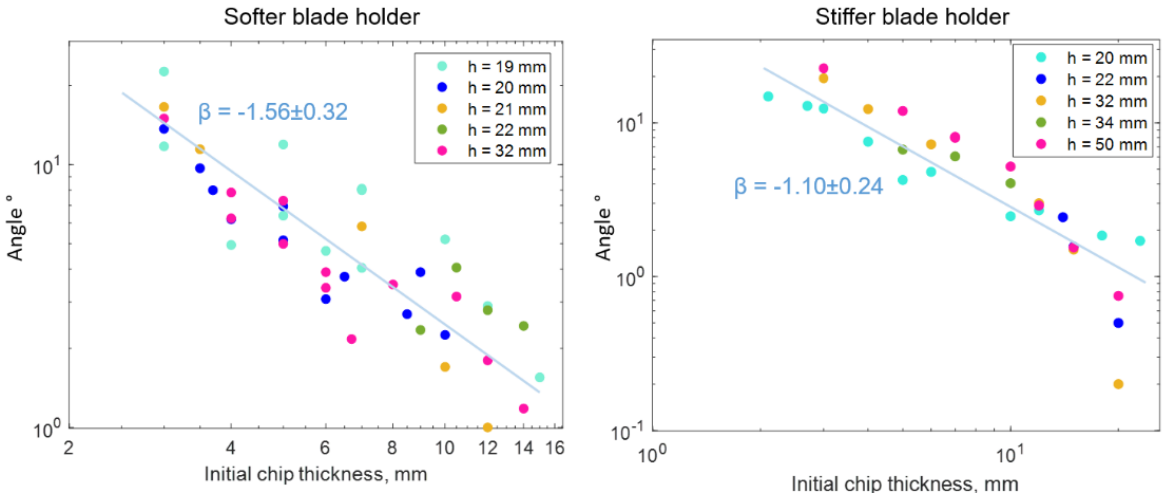

Figure 5.12: Log-log scale comparison of cutting samples E22 experiments with the softer blade holder.

These findings suggest that the flexibility of the blade has an impact on the cutting angles.

The combined results for the softer blade holder with both alginate and PDMS show a similar trend of cutting at different sample heights, as shown in Fig.5.13, where the power-law exponent is -1.5 ± 0.3.

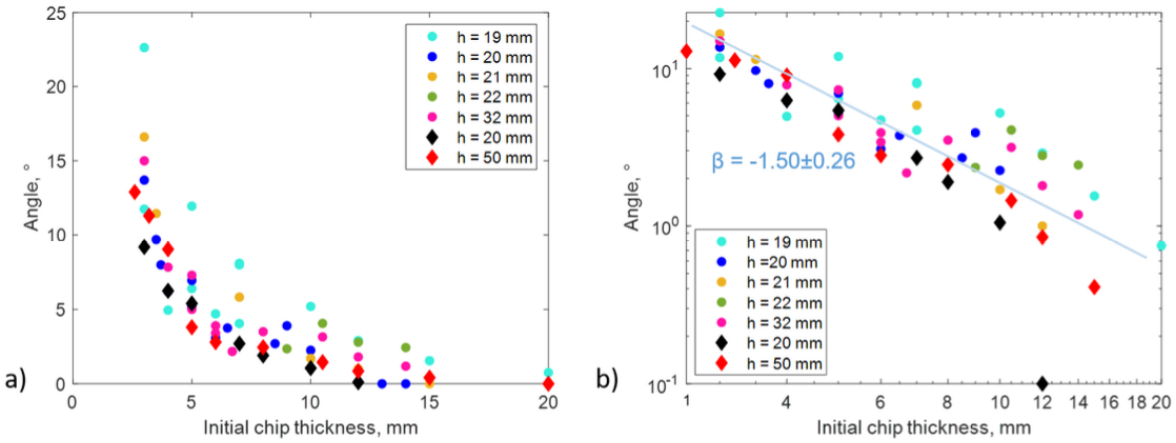

Figure 5.13: Comparison of cutting angles observed after experiments with the softer blade holder for ∘ PDMS and ♢ alginate.

Understanding the role of blade flexibility is crucial for accurately interpreting cutting angle data in studies of soft materials. The observed differences highlight the importance

of considering blade characteristics in experimental setups to ensure consistent and reliable results in research on cutting mechanics.

When cutting a PDMS sample with a softer holder, we observed a stronger trend of increasing force, reaching up to 15 mm as the chip thickness increased (Fig. 5.14). In contrast, with a stiffer holder, this threshold appears at nearly 5 mm.

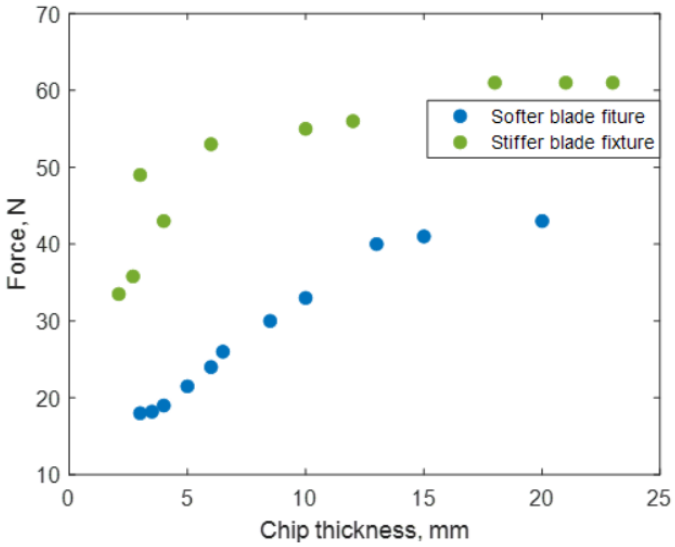

Figure 5.14: Different force measurements observed after cutting samples in E22 experiments as a function of the distance d from the edge.

If we consider the energy balance in the system while cutting just started the total energy release rate can be expressed as:

$$G = \frac{\delta U_{el}}{\delta A} + \frac{\delta W}{\delta A} = \Gamma_{\text{cut}} + \Gamma_{\text{friction}}$$

where $\frac{\delta U_{el}}{\delta A}$ decreases with reducing chip thickness for both softer and stiffer blade holders, while the work done by the blade is calculated as the ratio of the applied force F and the width b of the sample.

That could suggest that the trend that we see on the graph comes from two different possibilities: either Γ_{friction} is increasing, or there is a negative term in G that decreases with chip size, driving the energy away. This term is the elastic part of the energy, which

represents the energy stored in the material due to elastic deformation.

As the blade penetrates further, more energy is stored elastically; part of the work is converted into elastic energy. To achieve the same Γ_{cut}, if there is no significant friction effect, the force required for cutting would need to increase.

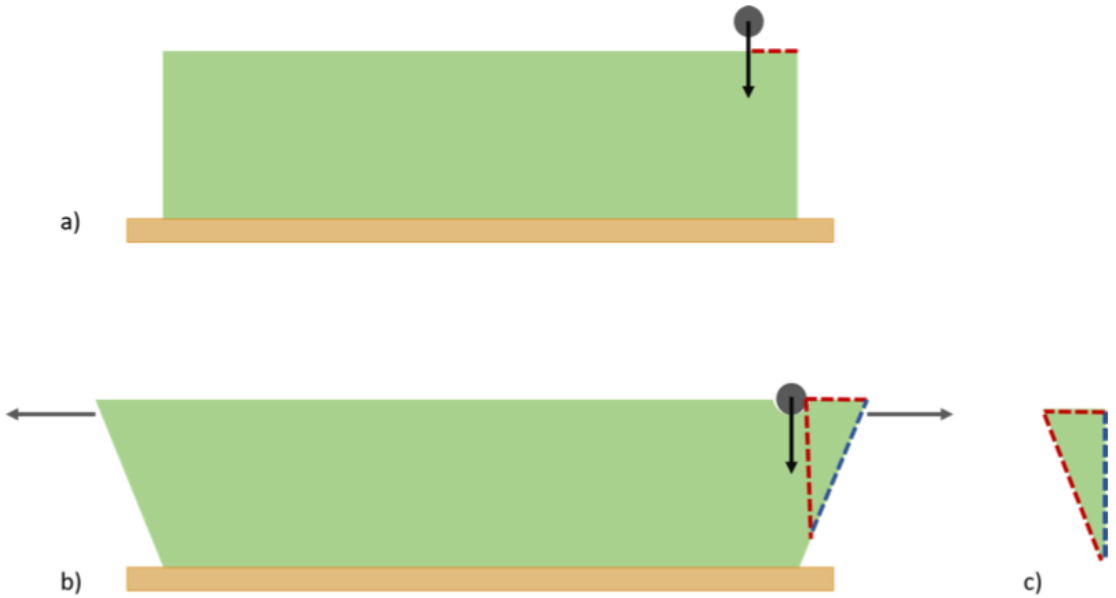

Figure 5.15: a) Original sample before the blade contacts the border, b) the blade moves into the sample, causing the sample to stretch under pressure after contact, until the cut is initiated and c) fragment of the sample after cutting.

Cutting generally maintains a steady cutting force. However, as the material becomes softer, the elastic energy increases. When cutting near the border, the sample behaves as if it is even softer, leading to higher strains and, consequently, higher elastic energies. This increase in energy could result in a negative G component.

Once cutting begins, the cutting force reaches a plateau, and the material can no longer be stretched further. During this phase, the bending remains constant, and the blade moves almost straight, as illustrated in the sketch (Fig. 5.15).

5.4 Conclusions

In this chapter, we designed an experiment to investigate the interplay between blade flexibility, material deformation, and cutting path, building on the insights from previous chapters. The introduction of a flexible blade holder allowed us to guide a stiff blade along a desired cutting path while maintaining the rigidity necessary for effective cutting. If the blade lacked stiffness, the cutting path would primarily be dictated by the back of the blade rather than the cutting edge, leading to significant nonlinear effects. These nonlinearities are central to the generation of the final chip shapes.

Our findings reveal that even when the curing process is locally symmetric, unwanted lateral deviations often arise. These deviations result from a combination of the nonlinear large deformation of the soft sample and the flexibility of the blade. Together, these effects play a critical role in shaping the cutting profile.

We propose that the dimensionless parameter d/l_{TE} is pivotal in understanding the cutting behavior of soft materials. This ratio is crucial because it defines the transition scale from a regime dominated by large elastic deformation to one governed by fracture mechanics. When d/l_{TE} is small, the forces required to provide the cutting energy are large enough to generate large strains of the whole chip.

For PDMS E22, with $\Gamma = 750 \pm 40\,\text{J/m}^2$ and $E = 709\,\text{kPa}$, corresponding to a tomoelastic length $l_{TE} = 1\,\text{mm}$, we observed persistent morphological changes up to a cutting distance $d = 15\,\text{mm}$. By comparing chip thickness with l_{TE}, we identified conditions under which morphogenesis arises.

As d/l_{TE} decreases, the material's tendency to follow a straight crack path diminishes, leading to complex cutting profiles. This behavior is indicative of a regime where the fracture energy cost is more significant than the energy to induce large strains, resulting in large deformation angles and potentially nonlinear crack paths. The experimental observations of morphogenesis in our samples can be attributed to this shift in the balance between elastic and fracture energies.

When considering flexible blades, the situation leads to increasing non-linearity. The

bending stiffness B of the blade introduces an additional length scale, complicating the dimensional analysis with respect to the stiffer blade scenario. Unlike the stiffer blade scenario. The bending of the blade can introduce further nonlinearity and larger shape changes.

Our results show that the softer blade holder tends to produce less pronounced cutting angles compared to stiff blades, particularly at smaller distances d more from the edge. This allows to obtain larger strains in the sample during the cutting process. The stiffness of the blade plays a critical role in inducing or preventing morphogenesis during cutting. While our primary goal is to avoid morphogenesis, which leads to unwanted issues, studying these effects requires us to intentionally create them. Therefore, our experimental setup was not optimized for ideal cutting but rather for studying these phenomena and understanding how to model and eventually avoid them. Although we have not yet developed a comprehensive model, our findings indicate that for achieving clean cuts, minimizing morphogenesis is crucial. Specifically, with softer materials, the cutting length is limited when attempting to create straight slices.

Chapter 6

General Conclusions and Prospects

Final remarks: This dissertation has investigated the intricate mechanics of cutting soft materials, focusing on polydimethylsiloxane (PDMS), gelatin, and alginate. Across the three experimental projects, a unifying theme emerged: the discovery and analysis of non-linear effects that arise during cutting processes and their role in generating complex morphogenetic features in the resulting chip shapes. These findings provide critical insights into the interplay between material deformation, fracture mechanics, and cutting tool dynamics.

In **Chapter 2**, the research concentrated on the cutting of thin PDMS elastomer sheets. The study systematically analyzed the effects of blade sharpness, cutting speed, and material properties on cutting behavior. The first part of the chapter focused on quantifying cutting energy under mixed loading, combining stretching and cutting. This provided a foundation for understanding the energetics of the process. The second part identified instabilities such as out-of-plane wrinkling and in-plane oscillations, linked to the material's mechanical properties and cutting conditions. By drawing an analogy with oscillating cracks observed during the quenching of glass plates, the chapter proposed a novel perspective on the origins of these instabilities.

Chapter 3 extended the study to wire-cutting of gelatin gels, where a new experimental configuration was introduced. The cutting force was imposed, while the direction of blade motion was allowed to remain free, offering the blade ”freedom” to determine its path. This unique approach demonstrated that the directionality of crack propagation is driven by the in-

teraction between stretching and cutting contributions, which influence the blade's trajectory in different ways. The study highlighted the strong instabilities that arise from this coupling, further emphasizing the sensitivity of the cutting process to material and loading conditions.

Finally, **Chapter 4** addressed the role of blade flexibility in shaping chips during the cutting of soft elastomers near their edges. This scenario presented a significant challenge due to the coupling of nonlinear strains in the material and the bending of the blade. The experiments revealed how these nonlinear effects can cause deviations from the intended cutting path, resulting in morphogenesis and reduced precision. By introducing the dimensionless parameter d/l_{TE}, where l_{TE} is the tomoelastic length, the study provided a framework for understanding the transition between regimes dominated by elastic deformation and those governed by fracture mechanics. The chapter further highlighted the impact of blade stiffness, showing how softer blade holders amplify nonlinearities and morphogenesis, while stiffer holders mitigate these effects.

Overall, this dissertation underscores the intricate interplay of material properties, cutting dynamics, and fracture mechanics in shaping the outcomes of cutting processes. It highlights the importance of controlling cutting parameters to mitigate unwanted nonlinearities and morphogenesis, while offering experimental and theoretical tools to guide future research. By systematically investigating a wide range of scenarios, this work contributes to the broader understanding of cutting mechanics in soft materials, with applications in manufacturing, biomedical engineering, and beyond.

Future perspectives: While this dissertation has improved the understanding of nonlinearities and instabilities in the cutting of soft materials, several avenues for future research remain. One potential direction is the development of predictive models that can predict the shape of the chips when cutting soft materials as a function of the nonlinear material properties, the shape and mechanical properties of the blade, and the specific driving of the blade. Additionally, exploring the application of these findings to other soft materials could further broaden the impact of this research.

In the cutting of thin sheets, a key area to explore is the identification and investigation

of materials with varying values of Γ/E, the tomoelastic length, which sets the characteristic length scale for the emergence of morphogenetic effects. Studying materials with a broader range of these ratios will enhance our understanding of how these properties influence cutting behavior and instabilities. Incorporating these findings into the existing model will be crucial for refining and extending its applicability across different types of soft materials. By increasing the diversity of materials studied, these models can be improved to better predict cutting outcomes and optimize processes for a wider array of materials in industrial applications.

An important area yet to be addressed is the development of a comprehensive theoretical model. Such a model would be crucial for predicting the onset and behavior of the observed instabilities under various cutting conditions. Although the experimental findings have provided valuable insights, a theoretical framework is necessary to fully explain the mechanisms driving these instabilities and to generalize the results across different materials and cutting scenarios.

Finally, the exploration of advanced cutting tools and techniques, such as those involving novel blade geometries or automated cutting systems, could further enhance the precision and efficiency of cutting soft materials. These efforts would not only build on the foundational knowledge established in this dissertation but also push the boundaries of what is achievable in the field of material cutting.

References

[1] Z. Liu et al. “Recent Advances in Soft Biological Tissue Manipulating Technologies”. In: *Chinese Journal of Mechanical Engineering* 35.1 (July 2022), p. 89.

[2] C. Wang, Z. Liao, and D. Wang. “Recent Advances in Processing of Biological Tissues”. In: *Chinese Journal of Mechanical Engineering* 35.1 (Aug. 2022), p. 102.

[3] A. G. Atkins, X. Xu, and G. Jeronimidis. “Cutting, by ‘Pressing and Slicing,’ of Thin Floppy Slices of Materials Illustrated by Experiments on Cheddar Cheese and Salami”. In: *Journal of Materials Science* 39.8 (Apr. 2004), pp. 2761–2766.

[4] Y. Luo et al. “Cutting Behavior of Cortical Bone in Different Bone Osteon Cutting Angles and Depths of Cut”. In: *Chinese Journal of Mechanical Engineering* 35.1 (July 2022), p. 91.

[5] S. Schuldt, Y. Schneider, and H. Rohm. “High-Speed Cutting of Foods: Cutting Behavior and Initial Cutting Forces”. In: *Journal of Food Engineering* 230 (Aug. 2018), pp. 55–62.

[6] B. Takabi and B. L. Tai. “A Review of Cutting Mechanics and Modeling Techniques for Biological Materials”. In: *Medical Engineering & Physics* 45 (July 2017), pp. 1–14.

[7] T. Mora and A. Boudaoud. “Buckling of Swelling Gels”. In: *Eur. Phys. J. E* 20.2 (June 2006), pp. 119–124.

[8] J. Guo et al. “Time Dependent Fracture of Soft Materials: Linear versus Nonlinear Viscoelasticity”. In: *Soft Matter* 16.26 (July 2020), pp. 6163–6179.

[9] G. Zhang et al. “Advancements in Phase-Field Modeling for Fracture in Nonlinear Elastic Solids under Finite Deformations”. In: *Mathematics* 11.15 (2023/0001), p. 3366.

[10] . “VI. The Phenomena of Rupture and Flow in Solids”. In: *Phil. Trans. R. Soc. Lond. A* 221.582-593 (Jan. 1921), pp. 163–198.

[11] C.E. Inglis. “Inglis Stress in a Plate Due to the Presence of Cracks and Sharp Corners”. In: *Fellow of King’s College, Cambridge* (1913).

[12] J. R. Low. “The Fracture of Metals”. In: *Progress in Materials Science* 12 (Jan. 1963), pp. 3–96.

[13] S. Ya. Yarema. “On the Contribution of G. R. Irwin to Fracture Mechanics”. In: *Mater Sci* 31.5 (Sept. 1996), pp. 617–623.

[14] Rong Long and Chung-Yuen Hui. “Crack Tip Fields in Soft Elastic Solids Subjected to Large Quasi-Static Deformation — A Review”. In: *Extreme Mechanics Letters* 4 (Sept. 2015), pp. 131–155.

[15] L. B. Freund and L. B. Freud. *Dynamic Fracture Mechanics*. Cambridge University Press, Mar. 1998.

[16] T. Goldman, A. Livne, and J. Fineberg. “Acquisition of Inertia by a Moving Crack”. In: *Phys. Rev. Lett.* 104.11 (Mar. 2010), p. 114301.

[17] T/ L. Anderson. *Fracture Mechanics — Fundamentals and Applications, Fourth Edition*. CRC Press, Mar. 2017.

[18] T. Baumberger, C. Caroli, and D. Martina. “Fracture of a Biopolymer Gel as a Viscoplastic Disentanglement Process”. In: *Eur. Phys. J. E* 21.1 (Sept. 2006), pp. 81–89.

[19] G. J. Lake and O. H. Yeoh. “Measurement of Rubber Cutting Resistance in the Absence of Friction”. In: 53(1) (1980), pp. 210–227.

[20] B. Zhang et al. “Y-Shaped Cutting for the Systematic Characterization of Cutting and Tearing”. In: *Exp Mech* 59.4 (Apr. 2019), pp. 517–529.

[21] T. Zhang et al. “Predicting Fracture Energies and Crack-Tip Fields of Soft Tough Materials”. In: *Extreme Mechanics Letters* 4 (Sept. 2015), pp. 1–8.

[22] B. Shrimali and O. Lopez-Pamies. “The “Pure-Shear” Fracture Test for Viscoelastic Elastomers and Its Revelation on Griffith Fracture”. In: *Extreme Mechanics Letters* 58 (Jan. 2023), p. 101944.

[23] D. Ahmad et al. “Crack Propagation Behaviour of Laterally Constrained Polymers Used as Dielectric Elastomers”. In: *Rubber Chemistry and Technology* (May 2021).

[24] T. Corre et al. “Experimental Full Field Analysis for Dynamic Fracture of Elastomer Membranes”. In: *Int J Fract* 224.1 (July 2020), pp. 83–100.

[25] H. P. Zhang et al. “Toughening Effect of Strain-Induced Crystallites in Natural Rubber”. In: *Phys. Rev. Lett.* 102.24 (June 2009), p. 245503.

[26] Yoshihiro Morishita, Katsuhiko Tsunoda, and Kenji Urayama. “Velocity Transition in the Crack Growth Dynamics of Filled Elastomers: Contributions of Nonlinear Viscoelasticity”. In: *Phys. Rev. E* 93.4 (Apr. 2016), p. 043001.

[27] C. T. McCarthy, M. Hussey, and M. D. Gilchrist. “On the Sharpness of Straight Edge Blades in Cutting Soft Solids: Part I – Indentation Experiments”. In: *Engineering Fracture Mechanics* 74.14 (Sept. 2007), pp. 2205–2224.

[28] C. T. McCarthy, A. Ní Annaidh, and M. D. Gilchrist. “On the Sharpness of Straight Edge Blades in Cutting Soft Solids: Part II – Analysis of Blade Geometry”. In: *Engineering Fracture Mechanics* 77.3 (Feb. 2010), pp. 437–451. ISSN: 0013-7944. DOI: 10.1016/j.engfracmech.2009.10.003.

[29] S. Schuldt et al. “Analysis of the Sharpness of Blades for Food Cutting”. In: *Journal of Food Engineering* 188 (Nov. 2016), pp. 13–20.

[30] S. Mora. “Effects of the Blade Shape on the Slicing of Soft Gels”. In: *Eur. Phys. J. E* 44.12 (Dec. 2021), p. 151.

[31] K. L. Johnson. *Contact Mechanics*. Cambridge: Cambridge University Press, 1985.

[32] B. Lawn. *Fracture of Brittle Solids*. 2nd ed. Cambridge Solid State Science Series. Cambridge: Cambridge University Press, 1993.

[33] J. A. Greenwood, J. B. P. Williamson, and Frank Philip Bowden. “Contact of Nominally Flat Surfaces”. In: *Proceedings of the Royal Society of London. Series A. Mathematical and Physical Sciences* 295.1442 (Jan. 1997), pp. 300–319.

[34] N. Amino. “Relationships Between the Friction and Viscoelastic Properties of Rubber”. In: *Tire Science and Technology* 28 (July 2000).

[35] B. Persson. “Theory of Rubber Friction and Contact Mechanics”. In: *The Journal of Chemical Physics* 115 (Aug. 2001).

[36] D. T. Nguyen et al. “Non–Amontons-Coulomb Local Friction Law of Randomly Rough Contact Interfaces with Rubber”. In: *EPL* 104.6 (Jan. 2014), p. 64001.

[37] K. Vorvolakos. “The Effects of Molecular Weight and Temperature on the Kinetic Friction of Silicone Rubbers — Request PDF”. In: *Langmuir* 19.17 (2003), pp. 6778–6787.

[38] A. Schallamach. “The Velocity and Temperature Dependence of Rubber Friction”. In: *Proc. Phys. Soc. B* 66.5 (May 1953), p. 386.

[39] A. Chateauminois and C. Fretigny. “Local Friction at a Sliding Interface between an Elastomer and a Rigid Spherical Probe”. In: *Eur. Phys. J. E* 27.2 (Oct. 2008), pp. 221–227.

[40] F. P. Browden and D. Tabor. “The Friction and Lubrication of Solids”. In: *Oxford University Press* (2001). (Visited on 08/20/2024).

[41] R.D. Mindlin. “Compliance of Elastic Bodies in Contact”. In: *J. Appl. Mech* 16(3) (1949), pp. 259–268.

[42] J. Scheibert et al. “Stress Field at a Sliding Frictional Contact: Experiments and Calculations”. In: *Journal of the Mechanics and Physics of Solids* 57 (Oct. 2009), p. 1921.

[43] A. Chateauminois. “Effects of Stretching on the Frictional Stress of Rubber.” In: *Soft Matter (RSC Publishing)* (2017). (Visited on 07/11/2024).

[44] R. S. Rivlin. “Rupture of Rubber. I. Characteristic Energy for Tearing”. In: *Journal of Polymer Science* (1953). (Visited on 08/06/2024).

[45] A. N. Gent. “A New Constitutive Relation for Rubber”. In: *Rubber Chemistry and Technology* 69.1 (Mar. 1996), pp. 59–61.

[46] S. B. Hutchens, S. Fakhouri, and A. J. Crosby. “Elastic Cavitation and Fracture via Injection”. In: *Soft Matter* 12.9 (Feb. 2016), pp. 2557–2566.

[47] S. I. Heizler, D. A. Kessler, and H. Levine. “Propagating Mode-I Fracture in Amorphous Materials Using the Continuous Random Network Model”. In: *Phys. Rev. E* 84.2 (Aug. 2011), p. 026102.

[48] F. Lechenault et al. “Soft Coring: How to Get a Clarinet out of a Flute?” In: *Extreme Mechanics Letters* 61 (June 2023), p. 101976.

[49] M. Marder and J. Fineberg. “How Things Break”. In: *Physics Today* 49.9 (Sept. 1996), pp. 24–29.

[50] J. Fineberg and M. Marder. “Instability in Dynamic Fracture”. In: *Physics Reports* 313.1 (May 1999), pp. 1–108.

[51] F. Tian and J. P. Gong. “Nonlinearity Tunes Crack Dynamics in Soft Materials”. In: (Aug. 2023).

[52] A. C. Maan et al. “Unstable Oscillation of the Cryogenic H Maser”. In: *Physica B: Condensed Matter*. Proceedings of the 19th International Conference on Low Temperature Physics 165–166 (Aug. 1990), pp. 21–22.

[53] E. Hamm, I. Sivak, and B. Roman. “Nature of Crack Path Instabilities in Thin Sheets Cut by Blunt Objects”. In: *Phys. Rev. Lett.* 124.17 (Apr. 2020), p. 174101.

[54] Van-Bac Pham et al. “Global Bifurcation Criterion for Oscillatory Crack Path Instability”. In: *Phys. Rev. E* 77.6 (June 2008), p. 066114.

[55] F. Tian. “Bifurcation Criterion and the Origin of Limit Crack Velocity in Dynamic Brittle Fracture — International Journal of Fracture”. In: *Springer* 224 (June 2020), pp. 117–131.

[56] Michel J. A. M. van Putten. “Dynamics in Two-Dimensional Systems”. In: *Dynamics of Neural Networks: A Mathematical and Clinical Approach*. Springer, 2020, pp. 71–109.

[57] A. Ghatak and M. K. Chaudhury. “Adhesion-Induced Instability Patterns in Thin Confined Elastic Film”. In: *Langmuir* 19.7 (Apr. 2003), pp. 2621–2631.

[58] R. D. Deegan et al. “Oscillating Fracture Paths in Rubber”. In: *Phys. Rev. Lett.* 88.1 (Dec. 2001), p. 014304.

[59] E. Bouchbinder, J. Fineberg, and M. Marder. “Dynamics of Simple Cracks”. In: *Annual Review of Condensed Matter Physics* 1.Volume 1, 2010 (Aug. 2010), pp. 371–395.

[60] P. M. Reis et al. “Unzip Instabilities: Straight to Oscillatory Transitions in the Cutting of Thin Polymer Sheets”. In: *EPL* 82.6 (June 2008), p. 64002.

[61] B. Yang and K. Ravi-Chandar. “Crack Path Instabilities in a Quenched Glass Plate”. In: *Journal of the Mechanics and Physics of Solids* 49.1 (Jan. 2001), pp. 91–130.

[62] M Adda-Bedia and L Mahadevan. “Crack-Front Instability in a Confined Elastic Film”. In: *Proceedings of the Royal Society A: Mathematical, Physical and Engineering Sciences* 462.2075 (May 2006), pp. 3233–3251.

[63] A. Ghatak and L. Mahadevan. “Crack Street: The Cycloidal Wake of a Cylinder Tearing through a Thin Sheet”. In: *Phys. Rev. Lett.* 91.21 (Nov. 2003), p. 215507.

[64] B. Roman et al. “Oscillatory Fracture Paths in Thin Elastic Sheets”. In: *Comptes Rendus Mécanique* 331.12 (Dec. 2003), pp. 811–816.

[65] G. J. Lake and O. H. Yeoh. “Measurement of Rubber Cutting Resistance in the Absence of Friction”. In: *Int J Fract* 14.5 (Oct. 1978), pp. 509–526.

[66] L. B. Freund. *Dynamic Fracture Mechanics*. Cambridge Monographs on Mechanics. Cambridge: Cambridge University Press, 1990.

[67] M. Marder J. Fineberg. “Instability in Dynamic Fracture”. In: 313.1-2 (May 1999), pp. 1–108.

[68] M. Adda-Bedia and Y. Pomeau. “Crack Instabilities of a Heated Glass Strip”. In: *Phys. Rev. E* 52.4 (Oct. 1995), pp. 4105–4113.

[69] J. B. Leblond. “Crack Paths in Plane Situations—I. General Form of the Expansion of the Stress Intensity Factors”. In: *International Journal of Solids and Structures* 25.11 (Jan. 1989), pp. 1311–1325.

[70] K. Larson. “Can You Estimate Modulus From Durometer Hardness for Silicones? Yes, but Only Roughly . . . and You Must Choose Your Modulus Carefully!” In: (Sept. 2017).

[71] R. S. Rivlin and A. G. Thomas. “Rupture of Rubber. I. Characteristic Energy for Tearing”. In: *Journal of Polymer Science* 10.3 (1953), pp. 291–318.

[72] Y. H. Zhao et al. “Influence of Specimen Dimensions and Strain Measurement Methods on Tensile Stress–Strain Curves”. In: *Materials Science and Engineering: A* 525.1 (Nov. 2009), pp. 68–77.

[73] H. W. Greensmith and A. G. Thomas. “Rupture of Rubber. III. Determination of Tear Properties”. In: *Journal of Polymer Science* 18.88 (1955), pp. 189–200.

[74] A. Livne. “Oscillations in Rapid Fracture”. In: *Phys. Rev. Lett.* 98 (2007).

[75] F. Corson et al. “Thermal Fracture as a Framework for Quasi-Static Crack Propagation”. In: *Int J Fract* 158.1 (July 2009), pp. 1–14.

[76] M. Marder. “Instability of a Crack in a Heated Strip”. In: *Phys. Rev. E* 49.1 (Jan. 1994), R51–R54.

[77] T. Baumberger, C. Caroli, and D. Martina. “Fracture of a Biopolymer Gel as a Viscoplastic Disentanglement Process”. In: *Eur. Phys. J. E* 21.1 (Sept. 2006), pp. 81–89.

[78] Members of the GMIA. “Gelatin Handbook - Gelatin Manufacturers Institute of America Home”. In: *Gelatin Manufacturers Institute of America* (2019).

[79] Y. Liu, C.-Y. Hui, and W. Hong. “A Clean Cut”. In: *Extreme Mechanics Letters* 46 (July 2021), p. 101343.

[80] A. Spagnoli et al. “Cutting Resistance of Soft Materials: Effects of Blade Inclination and Friction”. In: *Theoretical and Applied Fracture Mechanics* 101 (June 2019), pp. 200–206.

[81] C. T. McCarthy, M. Hussey, and M. D. Gilchrist. “On the Sharpness of Straight Edge Blades in Cutting Soft Solids: Part I – Indentation Experiments”. In: *Engineering Fracture Mechanics* 74.14 (Sept. 2007), pp. 2205–2224.

[82] M. Czerner, L. A. Fasce, and P. M. Frontini. “Wire Cutting Method to Assess Fracture Toughness of Gelatin Gels: Phenomenological Analysis and Limitations of Methodology”. In: *Materials Performance and Characterization* 3.3 (Sept. 2014), pp. 448–468.

[83] Y. Tanaka et al. “Determination of Fracture Energy of High Strength Double Network Hydrogels”. In: *J Phys Chem B* 109.23 (June 2005), pp. 11559–11562.

[84] T. Baumberger et al. “Magic Angles and Cross-Hatching Instability in Hydrogel Fracture”. In: *Phys. Rev. Lett.* 100.17 (May 2008), p. 178303.

[85] F. Baldi, F. Bignotti, and T. Riccò. “Determination of the Fracture Resistance of Polymer Gels via Cutting with Wire”. In: *12th International Conference on Fracture 2009, ICF-12* 1 (Jan. 2009), pp. 387–396.